People's Democratic Republic of Algeria

Ministry of Higher Education and Scientific Research

University of Echahid Hamma Lakhdar El-OUED

Faculty of Natural and Life Sciences

Department of Cellular and Molecular Biology

END OF STUDIES MEMOIR

Submitted to Obtain the Academic Master's Degre

Speciality: Toxicology

THEME

Synthesis, Characterization, and Multi-ModeI Evaluation of Anti-Inflammatory Activity of Four Porphyrin Derivatives: *In Vivo*, *In Vitro*, and *In Silico* Approaches

Presented by:

ZERROUD Farida

ZERROUD Nacer Allah

Jury Members:

President: Mrs.Tedjiani Aich	M.A.B, University of El Oued
Supervisor: Mrs. BOUDEBIA Ouafa	M.A.B, University of El Oued
Co-Supervisor: Mr. LANEZ Elhafnaoui	M.C.A, University of El Oued
Examiner: Mrs. Laib Ibtissam	M.A.B, University of El Oued

Incubator Representative: Mr. Zaghdi Zoubir

Economic Partner: Mr. Omeirat Mohammed Al-Amin

University Year: 2024/2025

شكـــــر و تقديـــــر

الحمد لله أولاً وآخراً، ظاهرًا وباطنًا، على نعمٍ لا تُعدّ ولا تُحصى، وعلى توفيقه الذي رافقنا في خطوات هذا المشوار العلمي، حتى تكللت جهودنا بثمرة هذه المذكرة.

في طريق العلم، لا يكون السير سهلاً ولا الدرب ممهّدًا، ولكن الله يهيّئ للمرء قلوبًا صافية، وأيادي بيضاء، تضيء له العتمة، وتشد من أزره في لحظات الوهن، وتقاسمه الحلم حتى يصبح واقعًا.

نتوجه بأسمى آيات الشكر والعرفان، وبمشاعر يغمرها الامتنان، إلى مشرفتنا الفاضلة، **الأستاذة بوضبية وفاء**، التي لم تكن فقط أستاذة وموجهة، بل كانت سندًا حقيقيًا في كل مراحل العمل. علّمتنا أن البحث العلمي ليس مجرد خطوات منهجية، بل هو صبر وعطاء وأخلاق. كان دعمها نورًا في لحظات الشك، وتشجيعها وقودًا يدفعنا للاستمرار كلما تعثرت خطواتنا. لها منا كل التقدير والدعاء الصادق بأن يجزيها الله عنا خير الجزاء.

ونخص بالشكر والتقدير **الدكتور الحفناوي العانز** المشرف المساعد، الذي رافقنا عن قرب، وواكب خطواتنا بحرص واهتمام، وكان دومًا من أول الداعمين لنا، حضورًا ومساندةً وتشجيعًا. كانت روحه الطيبة منارةً خفية في خلفية هذا النجاح.

كذلك نشكر **الدكتور بن عمر محمد العربي** على دعمه وتوجيهه، حيث انه لم يبخل علينا بالنصح والإرشاد، فله منا خالص الامتنان والتقدير.

ولا يمكننا أن نغفل عن توجيه شكر خالص وعميق **للدكتور شعوة حسين**، الذي كان حاضرًا في محطات كثيرة من رحلتنا، يمنحنا النصيحة الصادقة من قلبه، ويمدّ لنا يد العون كلما احتجنا إلى دعم أو توجيه. كان وجهه البشوش وموقفه الإيجابي دائمًا مصدر طمأنينة لنا، وصوته الهادئ يحمل دفء الأخوة وصدق النية. نشكره من أعماق قلوبنا على كل لحظة منحنا فيها من وقته، وكل مرة كان فيها سندًا نلجأ إليه بثقة وارتياح.

كما نعرب عن عميق شكرنا وامتناننا **للأستاذة العايب ابتسام**، التي لم تبخل علينا بتوجيهاتها ونصائحها، وكانت دومًا تسعى لمدّ يد العون، وتقديم ما يُعين على تخطي العقبات، فجزاها الله خيرًا على كل ما قدمته لنا من دعم صادق.

ولا يفوتنا أن نتوجّه بخالص الشكر **للدكتور بن ناصر كمال**، الذي كانت لمسته واضحة في هذا العمل، وقدّم لنا دعمه بكل سخاء ونبل. كان لتدخّله في الوقت المناسب الأثر الكبير في تسهيل مهمتنا وإنجاحها.

كما نعرب عن تقديرنا العميق لأعضاء لجنة المناقشة، **الأستاذة تجاني عائشة** رئيسة، و**الأستاذة العايب ابتسام** مناقِشة، الذين شرفونا بقبولهم مناقشة هذه المذكرة، وكان حضورهم مصدر فخر لنا، ونقاشهم قيمة علمية مضافة لهذا العمل.

ولا يسعنا أيضًا إلا أن نشكر **مهندسي المخابر بكلية علوم الحياة والعلوم الطبيعية بجامعة الوادي**، وعلى رأسهم **السيد عمر خنوفة** و**السيدة منى شريطي**، الذين كانوا خير عونٍ لنا، فبفضل جهودهم وتعاونهم استطاعت تجربتنا الميدانية أن ترى النور.

ونتقدّم بجزيل الشكر والعرفان إلى **أعضاء مخبرVTRS** ، الذين لم يترددوا يومًا في دعمنا، وكان لعطائهم الصامت والمستمر أثر كبير في إتمام هذا العمل.

إلى كل من وقف إلى جانبنا، ولو بكلمة، ولو بابتسامة، ولو بدعاء في ظهر الغيب. لكم منّا كل التقدير، ومن قلوبنا دعاء لا ينقطع، وذكرى لا تزول.

الاهـــــــداء

إلى من كانت الحضن الدافئ حين ضاق صدري، والكلمة الطيبة حين خفت صوتي، والنور الذي لم يخفت يومًا...

إليكِ أمي، يا من حملتِ عني التعب، وسهرتِ لأجلي، وصليتِ في صمتٍ أن أبلغ هذا اليوم. نجاحي هو امتداد لصبرك، وهذه اللحظة لا تكتمل إلا بكِ.

إلى أبي، الذي كان سندًا لا يميل، وظهرًا لا ينكسر، وصوتًا يشدُّ من أزري في كل لحظة ضعف.

كل خطوةٍ قطعتها، كنت فيها الأمان والطريق.

إلى إخوتي الذين كانوا دائمًا الوطن الآخر، الذين احتملوا قلقي، وتقبّلوا غيابي، وشاركوا دعواتهم وأمنياتهم دون أن أطلب.

إلى كل من مرّ في طريقي وترك أثرًا جميلًا، إلى من مدّ لي يدًا، أو منحني كلمة طيبة، أو صمت بجانبي وقت الحاجة...

أهدي هذا العمل لكل من أحبني بصدق، وآمن بي حين شككت في نفسي،

لأن النجاح لا يُصنع وحده، بل يُولد من قلوبٍ أحاطتك بالحبّ، وعيونٍ تمنت لك الخير في كل حين.

زرود فريدة

الاهـــــــداء

إلى المدافعين عن شرف الأمة

غزة تُقصف ونحن نبحث عن الكلماتِ
أطفالٌ ينامون على أصواتِ الصواريخِ
وأمهاتٌ ينتظرن خروج جثث أولادهن من تحت الركامِ
وشبابٌ يكتبون وصاياهم على أوراقٍ ممزقةٍ
غزة جرحٌ في قلبِ كلِّ من بقيت لديه إنسانية
غزة لا تطلب الكثير...فقط : ألا نخذلها بالصمتِ
لكِ الله يا غزة وأمة الخذلانِ أيضًا لها الله

إلى أبي

إلى العزيز الذي حملتُ اسمه فخرًا
إلى من كلّله الله بالهيبة والوقارِ
إلى من حصد الأشواك عن دربي
وزرع لي الراحة بدلًا منها

إلى أمي

إلى من علّمتني الأخلاق قبل أن أتعلمها
إلى الجسر الصاعد بي إلى الجنة
إلى اليد الخفية التي أزالت عن طريقي العقبات
ومن ظلّت دعواتها تحمل اسمي ليلًا ونهارًا
احبك يا اية الله
أمي محبوبتي و ملهمتي

إلى إخوتي وأصحابي

وإلى من وهبني الله نعمة وجودهم، إلى مصدر قوتي، وأرضي الصلبة، وجدار قلبي المتين إخوتي.
وإلى من إن ضاقت بي الدنيا وسعت بخُطاهم، وإن سقطت، كانوا أول من رفعوني بكلامهم
إلى من رافقني بالقلب قبل الدرب أصحابي الأحبة.

طويت صفحة من التعب وسجلت في تاريخي فخرا لا ينسى. لم أعد أتساءل عن ملامح الوصول فقد بعيوني. تلاشت غيوم التعب وابتسم الأفق بعد عتمة الانتظار. ها هي الخطى التي كانت تتعثر أحيانًا قد وجدت مستقرها في قمة الإنجاز، وبين طيات الطريق تنفست سلامًا وفرحًا وامتنانً. حققتها من أجل روح جدي.

زرود نصر الله

Abstract

This study is part of ongoing efforts to develop effective alternative treatments against inflammation. It focuses on evaluating the anti-inflammatory activity of four porphyrin derivatives synthesized in the laboratory and assessed through three complementary approaches: *in vitro*, *in vivo*, and *in silico*. Chronic inflammation poses a major medical challenge today, being linked to several serious diseases such as cancer, type 2 diabetes, multiple sclerosis, and neurodegenerative disorders, which highlights the need for new, safer, and more effective compounds.

This study evaluated the anti-inflammatory potential of four derivatives: *$NiTPPH_2$*, *$TbiPPH_2$*, *$TPPH_2$(o-methyl)*, and *$ZnTPPH_2$*, compared to diclofenac as a reference drug, using a glyphosate-induced inflammation model in rats, alongside cellular and computational assessments to determine efficacy, toxicity, and pharmacokinetic behavior.

The results of both *in vitro* and *in vivo* evaluations demonstrated a marked effectiveness of porphyrin derivatives as anti-inflammatory agents. In the bovine serum albumin (BSA) denaturation assay, these derivatives exhibited strong protein stabilization capacity, with inhibition rates ranging from 79.86% to 90.22% and IC_{50} values between 68.91 and 92.71 µg/mL. These findings indicate significant anti-inflammatory activity at the cellular level. In the rat inflammation model, treatment with porphyrin derivatives led to notable biological improvements, including a reduction in hepatic malondialdehyde (MDA) levels from 8.06 to 4.0 nmol/mg protein following administration of *$TPPH_2$(o-methyl)*, and an increase in brain reduced glutathione (GSH) levels from 5.8 to 10.53 nmol/mg protein with *$NiTPPH_2$*. The treatment also stabilized liver enzyme levels (ALT and AST) close to control values and normalized the weights of affected organs, particularly the liver and kidneys, compared to the glyphosate-only group. These results reflect the promising potential of porphyrin derivatives in modulating inflammation associated with oxidative stress.

Histological analysis supported these findings, showing clear structural improvement in liver, kidney, and brain tissues, with reduced inflammation.

In silico studies confirmed strong pharmacological potential, especially for *$TPPH_2$(o-methyl)* and *$NiTPPH_2$*, with COX-1 binding energies reaching (–10.3 kcal/mol), and favorable ADMET profiles in terms of absorption, distribution, and safety.

Abstract

The synthesized porphyrin derivatives, particularly *$TPPH_2$(o-methyl)* and *$NiTPPH_2$*, exhibit promising anti-inflammatory activity through multiple mechanisms, making them strong candidates as safer and effective alternatives to conventional NSAIDs like ibuprofen and diclofenac.

Keywords : Porphyrins, Anti-inflammatory, *In vitro, In vivo, In silico,* COX-1, ADMET**.**

Résumé

Cette étude s'inscrit dans le cadre des efforts visant à développer des alternatives thérapeutiques efficaces contre les inflammations. Elle porte sur l'évaluation de l'activité anti-inflammatoire de quatre dérivés de porphyrine, préparés en laboratoire et testés selon trois approches complémentaires : *in vitro, in vivo* et *in silico*. L'inflammation chronique constitue aujourd'hui un défi médical majeur, impliqué dans diverses pathologies telles que le cancer, le diabète de type 2, la sclérose en plaques et les maladies neurodégénératives, ce qui justifie la recherche de composés plus efficaces et moins toxiques.

Cette étude a évalué l'effet anti-inflammatoire de quatre dérivés : *NiTPPH₂*, *TbiPPH₂*, *TPPH₂(o-methyl)* et *ZnTPPH₂*, comparés au diclofénac comme substance de référence, dans un modèle d'inflammation induite par le glyphosate chez le rat, avec des analyses cellulaires et informatiques pour étudier leur efficacité, leur toxicité et leurs propriétés pharmacocinétiques.

Les résultats des évaluations *in vitro* et *in vivo* ont démontré une efficacité marquée des dérivés de porphyrine en tant qu'agents anti-inflammatoires. Dans le test de dénaturation de l'albumine sérique bovine (BSA), ces dérivés ont montré une forte capacité de stabilisation des protéines, avec des taux d'inhibition variant entre 79,86 % et 90,22 %, et des valeurs de CI_{50} comprises entre 68,91 et 92,71 µg/mL. Ces données indiquent une activité anti-inflammatoire notable au niveau cellulaire. Dans le modèle inflammatoire chez le rat, le traitement avec les dérivés de porphyrine a conduit à des améliorations biologiques significatives, notamment une réduction du taux hépatique de malondialdéhyde (MDA) de 8,06 à 4,0 nmol/mg de protéine après administration du *TPPH₂(o-méthyle)*, ainsi qu'une augmentation du taux cérébral de glutathion réduit (GSH) de 5,8 à 10,53 nmol/mg de protéine suite à l'utilisation du *NiTPPH₂*. Le traitement a également permis de stabiliser les enzymes hépatiques ALT et AST à des niveaux proches de ceux des témoins, tout en normalisant les poids des organes affectés, en particulier le foie et les reins, par rapport au groupe glyphosate seul. Ces résultats illustrent le potentiel prometteur des dérivés de porphyrine dans la modulation de la réponse inflammatoire liée au stress oxydatif.

L'analyse histologique a confirmé ces effets, montrant une amélioration structurelle marquée du foie, des reins et du cerveau, avec une diminution nette des lésions inflammatoires.

L'approche *in silico* a mis en évidence un fort potentiel pharmacologique, notamment pour *TPPH₂(o-methyl)* et *NiTPPH₂*, avec une énergie de liaison au site COX-1 atteignant (–10,3

kcal/mol), et de bons profils d'absorption, de distribution et d'innocuité selon les prédictions ADMET.

En conclusion, les dérivés porphyriniques étudiés, en particulier *$TPPH_2$(o-methyl)* et *$NiTPPH_2$*, montrent une activité anti-inflammatoire significative et multifactorielle, suggérant leur potentiel comme alternatives sûres et efficaces aux anti-inflammatoires classiques comme l'ibuprofène ou le diclofénac.

Mots clés: Porphyrines, anti-inflammatoire, *In vitro, In vivo*, COX-1, ADMET.

ملخص

تندرج هذه الدراسة ضمن الجهود المتواصلة لتطوير علاجات بديلة وفعالة ضد الالتهابات، وهي تتمحور حول تقييم النشاط المضاد للالتهاب لأربعة مشتقات من البورفيرين تم تحضيرها مخبريًا وتقييمها باستخدام ثلاث مقاربات تكاملية: *in vitro*، *in vivo*، و*in silico*. تشكل الالتهابات المزمنة اليوم تحديًا طبيًا رئيسيًا يرتبط بالعديد من الأمراض المستعصية مثل السرطان، السكري من النوع الثاني، التصلب اللويحي، وأمراض التنكس العصبي، مما يعزز الحاجة إلى مركبات فعالة ذات سمية منخفضة وانتقائية عالية.

هدفت هذه الدراسة إلى تقييم النشاط المضاد للالتهاب لأربعة مشتقات هي: *NiTPPH₂*، *TbiPPH₂*، *TPPH₂(o-methyl)*، و*ZnTPPH₂*، ومقارنتها بعقار الديكلوفيناك كمادة مرجعية، باستخدام نموذج التهاب محثوث بالغليفوسات في الجرذان، إلى جانب التقييم الخلوي والحاسوبي لتحديد الفعالية والسمية والخصائص الدوائية المتوقعة.

أظهرت نتائج التقييمين *in vitro* و *in vivo* فعالية ملحوظة لمشتقات البورفيرين كمضادات التهاب. في اختبار التثبيط الحراري لبروتين**BSA** ، بينت هذه المشتقات قدرة عالية على تثبيت البروتين، حيث تراوحت نسب التثبيط بين 79.86% و90.22%، وسُجلت قيم **IC_{50}** في حدود 68.91 إلى 92.71 ميكروغرام/مل. هذه النتائج تشير إلى كفاءة واضحة في منع تمسخ البروتين، ما يدعم التأثير المضاد للالتهاب على المستوى الخلوي. أما في نموذج الالتهاب في الجرذان، فقد أدى العلاج بمشتقات البورفيرين إلى تحسينات بيولوجية ملموسة، من بينها انخفاض مستوى المالون ثنائي الألدهيد (MDA) في الكبد من 8.06 إلى 4.0 نانومول/ملغ بروتين بعد المعالجة بـ*TPPH₂(o-methyl)* ، وارتفاع تركيز الجلوتاثيون المختزل (GSH)في الدماغ من 5.8 إلى 10.53 نانومول/ملغ بروتين باستخدام *NiTPPH₂*. كما ساهمت هذه المعالجات في تثبيت نشاط إنزيمي ALT و ASTعند مستويات قريبة من القيم الطبيعية، إلى جانب استعادة أوزان الأعضاء المتأثرة، خصوصًا الكبد والكلى، إلى حدودها الفسيولوجية بالمقارنة مع مجموعة الغليفوسات غير المعالجة. تعكس هذه النتائج الدور الواعد لمشتقات البورفيرين في التخفيف من التأثيرات الالتهابية المرتبطة بالإجهاد التأكسدي.

التحاليل النسيجية دعّمت هذه النتائج، حيث أظهرت الشرائح المجهرية تحسنًا هيكليًا واضحًا في الكبد والكلى والدماغ، مع استعادة البنية النسيجية الطبيعية وتقليل مناطق الالتهاب.

أخيرًا، أظهرت الدراسة الحاسوبية *in silico* نتائج قوية في التنبؤ بالتوافر البيولوجي والسمية، حيث سجلت المركبات خصوصًا *TPPH₂(o-methyl)₂* و *NiTPPH₂* درجات ارتباط عالية بموقع COX-1 بلغت 10.3 kcal/mol– ، إلى جانب نتائج إيجابية في اختبار ADMET على مستوى الامتصاص والتوزيع وعدم السمية الوراثية.

خلصت هذه الدراسة إلى أن المشتقات المحضّرة من البورفيرين، خاصة *TPPH₂(o-methyl)*و *NiTPPH₂* ، تمتلك نشاطًا مضادًا للالتهاب واعدًا، بآليات متعددة تشمل تثبيط البروتينات الالتهابية، خفض الإجهاد التأكسدي، وحماية البنى الخلوية، مما يؤهلها لأن تكون بدائل فعالة وأكثر أمانًا مقارنة بالعقاقير التقليدية مثل الإيبوبروفين والديكلوفيناك.

الكلمات المفتاحية: البورفيرينات، النشاط المضاد للالتهاب، اختبارات مخبرية، دراسات حية، COX-1،ADMET .

Abreviations list

%: Percentage

13C NMR: Carbon-13 Nuclear Magnetic Resonance

1H NMR: Proton Nuclear Magnetic Resonance

ADMET: Absorption, Distribution, Metabolism, Excretion, and Toxicity

ALT: Alanine Aminotransferase

AST: Aspartate Aminotransferase

BHT: Butylated Hydroxytoluene

BSA: Bovine Serum Albumin

CBC: Complete Blood Count

$CHCl_3$: Chloroform

COX-1: Cyclooxygenase-1

CRP: C-Reactive Protein

DFT: Density Functional Theory

DMSO: Dimethyl Sulfoxide

DTNB: 5,5′-Dithiobis-(2-nitrobenzoic acid) (Ellman's Reagent)

EDTA: Ethylenediaminetetraacetic Acid

EGAP: Energy Gap

GI: Gastrointestinal

GRA: Granulocytes

GSH: Reduced Glutathione

HCl: Hydrochloric Acid

HOMO: Highest Occupied Molecular Orbital

Hp: Haptoglobin

Abreviations list

IC_{50}: Half Maximal Inhibitory Concentration

IR: Infrared

LUMO: Lowest Unoccupied Molecular Orbital

LYM: Lymphocytes

MDA: Malondialdehyde

MR: Molar Refractivity

NBT: Nitroblue Tetrazolium

NSAIDs: Non-Steroidal Anti-Inflammatory Drugs

Pa: Probability to be Active

Pi: Probability to be Inactive

PLT: Platelets

RBC: Red Blood Cells

ROW: Relative Organ Weight

SD: Standard Deviation

SMILES: Simplified Molecular Input Line Entry System

SOD: Superoxide Dismutase

TBA: Thiobarbituric Acid

TbiPPH₂: tert-Butyl-Substituted Tetraphenylporphyrin

TBS: Tris Buffer Solution

TCA: Trichloroacetic Acid

TPP: Tetraphenylporphyrin

TPPH₂(o-methyl): Free base Tetraphenylporphyrin

UV-Vis: Ultraviolet–Visible Spectroscopy

VTRS: Valorisation et Technologie des Ressources Sahariennes

Abreviations list

WBC: White Blood Cells

ZnTPPH₂: Zinc Tetraphenylporphyrin

List of figures

List of figures

List of tables

Summary

Introduction

Introduction

Inflammation is a fundamental and evolutionarily conserved biological process that plays a pivotal role in the host's defense against infection and injury. It encompasses a complex interplay of vascular, cellular, and molecular mechanisms aimed at neutralizing harmful agents, removing necrotic tissue, and initiating repair. However, when dysregulated or prolonged, this protective process transforms into a pathological one, contributing to the onset and progression of numerous chronic diseases such as rheumatoid arthritis, cardiovascular pathologies, neurodegenerative disorders, and various types of cancer **(Soares *et al*., 2023)**.

Over the past decades, extensive research has revealed that inflammation is not merely a symptom or consequence, but often a primary driver in the etiology and pathogenesis of many non-communicable diseases. This paradigm shift has prompted the scientific community to reconsider therapeutic strategies and to place inflammation at the heart of modern pharmacological intervention.

Currently, the mainstay of anti-inflammatory therapy relies on two major drug classes: non-steroidal anti-inflammatory drugs (NSAIDs) and corticosteroids. Despite their clinical efficacy, these drugs are frequently associated with dose-limiting side effects. NSAIDs, by inhibiting cyclooxygenase enzymes (COX-1 and COX-2), reduce the synthesis of pro-inflammatory prostaglandins but concurrently impair gastric mucosa protection and renal perfusion, leading to ulceration and nephrotoxicity **(Wongrakpanich *et al*., 2018)**. Corticosteroids, although potent, often result in metabolic disturbances, immunosuppression, and osteoporosis with long-term use **(Heymonet, 2013)**. These limitations underscore the urgent necessity for safer and more targeted therapeutic alternatives with multi-target capabilities and lower toxicity profiles.

In response to this therapeutic void, porphyrins and their derivatives have emerged as highly promising molecular scaffolds in the development of novel anti-inflammatory agents. Porphyrins are naturally occurring macrocyclic compounds composed of four pyrrole subunits interconnected via methine bridges, forming a conjugated π-electron system. Their biological relevance is evident in essential biomolecules such as heme and chlorophyll. However, beyond their natural functions, synthetic porphyrins have demonstrated unique physicochemical and redox properties that allow them to interact selectively with various biological targets implicated in inflammation, including reactive oxygen species (ROS), metalloproteins, and key enzymes such as cyclooxygenases **(Kadish *et al*., 2010)**.

Recent studies have illustrated that porphyrins can exert potent antioxidant activity, scavenge free radicals, and modulate inflammatory pathways at both molecular and cellular levels. These multifaceted capabilities position porphyrins as potential smart drugs, capable of addressing the complex and interconnected nature of inflammatory disorders **(Senge and Smith, 2021)**. Moreover, structural functionalization of porphyrins through peripheral substitutions or metal chelation has opened the door to a wide array of derivatives with enhanced selectivity and bioactivity.

This thesis is structured in two main parts. The first part is devoted to the theoretical foundations and comprises three chapters: the first chapter is dedicated to porphyrins and presents their structures, properties, and synthetic methods; the second chapter provides an in-depth look at the inflammatory process; and finally, the third chapter explores classic anti-inflammatory drugs, their mechanisms of action, and their therapeutic limitations.

The second part corresponds to the experimental approach and is structured around a tripartite strategy: *in vitro, in vivo*, and in silico. The *in vitro* biological assays aim to evaluate the anti-inflammatory activity of the four porphyrin derivatives synthesized and characterized using spectroscopic techniques. The *in-silico* analysis includes ADMET predictions, drug-likeness assessments, a chemoinformatics study, and molecular docking investigations to establish structure-activity correlations (SAR). The in vivo study complements the approach and aims to demonstrate the pharmacological potential of the tested derivatives in animal models.

This work is distinguished by its integrative and multidisciplinary approach, at the interface of synthetic chemistry, pharmacology, molecular modeling, and toxicology. By correlating chemical structure with biological performance, it contributes to the rational design of new multitarget anti-inflammatory agents capable of overcoming the limitations of conventional therapies.

First part
Bibliography

Chapter one
Porphyrins

I. General Information on porphyrins

I.1.1. Definition, properties and applications of porphyrins

Porphyrin is a large ring compound that is created by four pyrrole units joined by methene linkages. The methene linkages create the four meso positions of the porphyrin, and the carbon atoms in the four pyrroles make up the α and β positions (Figure 01). There are 22 π electrons in this molecule, 18 of which are accountable for the aromaticity of the molecule, according to Hückel's rule of 4n + 2 delocalized electrons, where n equals 4 here. Porphine is the name for the fully unsubstituted porphyrin.

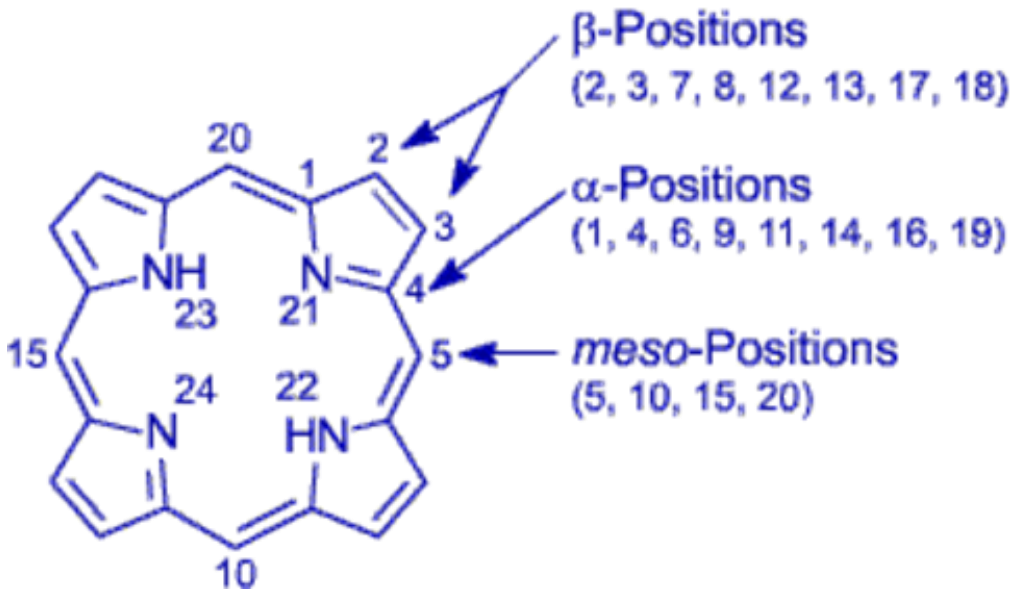

Figure 01: Structure of porphine**.**

Porphyrin can be found in two forms: as a 'freebase' (see Figure 01) and in a metal-complexed form (see Figure 02). In the latter, a metal cation (usually with an oxidation state of (+II) or (+III)) is coordinated.

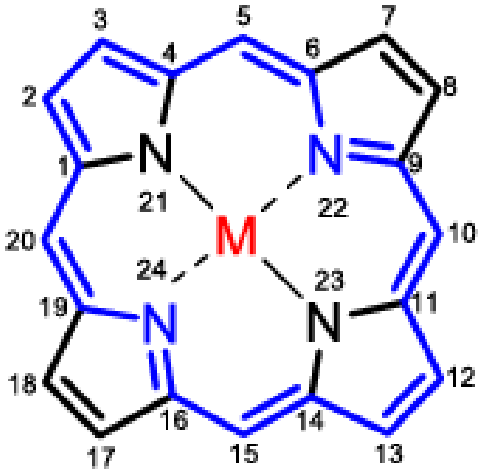

Figure 02: Metalized porphine (M = metal)**.**

Porphyrins are defined by a broad application range. Heme, a naturally occurring iron porphyrin in hemoglobin, is of essential importance in the transportation of oxygen to the different components of the body. Likewise, chlorophyll, a naturally occurring porphyrin, is of essential importance in the processes of photosynthesis. Porphyrins have applications in numerous areas, some of which include photodynamic therapy, biosensing devices, redox catalysis, synthetic photosynthesis, the development of photovoltaic cells, nonlinear optical properties, and molecular recognition **(Senge and Davis, 2010)**.

I.1.2. Spectroscopic and electrochemical characterizations of porphyrins

I.1.2.1. NMR nuclear magnetic resonance

I.1.2.1.1. Proton NMR spectroscopy (1H NMR)

Proton nuclear magnetic resonance for porphyrin macrocycles exhibits two characteristic signals. The α and β positions and the meso positions are observed.

Pyrrolic β protons at 8-9 ppm. Their multiplicity is decided by the symmetry of the porphyrin and the nature of substituents in the meso position.

The pyrrolic nitrogen protons are around -2ppm. These protons are exchangeable and produce a broad signal **(Iovine *et al*., 2000)**.

Due to the aromatic character of the porphyrin core, the protons of the core are inducted into an extremely strong shielding cone. The ring current produced by the magnetic field induces a large cone of magnetic anisotropy with its axis perpendicular to the macrocycle plane. Thus the

protons inside this cone (pyrrolic nitrogens H) are shielded to about 3ppm while the portons outside this cone (H. β.pyrrolic) are strongly deshielded **(Goff and Shimomura, 1980)**.

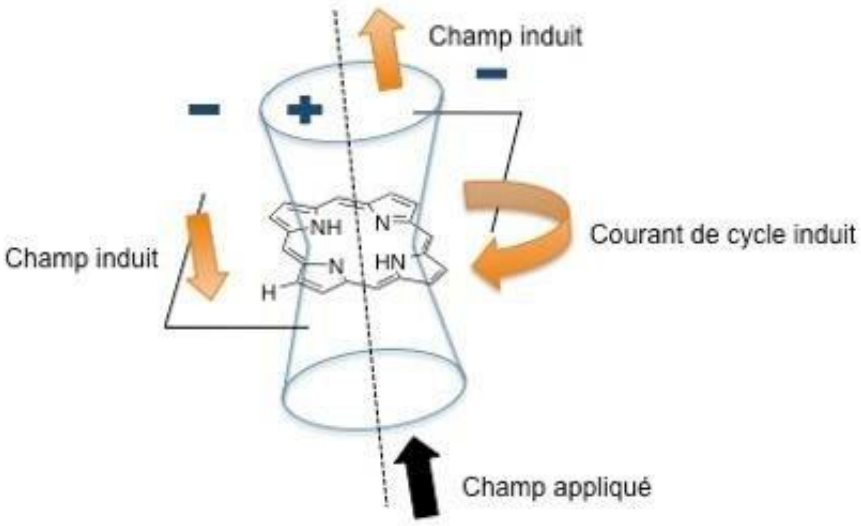

Figure 03: Anisotropy magnetic cone of a porphyrin**.**

The 1H NMR of porphine (unsubstituted porphyrin) is a triplet of three singlets at -3.76, 9.74, and 10.50 ppm **(Goff and Shimomura, 1980)**. They respectively refer to the nitrogen-bound protons, the β-pyrrolic protons, and methine protons (meso position). These latter are bound by carbons that are, in fact, electron-deficient and thus deshielded more than β-pyrrolic protons. Also, the uniqueness of the β-pyrrolic proton signals is explained via tautomerism of the internal NH protons. **(Craig, 1999)**, (Figure 04).

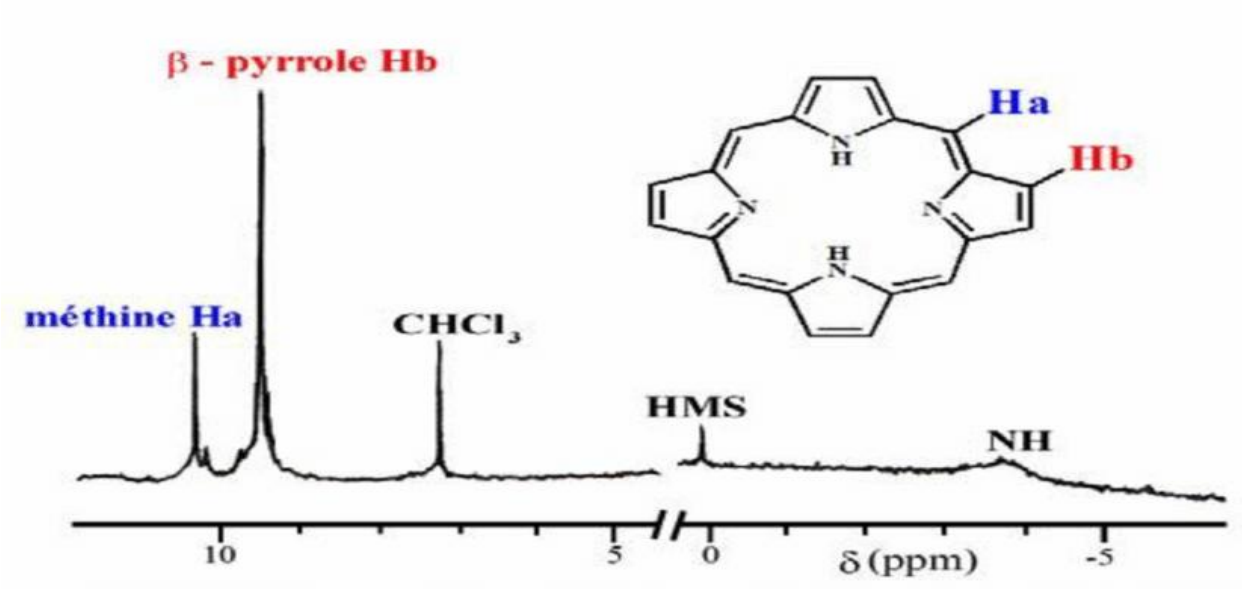

Figure 04: 1H NMR spectrum of porphyrin in CHCl3**.**

I.1.2.1.2. Carbon-13 NMR Spectroscopy (^{13}C NMR)

The ^{13} C NMR of the porphyrin could be distinguished into three distinct regions: alpha pyrrolic, betapyrrolic, and meso carbons. In the first two classes, alpha, and beta, there is a problem in identifying clearly their respective peaks due to NH tautomerism. These are more separated at low temperatures since NH tautomerism is sluggish when temperature is low.

Generally, alpha carbons have occurred at about 145 ppm. Moreover, there is a relatively unbroken chemical substance change (about 17 ppm) variation among your alpha carbon markers. Beta carbons, on the other hand, have shown up at about 130 ppm. The chemical substance shift variation among your beta carbons is smaller than in the case if there is alpha. It is between 5.3 and 6.9 ppm. For meso carbons, they are usually between 95 to 120 ppm.If porphyrin primary is metallated, the alpha and beta carbons' markers will be upshifted. In contrast, meso carbons show downfield shifts **(Whitlock and Bower, 1965)**.

I.1.2.2. UV-Visible Spectroscopy

In the UV-visible spectrum of porphyrins, it is possible to distinguish two types of absorption bands, which are caused by various electronic transitions. Porphyrins contain a widespread system of conjugated p-electrons **(Gouterman, 1961)**, which causes their absorption in the visible region and the formation of a characteristic pattern of absorption. This is due to transitions: $p \rightarrow p^*$, with a single strong band (with an extinction coefficient of more than 100000 L.mol-1.cm-1) in the range 390 to 430 nm (near UV), the Soret band or B band **(Krausz and Giannotti, 1983)**, and four additional bands in the range 480 to 700 nm (Visible). These latter bands all have intensities ten to twenty-fold weaker and are called Q bands.

The visible spectrum, which is in general structure-change sensitive, gives information regarding macrocycle substituents. Specifically, the four Q bands, numbered from I to IV with increasing energy, exhibit marked relative intensity changes as a function of both the nature and the position of the substituent **(Kobata *et al.*, 2007)**.

These are essentially four in type, which are etio, rhodo, oxorhodo, and phyllo.

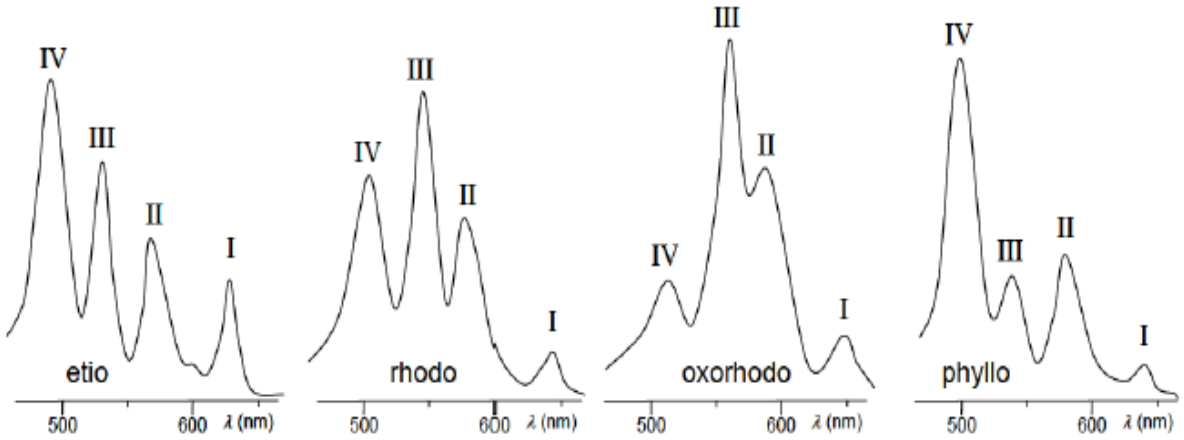

Figure 05: Different Q bands of free base porphyrins**.**

I.1.2.3. Cyclic Voltammetry

The electrochemical properties of porphyrin depend on whether it is in its free base or metal form, macrocycle substitution, and the solvent in which the investigation is conducted. Tetraphenyl porphyrin (TPP) is the most investigated porphyrin.

The electrochemical investigation of free-base porphyrins typically shows two single-electron oxidation steps and two to four single-electron reduction steps **(Clack and Hush, 1965; Felton and Linschitz, 1966; Wopschall and Shain, 1967; Furhop *et al*., 1973)**. The initial oxidation of the porphyrin results in the formation of a radical cation **(Wolberg and Manassen, 1970)**, which is further transformed into a dication at the second step of oxidation of the macrocycle. In the reduction

process, first an anion radical is generated, followed by the formation of a di-anion after the first two reduction steps. Notably, the electrochemical reduction of TPP shows that the third and fourth steps of porphyrin reduction are more complicated in nature **(Wilson and Peychal-Heiling, 1971; Dolphin *et al*., 1970)**.

The cation radicals generated by one-electron oxidation of free base porphyrins in the first step are found to be highly reactive and lead to protonation of the porphyrin **(Inisan *et al*., 1998)**.

Yves Le Mest and colleagues published a putative mechanism for TPP protonation through oxidation in 1998 (Scheme 1). For TPP, the monoprotonated form is demonstrated to be

unstable. Therefore, the deprotonation product is received following the elimination of two-electron equivalents. The hydrogen radicals are most likely from the solvent used.

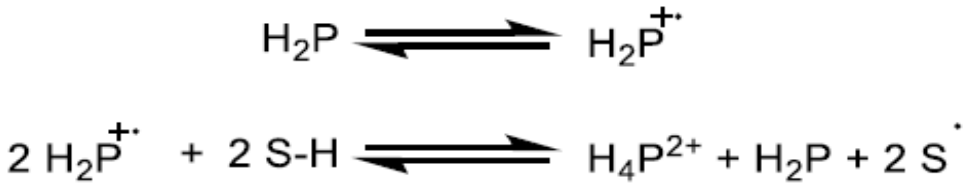

Schema I.1. Proposed mechanisms for the protonation of TPP during their first-stage oxidation.

For non-electroactive metal cation metallated metalloporphyrins, e.g., those metallated by Zn(II) or Mg(II), the redox behavior observed from cyclic voltammetry is identical with free base porphyrins. The metal influences the oxidation and reduction potential of the macrocycles primarily. These potential values directly relate to the electronegativity of the metal utilized within the metalloporphyrin **(Kadish and Van Caemelbecke, 2003)**. The higher the electronegativity of the metal of the metalloporphyrin, the easier the oxidation, and the harder the reduction process **(Brisach-Wittmeyer *et al*., 2005)**.

In the 1970s, Fuhrhop and co-workers asserted that the potential difference between the first oxidation and first reduction of a porphyrin (Δ|Red1-Ox1|) is 2.25 ± 0.15 V. Furthermore, they demonstrated that porphyrin's first and second oxidations are always distinguished by a potential difference of approximately 0.3 ± 0.1 V (Δ|Ox2-Ox1|), and that the first and second reductions of the macrocycle are distinguished by approximately 0.4 ± 0.1 V (Δ|Red2-Red1|) **(Furhop *et al*., 1973)** (Figure 06). It must be noted that these findings hold only for porphyrins containing a non-electroactive metal cation in the center.

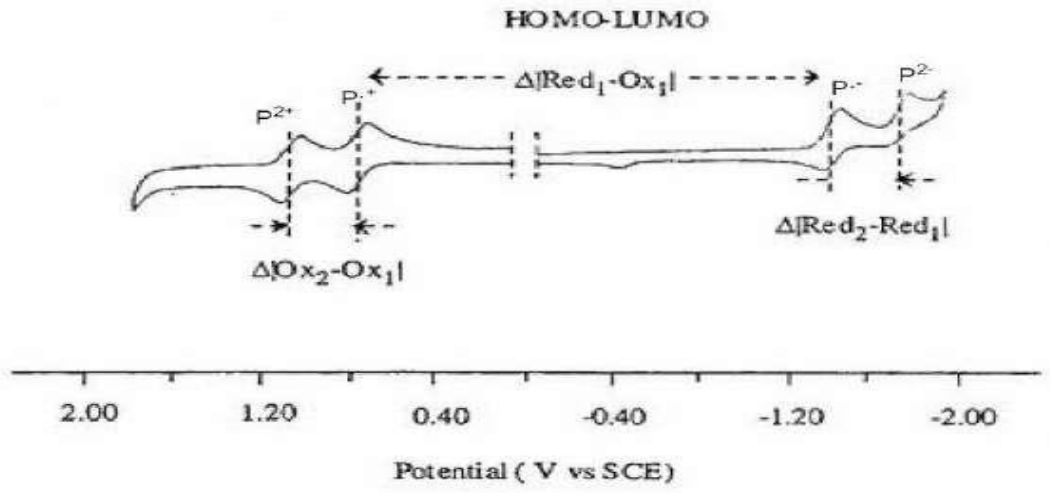

Figure 06: Cyclic voltammetry of TPP in CH2Cl2.

I.1.3. Description of porphyrin synthesis pathways

Porphyrins are obtainable by condensation of pyrrole with an aldehyde and acid and an oxidant (Rothemund procedure). Preparation of porphyrins which are substituted in the meso or the β position of porphine and specifically the formation of porphyrins have been the target of a huge amount of research work.

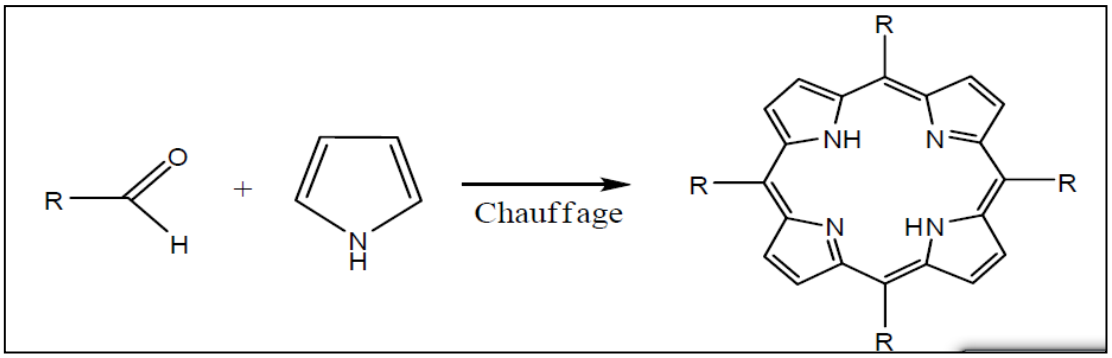

Figure 07: Method of Rothemund**.**

TPP is the most investigated porphyrin. Its synthesis, as illustrated by Adler and Longo in 1967, is directed by several factors like medium acidity, solvent, reaction temperature, oxygen availability, and concentration of initial reagents. Through the realization of various studies, the optimal synthesis procedure was defined: condensing four equivalents of pyrroles with benzaldehyde at reflux in propionic acid (141°C) to yield TPP in ca. 20% yields in crystalline

form and with reproducibility **(Rothemund and Menotti, 1941; Adler *et al.*, 1964; Adler *et al.*, 1967; Dolphin, 1970)**.

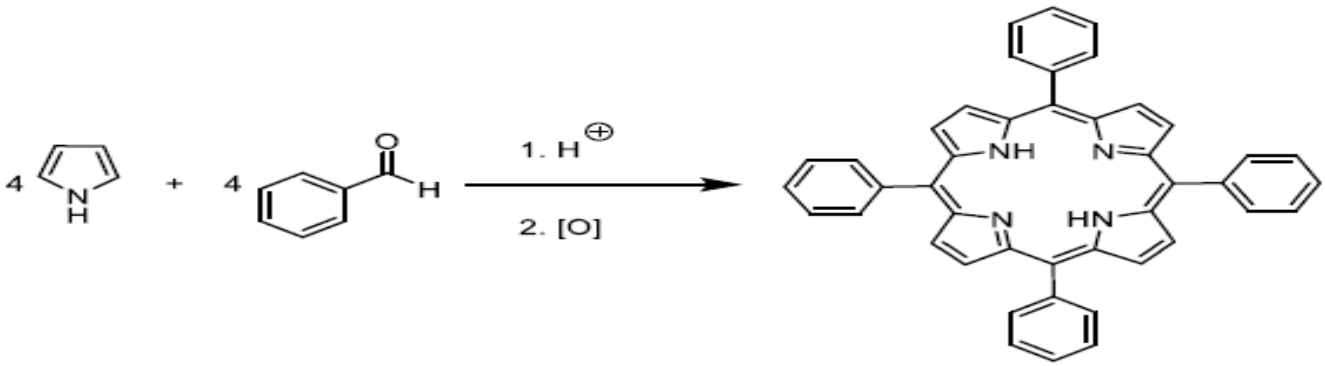

Figure 08: Method of Adler and Longo**.**

Lindsey and co-authors also helped to optimize the procedure of Adler and Longo **(Lindsey and Wagner, 1989; Geier and Lindsey, 1999; Feng and Senge, 2000; Geier *et al.*, 2001)**. Pyrrole is condensed with the aldehyde in a chlorinated solvent (chloroform or dichloromethane) in the presence of a catalytic amount of trifluoroacetic acid (TFA) or BF3·(Et)2O at room temperature. The resulting porphyrinogen is oxidized with an oxidant such as 2,3-dichloro-5,6-dicyano-1,4-benzoquinone (DDQ) to give meso-tetrasubstituted porphyrins, yield 30% to 40%.

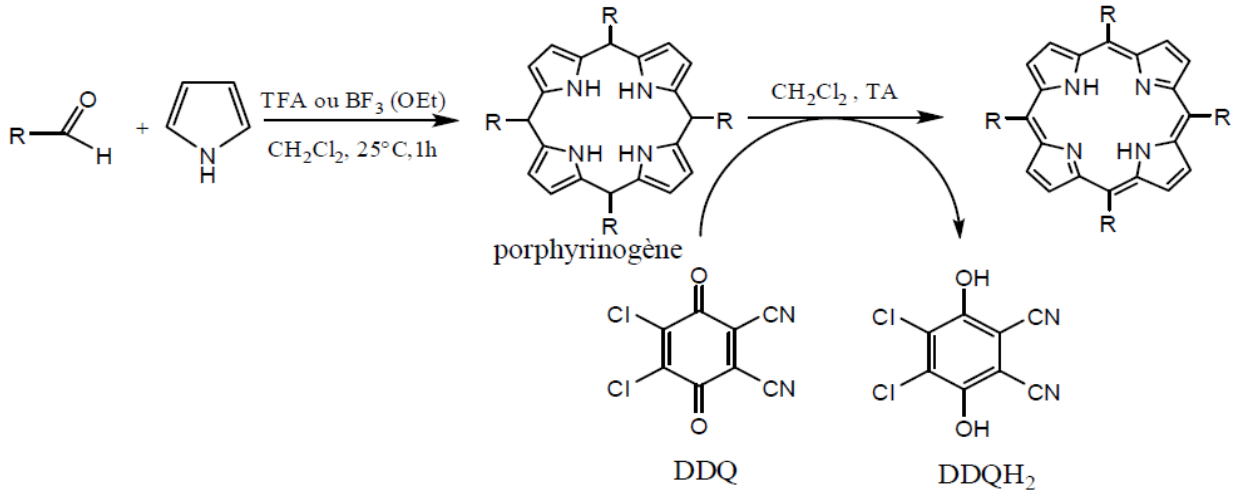

Figure 09: Method of Lindsey**.**

MacDonald describes a more targeted synthesis route in three stages **(Markonac and MacDonald, 1965)**, as illustrated in (Figure 10).The first step of the synthesis involves dipyrromethane, which is produced from the reaction of an aldehyde with an excess of pyrrole. Alternatively, it is possible to use multiple aldehydes and dipyrromethanes in the same so-called [2+2] condensation reaction by MacDonald **(Lindsey, 2010)**.

The main drawback of this type of condensation is the formation of statistical mixtures of isomers, which can prove challenging to separate and inevitably reduce yields if only one of the isomers is desired **(Smith, 1975)**.

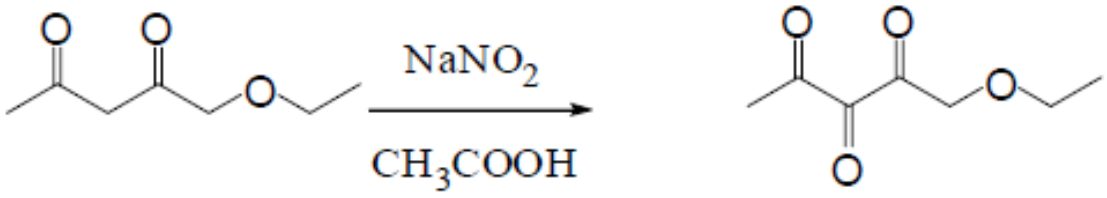

Figure 10: Method Mac Donald**.**

The introduction of functional groups at the β-pyrrolic positions is usually achieved through the synthesis of pre-functionalized pyrrolic intermediates. These intermediates are basic pyrroles, referred to as dipyrromethanes, and more complex structures like a,c-diladienes, which are oligomeric species of four pyrroles. Through systematic introduction of different functional moieties under controlled conditions, porphyrin derivatives can be derivatized.

One of the major synthesis pathways is the Knorr process that yields highly functionalized pyrroles from simple precursors **(Tamez Jr, 2006)**. Knorr's process, initially described in 1884, involves the stoichiometric condensation of ethyl acetoacetate with an oxime generated by treatment with sodium nitrite and then reduced by zinc in glacial acetic acid.(Figure 11)

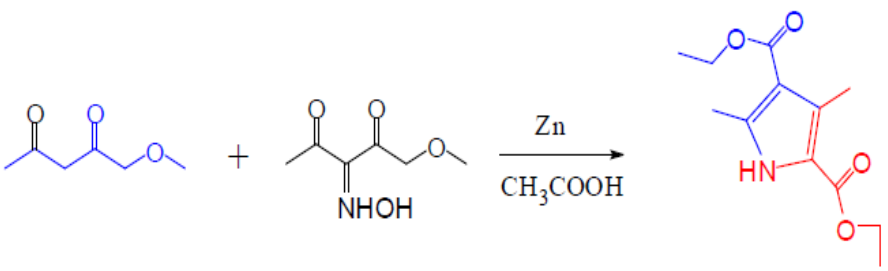

Figure 11: Method of Knorr**.**

Another significant pyrrole synthesizing process is the Barton-Zard process. The process is based on the use of a nitroacetate, which, upon removal of its acetate group by a base, gives a nitroalkane. It is then treated with an isocyanoacetate derivative to yield a cyclized product, which, upon removal of the nitro NO2 group, yields the desired pyrrole **(Bacton and Zard, 1935)**.

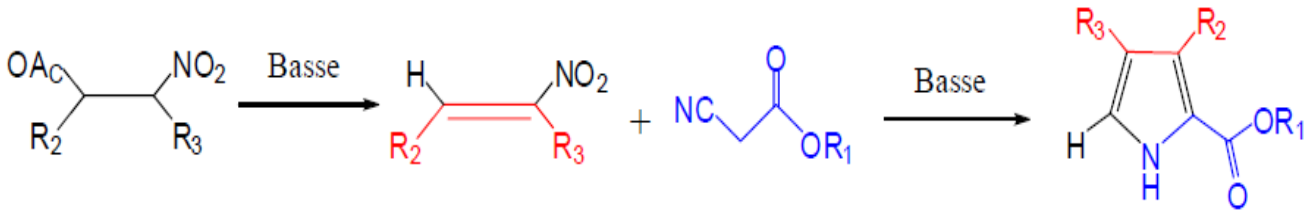

Figure 12: Method of Barton-Zard**.**

Chapter two

Inflammation

II.1.3. Inflammation

II.1. Definition

Inflammation is a complex biological response of the body's tissues to harmful stimuli, such as pathogens, damaged cells, or irritants. It is a protective mechanism that involves immune cells, blood vessels, and molecular mediators. The primary purpose of inflammation is to eliminate the initial cause of cell injury, clear out necrotic cells and tissues damaged from the original insult and the inflammatory process, and to initiate tissue repair. The cardinal signs of inflammation include redness, heat, swelling, pain, and loss of function, which are the result of increased blood flow, vascular permeability, and leukocyte recruitment to the site of injury or infection **(Soares *et al*., 2023).**

The inflammatory process is orchestrated by a variety of chemical mediators, including cytokines, chemokines, the kinin system, free radicals, nitric oxide, histamine, cell adhesion molecules, leukotrienes, prostaglandins, and the complement system. These mediators play crucial roles in the pathogenesis, diagnosis, and therapy of inflammatory diseases. They are responsible for the physiological changes that occur during inflammation, such as the dilation of blood vessels, increased permeability of the capillaries, and the migration of immune cells to the affected area **(Soares *et al*., 2023).**

II.2. Type of inflammation

Inflammation can be divided into three types based on the duration of the process that responds to the injurious cause; acute, which occurs immediately after injury and lasts a few days; chronic, which can last for months or even years if the acute inflammation does not resolve; and subacute, which is a transition period from acute to chronic that lasts from 2 to 6 weeks. **(Chen *and al*., 2018).**

II.2.1. Acute inflammation

Acute inflammation describes an immediate, adaptive, and relatively nonspecific response to numerous noxious stimuli. The name you see here (derived from Latin “acutus”) means “sharp” so it identifies this process.

The condition starts very quickly with sudden onset beyond which it continues for limited time. The time span of this process lasts several hours or multiple days according to the research of **(Damjanov, 2008).**

Soluble mediators including cytokines together with acute phase proteins and chemokines emerge after an acute injury to trigger acute inflammation. The mediators bring neutrophils and macrophages at the site while neutrophils stand as the predominant inflammatory cell type in all acute inflammatory reactions. The technique activates blood vessel expansion at the affected site which enhances bloodstream delivery to show symptoms including redness along with heat. The affected tissue experiences enhanced permeability of blood vessels as a result which enables extracellular fluid to enter the interstitial space leading to edema development. After the release of these mediators more inflammatory cells arrive at the site creating pain symptoms along with functional limitation **(Chen *and al*., 2018).**

Controlled acute inflammation provides beneficial effects because the body uses it as a defense mechanism against disease-causing microorganisms. The failure to control this process leads to severe negative results which septic shock **(Chen *and al*., 2018)** demonstrates. Chronic inflammation may develop from the response when neutrophil recruitment fails to eliminate the triggering adverse factor in some situations. **(Fleit, 2014)** (Figure 13)**.**

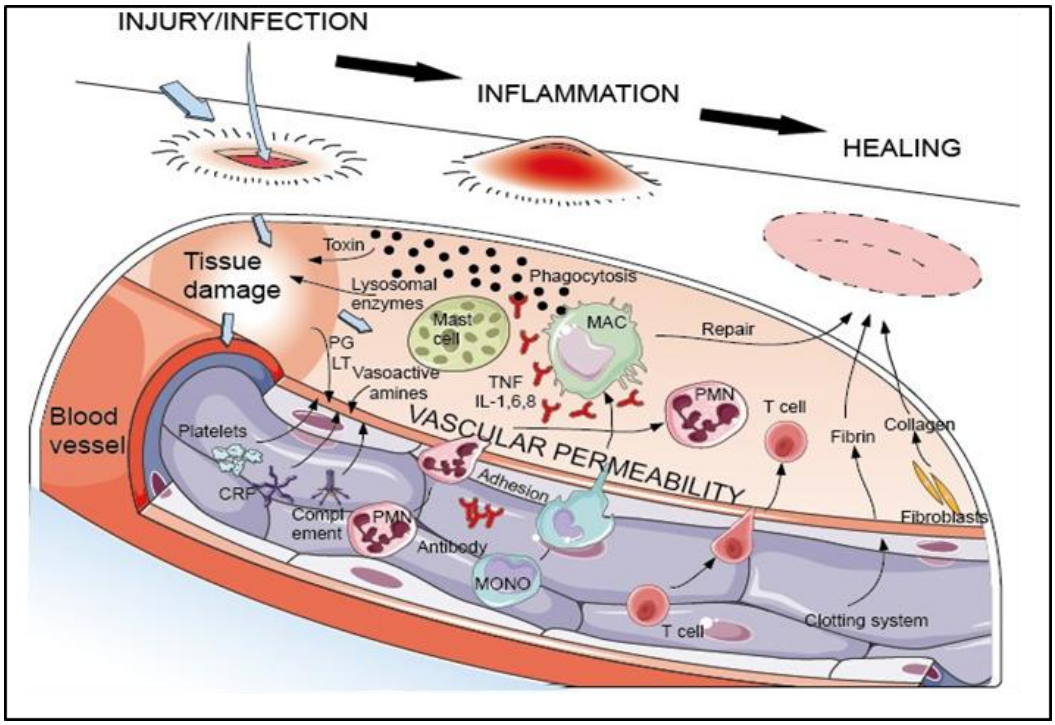

Figure 13: Cells and molecular mediators involved in acute inflammation **(Damjanov, 2008).**

II.2.2. Chronic inflammation

The inflammatory reaction known as chronic inflammation persists through time (chronos in Greek) after an inflammatory trigger where mononuclear leukocytes including lymphocytes and monocytes continually enter the affected tissue. Long-term inflammatory responses persist for extensive time intervals.

The duration of the inflammatory process spans multiple months through years to permanent timescales according to the nature of diseases such as atherosclerosis or autoimmune diseases or cancers or neurodegenerative diseases **(Damjanov, 2008).**

During chronic inflammation neutrophil circulation to tissue ends while tissue cells of monocyte and T lymphocyte lineage repeatedly enter the affected areas. The body transforms monocytes into macrophages upon their exit from blood circulation. The accumulation of macrophages together with lymphocytes in chronic inflammation promotes the increase of fibroblasts which ultimately results in organ malfunction **(Fleit, 2014).**

Table 01: Acute VS Chronic inflammation **(Šoltés *and al*., 2010).**

Inflammation	**Acute**	**Chronic**
Causative agent	Pathogens, injured tissues	Persistent acute inflammation due to non-degradable pathogens, persistent foreign bodies, or autoimmune reactions
Major cells involved	Neutrophils, mononuclear cells (monocytes, macrophages)	Mononuclear cells (monocytes, macrophages, lymphocytes, plasma cells, fibroblasts)
Primary mediators	Vasoactive amines, eicosanoids	INF- γ and other cytokines, growth factors, reactive oxygen species, hydrolytic enzymes
Onset	Immediate	Delayed
Duration	Few days	Up to many months or years
Outcomes	Resolution, abscess formation, chronic inflammation	Tissue destruction, fibrosis

II.3. Mediators of inflammation

The inflammatory response receives active mediation and regulatory power through chemical elements originating from circulation system components as well as inflammatory cells and damaged tissue. A mediator exists as a significant chemical element which supports the inflammatory reaction through essential functions **(Abdulkhaleq *et al*., 2018).**

II.3.1. Cellular component

The cellular aspect includes leukocytes which move from blood circulation to the inflammation site through extravasation because these cells exist primarily in the blood system. Certain leukocytes function as phagocytes which perform active bacterial viral and cellular debris cell engulfment. Participating leukocytes utilize enzymatic granules to achieve the destruction of penetrating pathogens. The inflammatory process gains strength and keeps going because leukocytes produce inflammatory mediators during synthesis.

Acute inflammatory conditions are generally associated with granulocytes yet mononuclear cells which incorporate monocytes and lymphocytes become active during chronic inflammation.

The cell entities use dynamic contact with soluble inflammatory mediators to set off immune responses which eliminate pathogens while fostering tissue repair conditions **(Serhan *et al*., 2005).**

II.3.2. Soluble Inflammatory Mediators

Inflammatory responses benefit from soluble proteins that function as essential agents to control the inflammatory process. The body contains soluble mediators in interstitial fluid together with blood which perform signaling roles to control every element of the inflammatory process. Cytokines and chemokines join the lipid mediators (prostaglandins and leukotrienes) alongside histamine and signal molecules which either promote or limit inflammation **(Serhan *et al*., 2005).**

The outcome of a specific immune response takes one of two forms: pro-inflammatory or anti-inflammatory along with cell-mediated or humoral characteristics depending on the initial cytokines generated to combat pathogens or tissue damage **(Shachar *et al*., 2013).**

The steady benefits from soluble mediators in inflammation resolution have shown that imbalanced cytokine and chemokine pathways drive multiple autoimmune pathologies **(Alvine *et al*., 2015).**

II.4. Biological markers of inflammation

II.4.1. C-reactive protein (CRP)

The discovery of C-reactive protein (CRP) occurred in 1930 at the infectious stage of illness through its polysaccharide C reaction which led to its naming as 'C-reactive protein'. The inflammatory glycoprotein functions as an acute inflammation-reflector. The rapid increase in CRP concentration makes it an early sign of the inflammatory response that develops quickly. The liver cell-derived protein serves as an antigen-activator because it triggers the complement pathway **(Le Gall *et al*., 2011).**

CRP characteristics:

- ✓ 6 to 8 hours half-life.
- ✓ At the physiological level CRP exists from below 4 to 6 mg/L (in rats).
- ✓ The inflammation process activates CRP from the point of the 6th hour onward.

Inflammation begins following its initiation and reaches normalcy after the inflammatory source vanishes away. This process typically requires 24 consecutive hours. The concentration of CRP increases significantly up to 500 or 1000 folds when acute inflammation occurs. A physiological CRP concentration serves as an important indicator of treatment effectiveness **(Le Gall *and al*., 2011).**

II.4.2. Determination of Fibrinogen (Fib) or Factor I

Fibrinogen (Factor I) is a liver-produced plasma protein. It exists in blood plasma and levels increase in inflammatory states. By thrombin influence, fibrinogen is transformed into fibrin, an insoluble protein that clots blood **(Hanss, 2005)**. It is involved in clot formation. The protein demonstrates a relatively mild variation (from 200 to 400 times normal), with a response time greater than usual (12 to 14 hours) and a long half-life (2 to 6 days), its measurement in the blood can be used to diagnose a range of syndromes, namely acute inflammatory syndromes **(Hanss, 2005).**

II.4.3. Determination of Haptoglobin (Hp)

Haptoglobin (Hp) or α2-glycoprotein synthesized by the liver has the capacity to bind in a stable complex with haemoglobin released into the circulation. Haptoglobin is therefore not a 'transport' protein in the strict sense, but rather a form of 'capture' of normal haemoglobin to prevent its urinary excretion.

In the absence of in vivo haemolysis or a deficiency of hepatic synthesis, Elevated haptoglobin is an excellent marker of an inflammatory syndrome **(Robert,2013)**. In the inflammatory response, haptoglobin increases with the increase in orosomucoid (an α1 immunoglobulin).

II.4.4. Serum protein electrophoresis

Inflammation proteins are examined in the serum. This is a crude test which provides an overview of a patient's protein status. Electrophoretic separation of plasma proteins provides 5 fractions, all of which include proteins involved in inflammation mechanisms **(De Nadaï *and al*., 2014).**

- Hypoalbuminemia is found in severe inflammatory syndromes.
- The rise in fraction 1 is noted at the onset of an inflammatory process, and a rise in fraction 2 is indicative of an established inflammatory syndrome.
- Isolated rises in globulins are indicative of elevated transferrin levels in martial deficiency **(De Nadaï *and al*., 2014).**

Chapter three
Anti-inflammatory drugs

III. Anti-Inflammatory Drugs

III.1. General information

Anti-inflammatory therapy focuses on controlling the excessive production aspecific reaction of tissues and preventing the acute form of inflammation becoming chronic **(Muster, 2005)**. It is normally carried out by artificial non-steroidal or steroidal anti-inflammatory molecules (corticoids). They are widely employed, but their side effects are sometimes drastic, particularly toxicity on renal and gastrointestinal systems (digestive irritations that can even induce gastric ulceration) **(Trabsa, 2015).**

III.2. Steroidal anti-inflammatory drugs (SIAs)

III.2.1. Definition

Steroidal anti-inflammatory or glucocorticoids are synthetic molecules that are obtained from cortisone, a naturally occurring release by the adrenal glands. Steroidal anti-inflammatory or glucocorticoids are potent anti-inflammatory agents with immunomodulatory and anti-allergic activity **(Heymonet, 2013)**. All of them have a hormonal effect on the control of metabolism (carbohydrate, protein and lipid particularly) and calm down the adrenals through a braking effect through the hypothalamic-pituitary **(Muster, 2005).** In contrast to the non-steroidal anti-inflammatory drugs (NSAIDs), glucocorticoids may inhibit all components of the inflammatory response. By their direct action on the vessels, they reduce the vascular features of inflammation. By their antiproliferative effect on histiocytes-monocytes-macrophages of all types, lymphocytes, plasma cells, fibroblasts and neutrophils, they reduce the early and late cellular features of inflammation **(Muster, 2005).**

III.2.2. Mechanism of action

Corticoids have new mechanisms of action that are mainly genomic (Transcriptional) characterized by the activation (Transactivation) or inhibition (Trans-repression) of numerous target genes **(Mekenza and Medjmedj, 2018)**. These are mediated in most cells involved in innate immunity (macrophages, polymorphs, mast cells), adaptive immunity (lymphocytes) but also in other cells (fibroblasts, epithelial and endothelial cells) **(Muster, 2005).**

Glucocorticoids are carried by the transport proteins albumin and transcortin. They pass through cell membranes by diffusion. Inside the cytoplasm, they bind to a specific receptor that belongs to the superfamily of steroid receptors. After binding of glucocorticoid, the glucocorticoid-receptor complex migrates to the nucleus and directly acts on DNA by binding

to specific sequences referred to as GREs (glucocorticoid response elements), thereby modulating (activating or suppressing) the transcription of target genes **(Heymonet, 2013)**. This stimulates the synthesis of a protein, lipocortin, which suppresses phospholipase A2, thereby reducing the release of arachidonic acid from phospholipids of membranes and therefore the synthesis of inflammation mediators, prostaglandins and leukotrienes. Glucocorticoids also diminish the production of a chain of proteins important to inflammatory phenomena, including interleukins and other cytokines, phospholipase A2 and cyclooxygenase 2 **(Lùllmann *et al*., 1996).** Corticoids also regulate cell activation and survival (apoptosis), which is responsible for their cytostatic effectiveness in certain haematological tumours **(Muster, 2005).**

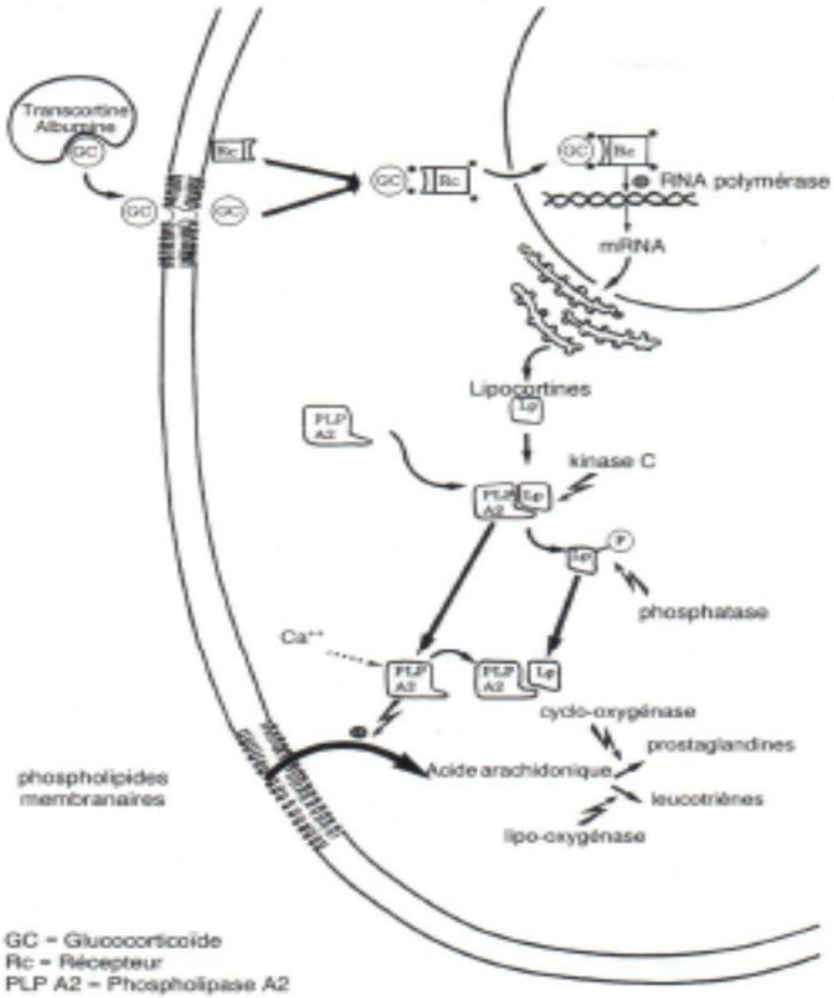

Figure 14: Mechanism of action of glucocorticoids **(Heymonet, 2013).**

III.2.3.Secondary effects

On brief administration, glucocorticoids even at high doses virtually have no side effects.

On long-term administration, they lead to a susceptibility to infection and interference with the healing process. Hyperactivity of glucocorticoids leads to:

- An increase in neoglucogenesis and release of glucose. Glucose is deposited as triglycerides (fat deposits: moon face and trunk thickening) due to the effect of insulin, and unless insulin release is enhanced sufficiently, 'steroid diabetes' is observed **(Lùllmann *et al*., 1996).**
- Increased breakdown of protein, skeletal muscle atrophy, osteoporosis, growth disturbances in children and skin atrophy. The mineralocorticoid action of cortisol has the following effects: retention of sodium and water, increase in blood pressure, oedema and potassium excretion with the possibility of hypokalaemia **(Lùllmann *et al*., 1996).**

III.3. Non-steroidal anti-inflammatory drugs (NSAIDs)

III.3.1.Definition

NSAIDs, unlike glucocorticoids, are a group of different synthetic chemical classes with a non-steroidal configuration **(Muster, 2005).** They are symptomatic drugs that may neutralize the inflammatory process, irrespective of etiology (mechanical, chemical, infectious, immunological), and are highly effective in pain and inflammation. Because of their characteristics, this therapeutic class is one of the most widely used in the world (4.5% of drug use in industrialised nations) **(Taïba *et al*., 2017)**. However, they are infamous for a number of negative effects, including gastrointestinal bleeding, cardiovascular and nephrotoxic side effects **(Wongrakpanich *et al*., 2018).**

III.3.2.Mechanism of action

Phospholipase A2 activation during inflammation results in membrane phospholipid breakdown to arachidonic acid that COX enzymes turn into prostaglandins (PGs) **(Neant, 2017)**. The inflammation process gets interrupted through the use of non-steroidal anti-inflammatory drugs which stop the production of cyclooxygenase to block prostaglandin formation. The enzyme-blocking effect shows either positive or adverse results according to a patient's medical state. The pain relieving properties along with the anti-inflammatory and antipyretic effects constitute the beneficial therapeutic effects. The therapeutic effect of

NSAIDs leads to stomach ulceration through their preventive action toward other prostaglandins that defend gastric mucosa. The inhibition of type I cyclooxygenases leads to almost all peptic ulceration and bleeding in the gut. The inhibition ability of NSAIDs on selective COX-2 activity matches the non-selective NSAIDs efficiency in treating inflammation and pain with lower rates of gastrointestinal side effects at the prescribed doses **(Heymonet, 2013).**

III.3.3.Secondary effects

The side effects of ANIS may be a result of inhibition of prostaglandin synthesis or diversion of arachidonic acid metabolism away from the cyclooxygenase pathway, i.e., to the lipo-oxygenase pathway.

Gastroduodenal effects: Prostaglandins play a protective role in the gastric mucosa, increasing the secretion of mucus and gastric blood perfusion and blocking the production of free radicals, except in the case of chronic NSAID use, when dyspepsia and peptic ulcers occur.

Renal effects: Renovascular effects: oedema due to sodium water retention, oliguria due to acute renal failure **(Annick, 2018).**

Cutaneous presentations: exfoliative dermatitis, Lyell and Stevens-Johnson syndromes. Various rashes and urticaria along with photosensitization affect patients who consume ketoprofen topical medication **(Sivry, 2014).**

The usage of propoxyphene can lead to hypertension resistance and hypertension relapse and congestive heart failure and it increases the risk of thrombotic artery issues when exposure exceeds standard durations or when using elevated doses **(Gungomer, 2015).**

Second part

Experimental

Chapter one
Materials and methods

I.1. Introduction

This study was carried out in collaboration with two specialist laboratories: the Laboratoire de Valorisation et Technologie des Ressources Sahariennes (VTRS) of the Faculté des Sciences Exactes, Département de Chimie, Université d'El Oued, and the Centre de Recherche Scientifique et Technique en Analyses Physico-Chimique (CRAPC) in Ouargla, Algeria. The VTRS laboratory facilitated the in vitro and *in silico* extraction of porphyrins. At the same time, the CRAPC carried out the precise GC/MS analysis of the extracted porphyrins. This collaborative effort enabled in-depth and precise experiments to be carried out, combining the expertise and resources of both institutions.

I.2. *Chemicals* and Reagents

- Bovine serum albumin (BSA, 5% w/v) from Sigma-Aldrich
- deionized water Plant extracts (0.1–1 mg/mL)
- AgO-NPs and ZnO-NPs
- Diclofenac sodium (positive control, anti-inflammatory drug)
- Deionized **water** – H_2O
- Diclofenac **sodium** – $C_{14}H_{10}Cl_2NNaO_2$
- Dimethyl sulfoxide (DMSO) – C_2H_6OS
- Tris buffer (TBS) – Tris ($C_4H_{11}NO_3$) + NaCl (Sodium chloride, NaCl)
- Coomassie Brilliant Blue G-250 – $C_{45}H_{44}N_3NaO_7S_2$
- Ethanol – C_2H_6O
- Phosphoric acid – H_3PO_4
- Whatman filter paper – cellulose-based, no formula
- Butylated hydroxytoluene (BHT) – $C_{15}H_{24}O$
- Trichloroacetic acid (TCA) – CCl_3COOH
- Thiobarbituric acid (TBA) – $C_4H_4N_2O_2S$
- Hydrochloric acid (HCl) – HCl
- 5,5′-Dithiobis-(2-nitrobenzoic acid) (DTNB or Ellman's reagent) – $C_{14}H_8N_2O_8S_2$
- Sulphosalicylic acid – $C_7H_6O_6S$
- Ethylenediaminetetraacetic acid (EDTA) – $C_{10}H_{16}N_2O_8$
- Phosphate buffer – typically contains KH_2PO_4 and Na_2HPO_4
- Nitroblue tetrazolium (NBT) – $C_{40}H_{30}Cl_2N_{10}O_6$
- Riboflavin (Vitamin B2) – $C_{17}H_{20}N_4O_6$

- Hydrogen peroxide (H_2O_2) – H_2O_2

I.3. *In vivo* inflammatory activities

I.3.1. Animals care

The present study was conducted on the total of 35 adult male Albino Wister rats, each weighing 120-150 grams, supplied by the Pasteur Institute in Algiers. The rats were conditioned for 16 days under the conditions of the animal house, which were maintained at a temperature of 25°C, 62% humidity, and a photoperiod of 12 hours light and 12 hours darkness. The animals were treated as per the guidelines laid down in the Guide for the Care and Use of Experimental Animals **(Albus, 2012)**. Polypropylene cages employed in this case are 50 x 35 x 20 cm and are subdivided into five rats per cage. The rats have free access to food and water. The cages are also covered with sawdust and are cleaned every two days until the termination of the experiment. The animals were fed routine food according to **(Southon *et al* 1984)**. Tap water was provided throughout the experiment for drinking.

I.3.2. Experimental process

The rats were acclimatized for 16 days and then separated into seven experimental groups of five rats per group. Each group was subjected to a different treatment schedule, as will be outlined in the subsequent sections:

- **Group 01 (control):** The control group was given normal drinking water and food throughout the experiment.
- **Group 02 (GLY):** These rats in this experiment received a normal food and drinking water that had also been mixxed with Glyphosate at a dose of 50 mg/kg for 33 days. Then we return pure water to them for 8 days
- **Group 03 (GLY+IBU):** These rats in this experiment received a normal food and drinking water that had also been mixxed with Glyphosate at a dose of 50 mg/kg for 33 days. Following this, By force-feeding, each rats received one milliliter of the IBU at a dose of 2 mg/kg over 8 days.
- **Group 04 (GLY+ *$NiTPPH_2$*):** These rats in this experiment received a normal food and drinking water that had also been mixxed with Glyphosate at a dose of 0.005% for 33

days. Following this, By force-feeding, each rats received one milliliter of the *$NiTPPH_2$* at a dose of 1ug/kg over 8 days.

- **Group 05 (GLY+ *$TbiPPH_2$*):** These rats in this experiment received a normal food and drinking water that had also been mixxed with Glyphosate at a dose of 50 mg/kg for 33 days. Following this, By force-feeding, each rats received one milliliter of the *$TbiPPH_2$* at a dose of 1ug/kg over 8 days.
- **Group 06 (GLY+ *$TPPH_2$(o-methyl)*):** These rats in this experiment received a normal food and drinking water that had also been mixxed with Glyphosate at a dose of 50 mg/kg for 33 days. Following this, By force-feeding, each rats received one milliliter of the *$TPPH_2$(o-methyl)*at a dose of 1ug/kg over 8 days.
- **Group 07 (GLY+*$ZnTPPH_2$*):** These rats in this experiment received a normal food and drinking water that had also been mixxed with Glyphosate at a dose of 50 mg/kg for 33 days. Following this, By force-feeding, each rats received one milliliter of the *$ZnTPPH_2$* at a dose of 1ug/kg over 8 days.

I.3.2.1. Relative Organ Weight (ROW)

Relative liver, kidney, and brain Weight

The liver, kidneys, and brain were carefully excised and weighed immediately after sacrifice. The relative organ weight (ROW) was calculated using the following formula:

Relative Organ Weight (ROW) = (Organ weight/final body weight) ×100

I.3.3. Methods of blood analysis

I.3.3.1. Hematological parameters assay

The hematological parameters (leucocytes (WBC), lymphocytes (LYM), granulocytes (GRA), erythrocytes (RBC), hemoglobin (HGB) and platelets (PLT)) are determined by the Coulter method using the Medonic type auto hematology analyzer specific to Complete Blood Count (CBC).

I.3.3.2. Biochemical parameters assay

Blood glucose

Beta-D-glucose in plasma is oxidised by glucose oxidase to D-glucono-1,5-lactone, producing hydrogen peroxide; the lactone is then slowly hydrolysed to D-gluconic acid. A peroxidase enzyme then converts the hydrogen peroxide to oxygen and water. The oxygen then reacts with an oxygen acceptor to form a coloured molecule, the concentration of which can be determined colorimetrically**. (Trinder, 1969).**

$$\text{Glucose} + \textbf{glucose oxidase} + O_2 \rightarrow \text{Gluconic Acid} + \mathbf{H_2O_2}$$

$$\mathbf{H_2O_2} + \text{Peroxidase} + \text{Oxygen acceptor (Colourless)} \rightarrow \text{H.O} + \text{Oxidised acceptor (}\mathbf{Coloured}\text{)}$$

C- reactive protein

The concentration of C-reactive protein (CRP) in the serum sample was determined by means of the turbidimetric method on a COBAS INTEGRA 400 analyser. The efficient monospecific antibody-based equilibrium turbidimetric immunoassay for blood C-reactive protein (CRP) employs polyethylene glycol-6000 to accelerate and enhance the immunoprecipitation reaction, and Tween-20 surfactant to reduce and stabilise the sample blank values **(Otsuji *et al*., 1982)**.

$$\text{Aspartate} + \text{2-Oxoglutarate} \xrightarrow{\text{AST}} \text{Oxalacetate} + \text{Glutamate}$$
$$\text{Oxalacetate} + \text{NADH} + \text{H}^+ \xrightarrow{\text{MDH}} \text{Lactate} + \text{NAD} +$$

Aspartate transaminase

In accordance with an enzymatic kinetic, the spectrophotometer measured the activity of the AST. The production of glutamate and oxaloacetate is catalysed by aspartate aminotransferase (AST), otherwise known as glutamate oxaloacetate-transaminase (GOT). This enzyme facilitates the transfer of an amino group from aspartate to -ketoglutarate. Malate dehydrogenase (MDH) and NADH are responsible for the conversion of oxaloacetate to malate. The rate of reduction in NADH content has been shown to be closely correlated with aspartate aminotransferase activity in the sample. As demonstrated by **Schumann *et al*. (2010),** spectrophotometric analysis is employed to facilitate the measurement of wavelengths of 340 nm **(Schumann *et al*., 2010)**.

$$\text{Aspartate} + \text{2-Oxoglutarate} \xrightarrow{\text{AST}} \text{Oxalacetate} + \text{Glutamate}$$

$$\text{Oxalacetate} + \text{NADH+H+} \xrightarrow{\text{MDH}} \text{Lactate} + \text{NAD+}$$

Alanine transaminase

The measurement of ALT activity was carried out by the spectrophotometer following an enzymatic kinetic method. Alanine aminotransferase (ALT), also referred to as glutamate-pyruvate-transaminase, is classified as a transaminase (GPT). The process of amino group transfer from L-alanine to -ketoglutarate is catalysed by ALT, resulting in the production of L-glutamate and pyruvate. Lactate dehydrogenase (LDH) and NADH are the enzymes responsible for the conversion of pyruvate to lactate. The alanine transferase activity exhibited by the sample demonstrated a positive correlation with the NADH concentration. At a wavelength of 340 nm, spectrophotometry is utilised to take the measurement **(Schumann *et al*., 2010).**

$$\text{Alanine} + \text{2-Oxoglutarate} \xrightarrow{\text{ALT}} \text{Pyruvate} + \text{Glutamate}$$

$$\text{Pyruvate} + \text{NADH} + \text{H} + \xrightarrow{\text{LDH}} \text{Lactate} + \text{NAD} +$$

I.3.4. Determination of oxidative stress parameters

I.3.4.1. Preparation of homogenates

One gram of tissue (liver, kidney, and testis) from each rat in the various experimental groups was utilised. Following a grinding and homogenising process of the tissues in TBS (50 mM Tris, 150 mM NaCl, pH 7.4), the cell suspension is subjected to a centrifugation process at 3000 rpm for a duration of 15 minutes. The resulting sample is then stored at 4°C for the subsequent analysis of oxidative stress parameters.

I.3.4.2. Determination of protein level

The Bradford method was utilised to spectrophotometrically measure the protein content of the extracts, with bovine serum albumin serving as a reference standard **(Bradford, 1976).** A quantity of 100 mg of Coomassie Brilliant Blue was dissolved in 50 ml of ethanol, thus producing the Bradford Reagent. This solution was then subjected to vigorous agitation for a period of two hours using an agitator. Subsequently, 850 millilitres of water and 100 millilitres of phosphoric acid should be incorporated to yield a solution of 1 litre. The utilisation of Whatman filter paper as a medium for the filtration of the Reagent is a notable observation. The homogenate and the standard were added to 2 ml of Bradford Reagent in tubes, which were then placed

in a dark environment, with a volume of 40 µl of each substance. Following a five-minute incubation period, the absorbances at 595 nm were measured. Protein concentrations are assessed by comparison to a standard range of bovine serum albumin carried out under identical conditions.

I.3.4.3. Determination of Malondialdehyde Level

The determination of malondialdehyde (MDA) level was conducted in accordance with the method originally described by **(Quintanilha, 1981).** Aliquots containing 1 ml of diluted homogenate mixed with 20 µl of 2% (w/v) ethanolic solution of BHT received 2 ml of MDA reagent (15% (w/v) trichloroacetic acid, 0.375% (w/v) thiobarbituric acid, and 0.25 N hydrochloric acid). The mixture was placed in a boiling water bath for 15 minutes, cooled, and then the precipitate was separated by centrifugation. Subsequently, the absorbances were determined at a wavelength of 532 nm. The concentration of MDA was expressed in nmol of MDA/mg protein.

$$MDA(\text{nmol/mg prot}) = \frac{OD \text{ sample} \times 10^6}{1 \times 1.56 \times 10^5 \times DF \times mg \text{ prot}}$$

Where: OD: Optical density at 532 nm, **1.56 x10^5 M^{-1} cm^{-1}**: Molar extinction coefficient of the MDA, **DF**: Dilution factor, **1**: Optical path length.

I.3.4.4. Determination of Reduced Glutathione Level

The GSH concentration is determined through the observation of a yellow colour that develops when 5,5′-Dithiobis-(2-nitrobenzoic acid) (DTNB) is added to compounds that contain sulfhydryl groups. The mixture of 0.8 ml tissue homogenate and 0.2 ml 0.25% sulphosalicylic acid was agitated, and then chilled at 4 °C for 15 minutes. Subsequently, the mixtures were subjected to a centrifugal process at a speed of 1000 revolutions per minute for a duration of 5 minutes. The final mixture comprised 0.5 ml of the upper layer, 1 ml of TBS (pH 7.4), and 0.025 ml of 0.01 M DTNB. Subsequently, the absorbances at 412 nm were measured after an interval of five minutes. The total GSH content was calculated as nmol GSH/mg protein, as previously described by Weckbecker and **(Cory, 1988).**

$$\text{GSH}\left(\frac{\text{nmol}}{mgprot}\right) = \frac{OD \times 10^6 \times 1.525}{13100 \times 0.8 \times 0.5 \times DF \times mg\ \text{prot}}$$

With: **1.525:** Total volume of solutions used in the GSH assay at the level of supernatant (0.5 ml, supernatant +1ml Tris + 0.025ml DTNB), **13100 M-1**: Molar extinction coefficient of -SH group at 412 nm, **0.8:** Volume of the homogenate, **0.5:** Volume of the supernatant, **DF**: Dilution factor.

I.3.4.5. Determination of Superoxide Dismutase Activity

The method of assaying SOD activity using NBT by the superoxide anion (O_·) is utilised as a basis for detecting the presence of SOD **(Beauchamp and Fridovich, 1971).** The following reagents are required: 500 µL of EDTA-Met, 900 µL of Phosphate Buffer (pH = 7.8), 25 µL of sample and 50 µL of NBT. The mixture is then placed in a water bath at 25°C for a period of five minutes. Following this, 25 µL of riboflavin is added to the mixture. The mixture is then exposed to light for a period of 20 minutes. The same steps are repeated for the control, with 0 µL of the sample replaced by the addition of 25 µL of buffer phosphate. The absorbances are then measured at a wavelength of 560 nm.

$$I\% = \frac{OD_c - OD_s}{OD_c} \times 100$$

With: **I%**: % inhibition of NBT reduction by SOD, **OD**c: Optical density of the control, **OD**s: Optical density of the sample.

And: The 50% inhibition is equal to 1 unit of enzyme. 50% inhibition = 1 unit of SOD, so the antioxidant activity of the enzyme equals SOD units / mg of pro.

I.3.4.6. Determination of Catalase Activity

The determination of catalase activity was conducted in accordance with the methodology established by **(Aebi, 1984).** The reaction was initiated by the mixing of 20ml of the upper layer with 780ml of a phosphate buffer solution (KH2PO4, 0.1M; pH 7.5) and 200µl of H2O2 (0.030M). The decrease in light absorption at a wavelength of 240 nanometres was measured at 30-second intervals for a period of two minutes, with the objective of monitoring the decomposition of H2O2. The enzymatic activity

was expressed in international units per minute and per gram of protein (IU/min/g of protein).

$$\text{Catalase } ((UI/\text{min})/g) = \frac{(2.3033/T) \times (\log\ A1/A2)}{DF \times g \text{ prot}}$$

Where*:* **A1**: Absorbance at the first minute, **A2**: Absorbance at the second minute, **T:** Time interval in minutes.

I.3.5. Histopathological study

For the histological study, fragments of the organs from all batches are taken. It is imperative that they are removed expeditiously in order to prevent autolysis, a process that occurs in the moments following the animal's demise. Following a thorough rinsing process with distilled water and 0.9% NaCl, the samples are then subjected to immediate immersion in a fixative solution comprising 10% formaldehyde **(Leclerc-Mercier *et al.*, 2016).** The technique employed comprises the following steps: the placement of the tissue samples in special cassettes with turned walls to allow the passage of liquids. Subsequently, the samples are dehydrated using an automatic device that facilitates the automated and progressive passage of the samples through ethanol baths of increasing concentration (70%, 95%, and 100%). Subsequently, the components are immersed in baths of liquid paraffin. The tissues are maintained and soaked in paraffin, and the embedding stage is then initiated. This stage involves the inclusion of the impregnated tissue in a block of paraffin, which, by solidifying, will allow it to be cut. The operation is characterised by the utilisation of "inclusion" devices, which facilitate the closure of a reservoir of paraffin maintained in a liquid state by a heating system, a small tap, and a refrigerated metal plate. This process enables the rapid solidification of the paraffin block containing the tissue. The production of thin sections of a few microns (5 µm on average) is possible thanks to specialised devices known as "microtomes". These sections are then spread on microscope slides, smoothed, and fixed on the slide by the application of heated gelatinous water. The staining technique employed in this study involves the use of hematoxylin-eosin, also known as hematein-eosin, as described by **(Elmalti *et al.* 2007).** This method necessitates the preparation of an acid alcohol solution, comprising 100 ml of 70% ethyl alcohol and 50 ml of HCl acid, as well as ammoniacal water, consisting of 100 ml of distilled water and 2 ml of ammonia. The staining

process further requires an eosin solution, which consists of 100 ml of 3% aqueous eosin, 125 ml of 95% ethyl alcohol, 375 ml of distilled water, and 2 drops of acetic acid. The staining procedure is outlined below:

Initially, deparaffinization and hydration of the slides is conducted using tap water. This is followed by rinsing with distilled water. Subsequently, the samples are immersed in a Harris hematoxylin bath for a period of 15 minutes. This process results in the colouration of the basophilic structures (nuclei) with a purplish hue. The blades are immersed in acid alcohol (1 to 2 dives); then in a tap water bath, with verification of the differentiation under the microscope. The first step in the procedure is to place the sample in an ammoniacal water bath. This is then followed by the addition of the sample to an eosin bath, where it is left for a period of between 15 seconds and 2 minutes. The result of this process is the colouring of the acidophilic structures (cytoplasm) of the sample a pink hue. It is notable that all of these baths are separated by tap water washes. Finally, the preparations were subjected to microscopic observation. This entailed the drying of the preparations, followed by their observation under an optical microscope. Photographic documentation was then undertaken using a camera **(Bremond-Gignac *et al*., 2004).**

I.4. *In Vitro* Bioassays

I.4.1. Equipment and Apparatus

- A Shimadzu UV-1800 spectrophotometer equipped with a 96-well microplate adapter was used for absorbance measurements.
- Micropipettes (1–1000 µL) – for accurate liquid handling
- Analytical balance – for precise weighing of chemicals and extracts
- Incubator (25°C, dark conditions) – for controlled reactions
- Water bath (70°C) – used in the BSA denaturation assay

I.4.2. Anti-inflammatory Activity

I.4.2.1. Bovine Serum Albumin (BSA) Denaturation Assay

Overview

Protein denaturation is a key event in the progression of inflammatory disorders **(Farooq et al., 2025)**, making the BSA denaturation assay a valuable model for evaluating anti-inflammatory activity **(Smati et al., 2025)**. This study investigates the ability of *$NiTPPH_2$*, *$TbiPPH_2$*,

$TPPH_2$(o-methyl), and *$ZnTPPH_2$* to inhibit protein denaturation, suggesting their potential therapeutic relevance in inflammation-related diseases.

Procedure

In the present study, the assay was conducted following established methodologies **(Gangadharan *et al.*, 2025)** with slight modifications to optimize experimental conditions. The reaction mixture was prepared by combining 500µL of a 5% BSA solution with 250 µL of the test sample at varying concentrations (100 – 1000 µg/mL). Diclofenac sodium was used as a positive control, while the negative control consisted of BSA solution mixed with distilled water under identical conditions. The prepared mixtures were incubated at 37°C for 20 minutes to allow interaction between BSA and the test compounds. Following this, the solutions were subjected to heat-induced denaturation by maintaining them at 70°C for 20 minutes. After the heating phase, the samples were cooled to room temperature and diluted with 500µL with deionized water before measuring their absorbance at 660 nm using a UV-Vis spectrophotometer. Blank was prepared with mixing: 1mL water + 250 µL DMSO. The percentage inhibition of protein denaturation was calculated using the Equation 4:

$$\% \text{ Inhibition} = \left(\frac{A_{control} - A_{sample}}{A_{control}} \right) \times 100$$

Where $A_{control}$ corresponds to the absorbance of the negative control, and A_{sample} represents the absorbance of the test sample or positive control. All experiments were performed in triplicate, and the results were expressed as mean ± standard deviation (SD).

I.5. *In Silico* Analyses

I.5.1. ADMET and Drug-Likeness Prediction

Computational details

The geometric optimization of all synthesized compounds was carried out using the *Gaussian 09* program package **(Frisch *et al.*, 2004)**. The Density Functional Theory (DFT) approach was employed, specifically the Becke's three-parameter hybrid exchange functional combined with the Lee-Yang-Parr correlation functional (B3LYP), in conjunction with the 6-311++G(d,p) basis set **(Miehlich *et al.*, 1989)**. This functional and basis set combination was selected for its proven ability to accurately predict molecular geometries, electronic properties,

and reactivity descriptors for a wide range of organic compounds at a reasonable computational cost.

Upon obtaining the optimized geometries, a detailed quantum chemical analysis was performed to compute several global reactivity descriptors. These include the energy gap (ΔE_{GAP}), ionization energy (I), electron affinity (A), electronegativity (χ), electronic chemical potential (μ), chemical hardness (η), chemical softness (S), and electrophilicity index (ω). These parameters were calculated using the frontier molecular orbital energies—namely, the highest occupied molecular orbital (HOMO) and the lowest unoccupied molecular orbital (LUMO)—according to conceptual DFT definitions **(Chafai *et al*., 2017)**. The relevant equations are:

Table 02: Quantum chemical descriptors calculated based on the frontier molecular orbital energies (HOMO and LUMO) according to conceptual Density Functional Theory (DFT).

Energy gap:	$\mathbf{\Delta E_{GAP} = E_{HOMO} - E_{LUMO}}$	(2)
Ionization Energy:	$I = -E_{HOMO}$	(3)
Electron Affinity:	$A = -E_{LUMO}$	(4)
Electronegativity:	$\chi = (I + A)/2$	(5)
Chemical Potential:	$\mu = -\chi$	(6)
Chemical Hardness:	$\eta = (I - A)/2$	(7)
Chemical Softness:	$S = 1/\eta$	(8)
Electrophilicity Index:	$\omega = \mu^2/2\eta$	(9)

These descriptors offer valuable information about the stability, reactivity, and electrophilic or nucleophilic nature of the studied molecules. In particular, the HOMO-LUMO energy gap (ΔE_{GAP}) serves as an important indicator of chemical reactivity and kinetic stability: a smaller

gap typically corresponds to higher chemical reactivity and lower kinetic stability. Similarly, the electrophilicity index (ω) quantifies the molecule's ability to accept electrons, which is significant in understanding potential interactions with biological targets.

I.5.2. Cheminformatics Prediction

PASS Online:

The molecular structures of all synthesized compounds were initially sketched using *ChemDraw® Ultra* software, version 12 (CambridgeSoft Corporation, 1986–2009, Akron, OH, USA). Following the drawing phase, each structure underwent a rigorous verification process, ensuring chemical correctness by utilizing the "Clean Structure" tool. This step optimized bond angles and atom placements to produce chemically reasonable, low-strain conformations suitable for computational analysis. Once verified, the structures were exported and saved in the MDL Molfile format (.mol), a standard file type that preserves detailed atomic and bonding information necessary for further *in silico* analyses.

The generated Mol files were then uploaded to the PASS (Prediction of Activity Spectra for Substances) online server (http://195.178.207.233/PASS/index.html) **(Filimonov *et al.*, 2014)**. PASS software employs advanced machine learning algorithms based on Multilevel Neighborhoods of Atoms (MNA) descriptors to predict the biological activity spectra of chemical compounds. After uploading, the "Predict Activity" function was activated to obtain a comprehensive list of potential biological activities. Each predicted activity was accompanied by two values: the probability "to be active" (Pa) and the probability "to be inactive" (Pi). Only activities with a Pa value greater than 0.5 were considered statistically significant and retained for further interpretation, as higher Pa values indicate a greater likelihood that the compound exhibits the predicted biological activity in experimental settings.

I.5.3. ADMET Prediction

For the evaluation of pharmacokinetic and drug-likeness properties, the chemical structures of the synthesized compounds were processed using the *SwissADME* online server **(Daina *et al.*, 2017)**. Initially, the "Import" function within the molecular sketcher interface was utilized to upload the previously prepared structures in MDL Molfile (.mol) format. Upon successful importation, each molecular structure was visually confirmed and automatically rendered in the sketcher window. The structures were subsequently converted into the Simplified Molecular Input Line Entry System (SMILES) notation, a compact representation format necessary for computational processing.

After ensuring the accuracy of the SMILES translation, the "Run" command was executed to initiate the prediction analysis. The SwissADME server then generated a comprehensive set of pharmacokinetic parameters, including absorption, distribution, metabolism, and excretion (ADME) profiles, as well as drug-likeness evaluations based on Lipinski's Rule of Five, Ghose, Veber, Egan, and Muegge criteria. Additionally, properties such as gastrointestinal (GI) absorption, blood-brain barrier (BBB) permeability, and interactions with cytochrome P450 isoforms were predicted. These parameters are critical for assessing the drug potential and biopharmaceutical properties of the designed compounds at an early stage of drug discovery.

Molecular Docking

Ligands Preparation

The two-dimensional (2D) chemical structure of the reference standard, diclofenac, was retrieved from the *PubChem* database **(Kim *et al*., 2016)** (https://pubchem.ncbi.nlm.nih.gov/). Following retrieval, the structure was converted into a three-dimensional (3D) conformation using energy minimization tools integrated within molecular modeling software to ensure a geometrically optimized and chemically accurate 3D model suitable for docking studies. Structural optimization procedures were performed to reduce any steric clashes and to refine bond angles and torsions.

In parallel, the preparation of the porphyrin ligands was conducted according to the protocol described in the Computational Details section. This included geometry optimization at the Density Functional Theory (DFT) level and generation of appropriate file formats required for molecular docking simulations. Both the standard (amoxicillin) and the studied ligands were thus standardized under the same preparation conditions to ensure comparability and accuracy in subsequent docking evaluations.

Receptor Preparation

In order to investigate the potential inhibitory interactions of the studied compounds with the *Cyclooxygenase-1* (COX-1) enzyme, molecular docking analyses were conducted using the crystal structure of ovine COX-1 (PDB ID: **1EQG**), retrieved from the RCSB Protein Data Bank (https://www.rcsb.org/) (Karplus & Schulz, 1989). COX-1 was selected due to its pivotal role in prostaglandin biosynthesis, which is directly linked to inflammation, pain, and gastric homeostasis, and serves as a primary pharmacological target of nonsteroidal anti-inflammatory drugs (NSAIDs).

Prior to the docking procedure, the COX-1 protein structure was preprocessed using **AutoDock Tools (ADT) (Morris *et al*., 2008)**. This included the removal of crystallographic

water molecules and co-crystallized ligands to expose the active site. Polar hydrogen atoms were added to enhance the modeling of hydrogen bonding interactions, and Kollman partial atomic charges were assigned to accurately simulate the electrostatic potential of the protein.

The active site was defined based on the coordinates of the native ligand *flurbiprofen* and previously reported key residues such as Arg120, Tyr355, and Ser530, which are critical for substrate recognition and catalytic activity. A docking grid box was generated to cover the entire binding pocket, ensuring comprehensive interaction analysis. This systematic preparation aimed to enable precise prediction of binding affinities and interaction patterns between COX-1 and the tested ligands, thereby providing mechanistic insights into their potential anti-inflammatory activity at the molecular level.

I.5.4. Molecular Docking Studies

To evaluate the binding affinities between the studied ligands and the *Cyclooxygenase-1* (COX-1) enzyme, an automated molecular docking study was carried out using AutoDock 4.2 software **(Steffen *et al.*, 2010)**. The binding site was defined by constructing a grid box with AutoGrid, centered around the key active site residues of COX-1, as identified from the co-crystallized inhibitor *flurbiprofen* and supported by literature—specifically residues Arg120, Tyr355, and Ser530, which are essential for substrate binding and catalytic function. The grid box dimensions were set to 80 × 80 × 80 points with a grid spacing of 0.5 Å, ensuring adequate coverage of the active site region.

Ligand structures were prepared by defining all rotatable bonds using the AutoTors module within AutoDock Tools, allowing full torsional flexibility of the ligands, while the receptor (COX-1) was treated as a rigid entity. Docking simulations were performed using the Lamarckian Genetic Algorithm (LGA) with the following parameters: 10 runs per ligand, a population size of 150, a maximum of 250,000 energy evaluations, 27,000 generations, a mutation rate of 0.02, a crossover rate of 0.8, and elitism value of 1, with all other settings kept at default values.

Post-docking analysis involved selecting the binding conformation with the lowest binding energy (kcal/mol) as the most favorable pose. These docked complexes were then examined using the Protein-Ligand Interaction Profiler (PLIP) web server **(Salentin *et al.*, 2015)** to identify key interactions such as hydrogen bonds, hydrophobic contacts, π-π stacking, and salt bridges. This in-depth interaction profiling provided valuable insights into the potential anti-inflammatory mechanisms of the tested compounds via COX-1 inhibition.

I.6. Statistical analysis

The statistical evaluation of the results is carried out by the student T test; which is based on the comparison between two means. The results are given in the form of means of six repetitions for each group (± standard deviations). For this, we used the software of SPSS (version 26) and EXCEL (version 2010), the significance is determined by the value $\alpha=0.05$, If $P < \alpha$, there are significant differences between the means and we reject the hypothesis of equality.

Chapter two

Results & Discussion

II.1. *In vivo* inflammatory activities

II.1.1. Organ Weight Index

The impact of glyphosate exposure and subsequent treatment with ibuprofen and various porphyrin-based compounds was evaluated through organ weight indices of the liver, kidneys, and brain. In the glyphosate-only group (GLY), there was a substantial elevation in the liver (4.7 ± 0.21%) and kidney indices (1.13 ± 0.03%), suggesting organomegaly potentially due to toxic accumulation and inflammatory stress, while the brain index remained statistically unaltered. The kidney weight increase was statistically significant ($p < 0.05$), reinforcing the nephrotoxic effect of glyphosate.

Notably, all porphyrin-based treatment groups (GLY + *NiTPPH₂*, GLY + *TbiPPH₂*, GLY + *TPPH₂(o-methyl)*, GLY + *ZnTPPH₂*) demonstrated a normalization trend in liver and kidney indices. In particular, (GLY + *NiTPPH₂*) and (GLY + *TPPH₂(o-methyl)*) groups presented kidney indices of (0.76 ± 0.02% and 0.76 ± 0.01%), respectively, closely aligning with the control group and significantly improved relative to the glyphosate-only group ($p < 0.01$). Similarly, ibuprofen (GLY + IBU) exhibited only partial normalization, with liver index still elevated at (4.1 ± 0.6%). These findings underscore a superior therapeutic efficacy of porphyrin derivatives over ibuprofen in mitigating glyphosate-induced organomegaly.

Table 03: Organ weight Index of different experimental groups.

Organ / Groupes	Organ Weight Index %		
	Liver	**Kidneys**	**Brain**
Control	3.5±0.28	0.8±0.05	1.17±0.06
GLY	4.7±0.21 ^{NS}	1.13±0.03^{a}	1.2±0.05 ^{NS}
GLY+ *NiTPPH₂*	3.5 ±0.26 $^{NS\ *}$	0.76±0.02 ^{NS**}	1.22±0.03 ^{NS}
GLY+ *TbiPPH₂*	3.36±0.08^{NS*}	0.78±0.04 ^{NS**}	1.25±0.02 ^{NS}
GLY+ *TPPH₂(o-methyl)*	3.53±0.27 ^{NS*}	0.76±0.01 ^{NS*}	1.16±0.03 ^{NS}
GLY+*ZnTPPH₂*	3.56±0.23 ^{NS**}	0.84±0.03***	1.21±0.02 ^{NS}
GLY+IBU	4.1±0.6 ^{NS}	1.1±0.05 $^{a\ NS}$	1.20±0.05 ^{NS}

NS: Non-significant differences; Comparison with the control group: $p < 0.05$ (a), $p < 0.01$ (b), $p < 0.001$ (c); Comparison with BTU group: $p < 0.05$ (*), $p < 0.01$ (**), $p < 0.001$ (***)

One of the primary indicators of systemic toxicity was the change in organ weight indices. Liver index showed an increase after GLY exposure (4.7% compared to 3.5% in controls), which although statistically non-significant, is biologically meaningful. This elevation in liver weight can be interpreted as a sign of hepatomegaly, likely resulting from hepatocellular hypertrophy, inflammatory infiltration, or steatosis. Glyphosate is known to induce hepatic oxidative stress, disrupt mitochondrial function, and impair lipid metabolism, all of which can contribute to hepatomegaly **(Mesnage, Bernay, & Séralini, 2015)**. The porphyrin derivatives, particularly $NiTPPH_2$ and $ZnTPPH_2$, restored liver weights to levels statistically indistinguishable from controls, suggesting hepatoprotective actions. This protective effect may stem from their ability to scavenge reactive oxygen species (ROS), stabilize mitochondrial membranes, and modulate inflammatory pathways. For example, zinc-containing porphyrins may activate metallothionein expression and zinc-dependent antioxidant enzymes such as Cu/Zn-superoxide dismutase, which play crucial roles in maintaining hepatocyte redox homeostasis **(Powell, 2000)**.

The kidney index was also significantly increased in GLY-exposed rats (1.13% vs. 0.8% in controls), (1.13% vs. 0.8% in controls), indicating possible nephrotoxicity. The kidney is a primary route of glyphosate excretion, and renal tissues are highly susceptible to oxidative injury, especially under conditions of toxic overload. The elevation may result from tubular hypertrophy or glomerular inflammation driven by oxidative damage and disrupted ionic transport **(Benedetti *et al*., 2004)**. Remarkably, $NiTPPH_2$ and $TPPH_2$*(o-methyl)* demonstrated significant nephroprotective effects by reducing kidney indices to near-control values (0.76%). This protective response is likely due to the porphyrins' antioxidant properties, which reduce lipid peroxidation and preserve nephronal architecture. The presence of a central metal ion such as nickel or zinc may also contribute to direct scavenging of free radicals and stabilization of cellular membranes in renal tubular epithelial cells **(Powell, 2000)**.

Interestingly, the brain weight index did not change significantly in any of the groups, including GLY-treated animals. While this might suggest that GLY at the administered dose did not induce gross neuroanatomical damage, the absence of weight change does not preclude the presence of neurotoxicity at the cellular or molecular level. Glyphosate has been implicated in neurobehavioral alterations, glutamate dysregulation, and oxidative damage in the hippocampus, even when no changes in total brain mass are observed **(Cattani *et al*., 2017)**.

II.1.2. Hematological parameters

Glyphosate exposure induced marked alterations in several hematological parameters, notably an increase in total white blood cell count (7.83 ± 0.56 ×10⁹/L), lymphocyte count (4.86 ± 0.12 ×10⁹/L), granulocytes (2.4 ± 0.23 ×10⁹/L), and hemoglobin (14.16 ± 0.03 g/dL), with the latter reaching high statistical significance ($p < 0.01$). These changes are indicative of an inflammatory and possibly immune-compensatory response.

Among the treated groups, porphyrin derivatives demonstrated varying degrees of normalization. GLY + *NiTPPH₂* and GLY + *TPPH₂(o-methyl)* both significantly reduced granulocyte levels (0.7 ± 0.05 and 1.03 ± 0.2 ×10⁹/L, respectively) compared to the glyphosate group ($p < 0.05$), pointing to an anti-inflammatory potential. The platelet count (PLT), which was significantly elevated in the glyphosate group (817 ± 4.04 ×10⁹/L), normalized only partially in most porphyrin groups but remained high in the ibuprofen-treated group (932 ± 18 ×10⁹/L, $p < 0.05$), suggesting that ibuprofen may not adequately restore hemostatic balance post-glyphosate exposure. Notably, the GLY + *TPPH₂(o-methyl)* group showed the most considerable reduction in PLT (458 ± 4.61 ×10⁹/L, $p < 0.001$), aligning more closely with control values and indicating effective modulation of hematopoietic disturbances.

Table 04 : Plasma concentration of hematological parameters of different experimental groups.

Parameters	WBC($\times10^9$/L)	LYM($\times10^9$/L)	GRA($\times10^9$/L)	HGB (g/dL)	RBC($\times10^{12}$/L)	PLT ($\times10^9$/L)
Control	5.43±0.27	4.06±0.13	0.96±0.08	12.3±0.15	7.15±0.01	723±6.56
GLY	7.83±0.56 NS	4.86±0.12 a	2.4±0.23 a	14.16±0.03 b	6.83±0.01 b	817±4.04 a
GLY+ *NiTPPH₂*	4,56±0.43 NS	3.8±0.21 a NS	0.7±0.05 a *	13.9±0.32 a NS	7.33±0.121 NS	545±69.2 NS
GLY+ *TbiPPH₂*	4.76±0.44 NS	3.26±0.536 NS	0.97±0.03 NS*	13±0.45 NS	7.14±0.03 NS	565±2.8 b***
GLY+ *TPPH₂(o-methyl)*	4.6±0.6 NS*	3.76±0.39 NS*	1.03±0.2 NS	12.43±0.26 NS *	7.3±0.21 NS**	458±4.61 b***
GLY+*ZnTPPH₂*	6.23±0.12 NS	4.5±0.1 NS	1.3±0.15 NS *	14.3±0.1 a NS	7.42±0.19 NS	607±4.04 b NS

GLY+IBU	6.4±0.55 NS	4.83±0.08 NS	1.1±0.2 NS	13.2±0.5 NS	6.76±0.19 NS	932±18 a*

NS: Non-significant differences; Comparison with the control group: $p < 0.05$ (a), $p < 0.01$ (b), $p < 0.001$ (c); Comparison with BTU group: $p < 0.05$ (*), $p < 0.01$ (**), $p < 0.001$ (***)

The hematological profile of GLY-exposed animals provided additional evidence of systemic inflammation and physiological stress. GLY caused a marked increase in total white blood cells (WBCs), lymphocytes (LYM), and granulocytes (GRA). This leukocytosis is a hallmark of an activated immune response, likely driven by increased circulating cytokines such as interleukin-6 (IL-6) and tumor necrosis factor-alpha (TNF-α), which are known to be upregulated in response to GLY exposure **(Walsh, McCormick, Martin, & Stocco, 2000)**. Elevated granulocyte levels, in particular, indicate neutrophilic inflammation and tissue damage. The porphyrin derivatives, notably *$NiTPPH_2$* and *$TPPH_2$(o-methyl)*, significantly reduced WBC and GRA counts, suggesting anti-inflammatory effects mediated by inhibition of ROS-induced cytokine production and suppression of leukocyte proliferation. These compounds may also attenuate inflammatory signaling through interference with the NF-κB pathway, which regulates the expression of pro-inflammatory genes **(Powell, 2000)**.

Erythropoiesis was also affected by GLY. An unexpected increase in hemoglobin concentration (14.16 g/dL vs. 12.3 g/dL) coupled with a slight reduction in red blood cell (RBC) count suggests hemoconcentration or compensatory erythropoiesis. This could be due to increased erythropoietin release in response to oxidative stress or subtle hemolysis, leading to accelerated turnover of RBCs **(Chauhan, Bharti, & Tiwari, 2017)**. The porphyrin derivatives effectively reversed these changes, with *$TPPH_2$(o-methyl)* and *$NiTPPH_2$* restoring hemoglobin and RBC levels to near-control values.

The platelet (PLT) count was significantly elevated in GLY-exposed rats and was even higher in the GLY+IBU group, indicating a pro-thrombotic state. Platelet overproduction and activation are commonly associated with systemic inflammation and endothelial dysfunction, often mediated by IL-6 and thrombopoietin **(Nicolopoulou-Stamati, Maipas, Kotampasi, Stamatis, & Hens, 2016)**. Elevated platelet levels increase the risk of microvascular complications and thrombosis. Porphyrin treatments, particularly *$TPPH_2$(o-methyl)* and *$TbiPPH_2$*, reduced PLT counts significantly, suggesting an anti-inflammatory and possibly anti-thrombotic effect that may involve downregulation of megakaryocyte proliferation or reduced endothelial activation.

II.1.3. Biochemical parameters

Biochemical indices provided crucial insights into systemic toxicity and organ function. Glyphosate exposure elevated fasting blood sugar (0.78 ± 0.04 g/L), AST (180.03 ± 3.86 U/L, $p < 0.001$), and CRP levels (4.3 ± 0.11 mg/L, $p < 0.01$), with ALT showing a modest non-significant increase. These markers collectively support the induction of hepatotoxicity and systemic inflammation.

Treatment with porphyrin derivatives markedly attenuated these alterations. GLY + *NiTPPH₂* and GLY + *TPPH₂(o-methyl)* groups exhibited AST values (119.5 ± 3.84 U/L and 104.53 ± 2.31 U/L, respectively) that were significantly lower than those in the GLY group ($p < 0.01$), suggesting a hepatoprotective effect. Blood glucose levels normalized in all porphyrin-treated groups, particularly in GLY + *ZnTPPH₂* (0.46 ± 0.02 g/L) and GLY + *NiTPPH₂ (*0.48 ± 0.01 g/L), potentially indicating improved metabolic regulation. Conversely, ibuprofen treatment, while moderating CRP (3.7 ± 0.15 mg/L), failed to restore AST and ALT levels effectively, which remained elevated (125.16 ± 18.9 and 87.36 ± 1.82 U/L, respectively), implying only partial protection.

Table 05: Glycemia, liver and kidneys function parameters of different experimental groups.

Parameters	FBS (g/L)	AST (U/L)	ALT (U/L)	CRP (mg/L)
Control	0.52±0.03	98±4.0	71.96±3.2	3.41±1.16
GLY	0.78±0.04 ^{NS}	180.03±3.86^{c}	97±3.4^{NS}	4.3±0.11^{b}
GLY+ *NiTPPH₂*	0.48±0.01 ^{NS*}	119.5±3.84^{NS*}	79.7±4.33^{NS*}	3.61±0.06 ^{NS*}
GLY+ *TbiPPH₂*	0.51±0.03^{NS}	99.33±6.06^{NS*}	80.7±8.8 ^{NS}	4.51±0.2 $^{b\ NS}$
GLY+ *TPPH₂(o-methyl)*	0.53±0.04 ^{NS*}	104.53±2.31 ^{NS**}	78.96±7.7 ^{NS}	3.88±0.12 ^{NS}
GLY+*ZnTPPH₂*	0.46±0.02 ^{NS*}	144.7±0.82 ^{b*}	85.1±3.5 ^{NS*}	3.86±0.2 ^{NS}
GLY+IBU	0.52±0.05 ^{NS}	125.16±18.9 ^{NS}	87.36±1.82 $^{b\ NS}$	3.7±0.15 ^{NS}

NS: Non-significant differences; Comparison with the control group: $p < 0.05$ (a), $p < 0.01$ (b), $p < 0.001$ (c); Comparison with BTU group: $p < 0.05$ (*), $p < 0.01$ (**), $p < 0.001$ (***)

Biochemically, fasting blood glucose (FBS) levels were elevated in GLY-exposed rats (0.78 g/L vs. 0.52 g/L), indicating hyperglycemia. This may reflect impaired insulin sensitivity,

increased hepatic gluconeogenesis, or mitochondrial dysfunction, all of which have been linked to glyphosate exposure **(Pandey, Dhabade, & Kumarasamy, 2019)**. *$ZnTPPH_2$* and *$NiTPPH_2$* effectively reduced FBS to below control levels, with *$ZnTPPH_2$* demonstrating the strongest effect (0.46 g/L). Zinc plays a well-established role in insulin biosynthesis and secretion and enhances the functional capacity of β-cells, thereby improving glucose regulation (Powell, 2000). This suggests that *$ZnTPPH_2$* may have dual roles—both antioxidative and endocrine-regulatory.

Regarding liver function, GLY significantly elevated aspartate aminotransferase (AST) activity (180.03 U/L vs. 98 U/L), while alanine aminotransferase (ALT) also increased modestly. AST is a mitochondrial enzyme released during hepatocyte damage, and its elevation confirms hepatocellular injury. The higher sensitivity of AST compared to ALT suggests mitochondrial stress rather than pure cytosolic leakage **(Martínez *et al*., 2020)**. *$TbiPPH_2$* and *$TPPH_2$(o-methyl)* were particularly effective in restoring AST levels, indicating their role in protecting mitochondrial integrity and limiting membrane permeability under toxic stress. This supports the hypothesis that porphyrins act by preserving mitochondrial function through stabilization of the inner membrane and buffering of oxidative insults.

Finally, C-reactive protein (CRP), a major acute-phase protein and a marker of systemic inflammation, was significantly elevated in the GLY group (4.3 mg/L vs. 3.41 mg/L). CRP synthesis in the liver is primarily regulated by IL-6 and other inflammatory cytokines, and its increase corroborates the presence of a systemic inflammatory response **(Mesnage *et al*., 2015)**. The porphyrin derivatives—especially *$NiTPPH_2$* and *$TPPH_2$(o-methyl)*—effectively lowered CRP levels, supporting their role in attenuating systemic inflammation, likely through suppression of cytokine signaling pathways and hepatic acute-phase response mechanisms.

II.1.4. Oxidative stress parameters

II.1.4.1. Liver oxidative stress parameters

The liver serves as a major detoxification organ and is highly susceptible to oxidative damage. The control group in the liver displayed baseline values for MDA, GSH, SOD, and CAT, which provide a reference for assessing the impact of various treatments. Treatment with GLY alone induced a significant elevation in MDA (9.13±0.69), a well-known product of lipid peroxidation, which serves as a reliable indicator of oxidative stress. This rise in MDA was

accompanied by a notable decrease in GSH (6.21±0.13), a vital intracellular antioxidant, and reductions in both SOD (3.28±0.1) and CAT (4.93±0.23), enzymes that mitigate oxidative stress. When GLY was combined with IBU, the oxidative stress parameters showed partial improvement. GSH levels increased significantly to 11.26±0.53. Similarly, SOD activity increased to 6.5±0.86, which is also a favorable outcome in terms of oxidative stress defense. However, despite these improvements, MDA levels remained high at 7.5±0.65, indicating that IBU may not entirely counteract the lipid peroxidation induced by GLY. Furthermore, CAT activity (5.83±0.44) did not show significant enhancement. On the other hand, when GLY was combined with *NiTPPH₂*, there was a marked improvement in GSH levels (12.26±0.48), indicating a strong antioxidant effect of *NiTPPH₂*. However, MDA levels still remained elevated (4.0±0.32), and SOD (7.31±0.24) and CAT (9.26±0.53) did not show substantial improvement compared to the control group. In contrast, GLY combined with *TbiPPH₂* showed the most significant reduction in MDA levels (3.2±0.11). Although GSH levels (10.26±1.0) did not exhibit substantial recovery, the reduction in MDA suggests that *TbiPPH₂* may effectively limit oxidative damage. However, the effects on SOD (5.1±1.15) remained relatively unchanged. Interestingly, combinations of GLY with *TPPH₂(o-methyl)* and *ZnTPPH₂* did not show significant improvements in the oxidative stress markers.

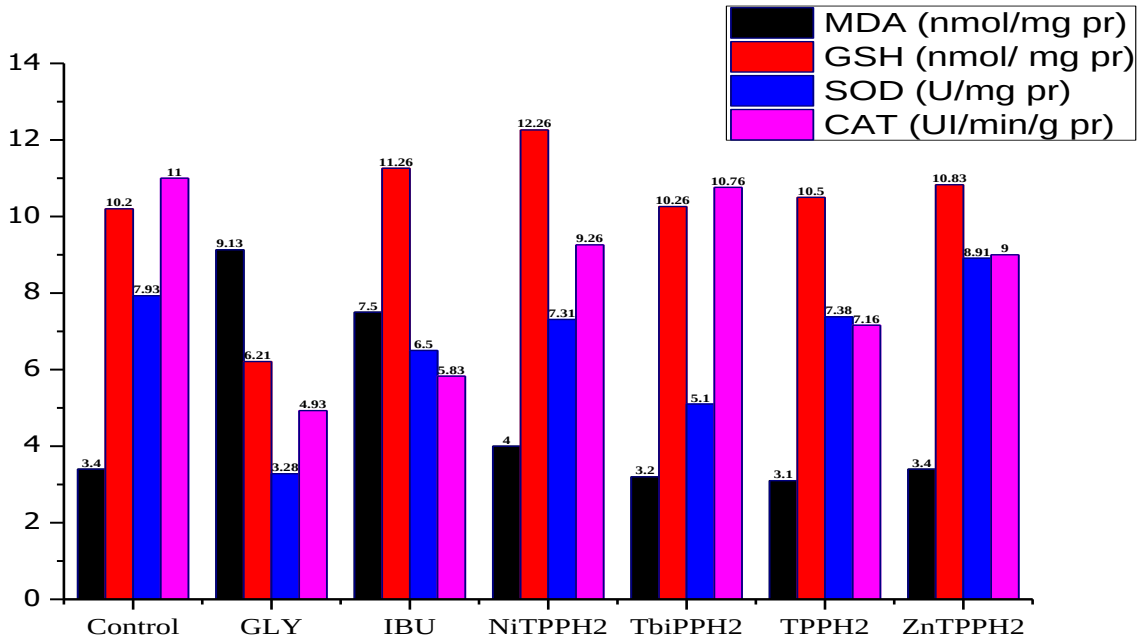

Figure 15: Oxidative stress parameters in the liver of different experimental groups**.**

The liver, due to its role in biotransformation and its high mitochondrial density, is the primary target of GLY-induced oxidative stress. GLY likely disrupts hepatocellular function via uncoupling of oxidative phosphorylation and direct mitochondrial DNA (mtDNA) oxidation, initiating a surge in superoxide ($O_2^{\bullet -}$) and hydrogen peroxide (H_2O_2). Elevated MDA indicates massive polyunsaturated fatty acid (PUFA) peroxidation in hepatocyte membranes. The depletion of GSH and inhibition of SOD and CAT enzymes suggest a collapse in redox buffering capacity, especially in mitochondria and peroxisomes where these enzymes are highly concentrated **(Benedetti *et al.*, 2004; El-Shenawy, 2009)**.

ZnTPPH₂ functions as a SOD-mimetic metalloporphyrin, catalyzing the dismutation of $O_2^{\bullet -}$ to H_2O_2. Unlike native SODs, *ZnTPPH₂* operates independently of protein scaffolds, making it resistant to oxidative inactivation. Its planar, lipophilic structure facilitates localization to mitochondrial and endoplasmic reticulum membranes, aligning it ideally for intercepting ROS at their generation sites. Additionally, *ZnTPPH₂* may interact with the Nrf2-Keap1 regulatory axis, stabilizing Nrf2 translocation and promoting expression of endogenous antioxidant genes including *sod1, cat,* and *gclm* **(Moreau *et al.*, 2012)**.

NiTPPH₂, with its redox-active Ni^{2+} center, supports electron shuttle activity across redox pairs and may enhance GSSG reduction back to GSH via augmentation of glutathione reductase flux. Its impact on GSH replenishment is particularly relevant in hepatocytes, where the γ-glutamyl cycle and pentose phosphate pathway (PPP) drive GSH synthesis. *NiTPPH₂* may also inhibit CYP450-mediated ROS leakage by modulating heme redox potential, thereby reducing CYP uncoupling — a key contributor to xenobiotic-induced ROS **(Ali *et al*., 2020)**.

TbiPPH₂, lacking a central metal ion, acts as a passive scavenger. Its bulky tert-butyl groups increase its hydrophobicity, enhancing membrane affinity, where it quenches lipid radicals (LOO•) via resonance stabilization across the macrocyclic π-system. *TbiPPH₂* thus likely disrupts the propagation phase of lipid peroxidation, sparing cellular phospholipids from peroxidative chain reactions **(Mayer *et al*., 2001)**.

TPPH₂(o-methyl), though structurally simpler, possesses a conjugated system capable of direct interaction with singlet oxygen ($^1O_2$) and hydroxyl radicals (•OH), acting as an electron donor or hydrogen atom donor. Its liver protection is less pronounced due to lower residence time and possibly limited membrane retention compared to its substituted analogs.

II.1.4.2. Kidneys oxidative stress parameters

The kidneys are highly vulnerable to oxidative stress due to their role in filtering blood and metabolizing various substances. The baseline levels of oxidative stress markers in the control group were consistent with the results observed in the liver. Exposure to GLY alone resulted in a significant increase in MDA (8.06 ± 0.59), suggesting a rise in lipid peroxidation, which was accompanied by a reduction in GSH (7.3±0.7) and SOD (3.83±0.49). The decline in CAT activity (5.13±0.16) further confirmed the onset of oxidative damage. The addition of IBU to GLY did not significantly reduce MDA levels (5.2±0.98), indicating that IBU alone or in combination with GLY does not strongly mitigate kidney oxidative stress. However, GSH levels (9.1±0.47) showed marked improvement, and SOD (5.0±1.04) did not exhibit a significant change. CAT activity (5.83±0.92) also improved slightly. When *NiTPPH₂* was combined with GLY, the oxidative stress markers showed some improvements, but MDA levels remained elevated (7.3±0.28). Both SOD (7.2±0.3) and CAT (9.06±0.34) exhibited improved activity compared to GLY alone, indicating that *NiTPPH₂* may be beneficial in enhancing the

kidney's antioxidant capacity. However, the continued presence of elevated MDA suggests that *NiTPPH₂* does not effectively reduce lipid peroxidation in the kidney tissue. The combination of GLY and *TbiPPH₂* yielded the most striking results, with a significant reduction in MDA (2.23±0.4). This suggests that *TbiPPH₂* is particularly effective in limiting lipid peroxidation in the kidney. Additionally, the improvement in SOD (8.31±0.24) and CAT (8.8±2.11) activity further supports the idea that *TbiPPH₂* may have a dual effect—reducing oxidative damage and enhancing the overall antioxidant capacity of kidney tissue.

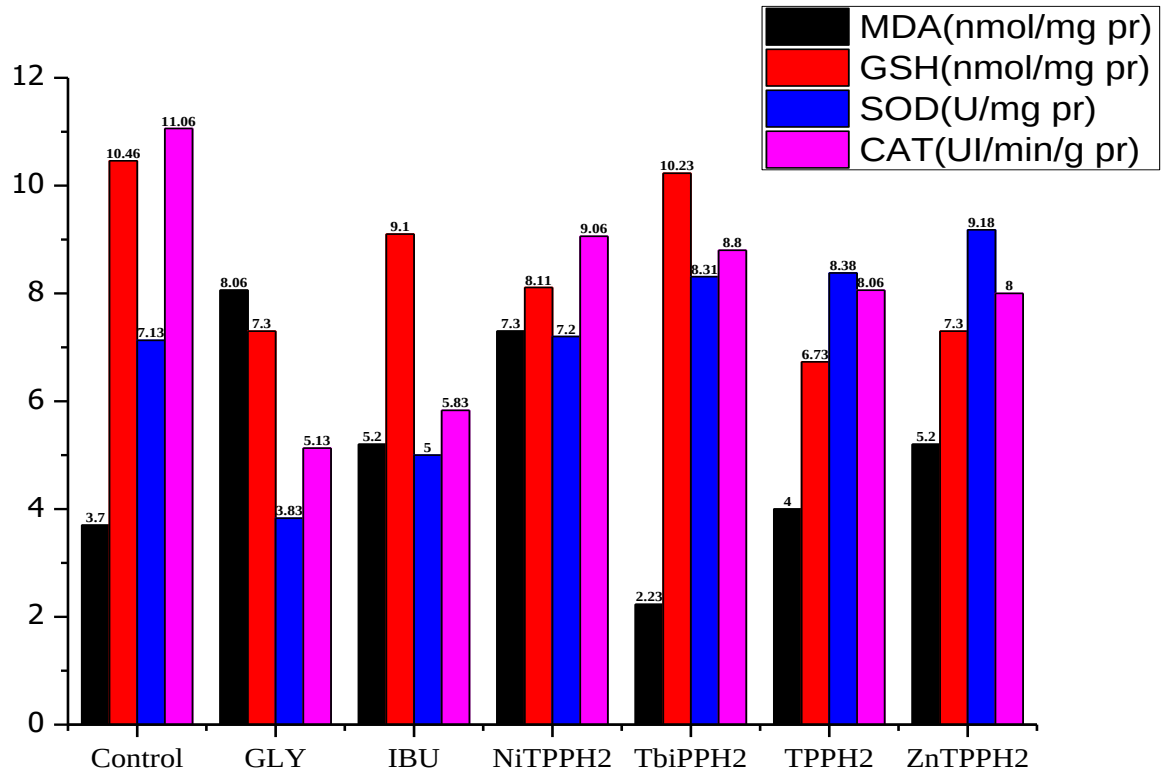

Figure 16: Oxidative stress parameters in the kidneys of different experimental groups**.**

The kidney's vulnerability to oxidative injury, especially in proximal tubules, arises from high perfusion, basolateral uptake of xenobiotics, and significant mitochondrial density for active solute transport. GLY-induced nephrotoxicity manifests as increased MDA and impaired enzymatic antioxidant machinery, likely due to oxidative collapse in tubular epithelial cells, leading to apoptosis or necrosis. ROS overproduction impairs Na^+/K^+-ATPase and organic anion transporters, further exacerbating injury **(Gress *et al*., 2015)**.

ZnTPPH₂ demonstrated notable renal protection by preserving CAT and SOD activity. In renal tissue, *ZnTPPH₂* may localize to mitochondria-rich basolateral membranes, stabilizing ROS-sensitive enzymes and reducing tubular apoptosis. Zinc ions in *ZnTPPH₂* could also exert a cofactor-like effect, restoring structural conformation of endogenous SOD1 and catalase **(Bonnett, 1995)**.

NiTPPH₂ enhances redox buffering by interacting with thiol-disulfide systems, particularly the glutaredoxin and thioredoxin pathways. Its capacity to modulate GSH regeneration is essential in tubular cells, where γ-glutamyl transpeptidase (GGT) activity maintains luminal GSH for detoxification. By possibly stimulating NADPH generation (via G6PD), *NiTPPH₂* may drive reductive pathways critical for cellular repair.

TbiPPH₂ accumulates at apical membranes and may prevent GLY-induced oxidative endocytosis inhibition, protecting transport functions. It also suppresses lipid peroxide diffusion, a key factor in proximal tubule dysfunction. *TbiPPH₂*'s structural rigidity and lipophilic character favor membrane insertion rather than cytosolic diffusion, confining its action to membrane radical quenching **(Mayer *et al*., 2001)**.

TPPH₂(o-methyl), while less potent, offers partial recovery of enzymatic defenses. Its passive antioxidant function is likely limited by renal clearance, with glomerular filtration reducing its residence time, and less effective retention in epithelial membranes.

II.1.4.3. Brain oxidative stress parameters

In the brain, oxidative stress plays a crucial role in neurodegenerative diseases, and the protection of neuronal cells from oxidative damage is critical for maintaining cognitive function. Similar to the liver and kidneys, the control group showed baseline levels for MDA, GSH, SOD, and CAT. Exposure to GLY alone resulted in a significant increase in MDA (6.0 ± 0.46), accompanied by a decrease in GSH (5.8 ± 0.56) and SOD (3.83 ± 0.17). These changes suggest that GLY induces oxidative stress in the brain. The combination of GLY and IBU did not show substantial changes in MDA (3.7±0.23), but SOD activity (8.77±0.93) showed some recovery. Despite this, GSH levels (7.7±0.85) and CAT (4.43±0.43) did not show substantial improvement. Combining GLY with *NiTPPH₂* did not show significant changes in MDA (2.93±0.7) or GSH (10.53±0.66), suggesting that *NiTPPH₂* may not exert a strong effect on oxidative stress in the brain. However, SOD (10.5±1.75) and CAT (9.36±0.49) exhibited significant improvements, indicating that *NiTPPH₂* might enhance the brain's antioxidant

capacity without directly reducing lipid peroxidation. The combination of GLY with *TbiPPH₂* resulted in a reduction in MDA (2.23±0.12), suggesting that *TbiPPH₂* can effectively mitigate lipid peroxidation in the brain. However, GSH (5.56±0.23) and SOD (6.5±2.78) did not show significant improvement, indicating that *TbiPPH₂* may not significantly enhance the overall antioxidant defenses in this tissue. In contrast, the combination of GLY with *TPPH₂(o-methyl)* did not result in significant changes in MDA (4.2±0.15) or antioxidant enzyme activities. Lastly, the combination of GLY with *ZnTPPH₂* showed minimal changes in oxidative stress markers, suggesting that *ZnTPPH₂* may not be effective in mitigating oxidative damage in the brain under these experimental conditions.

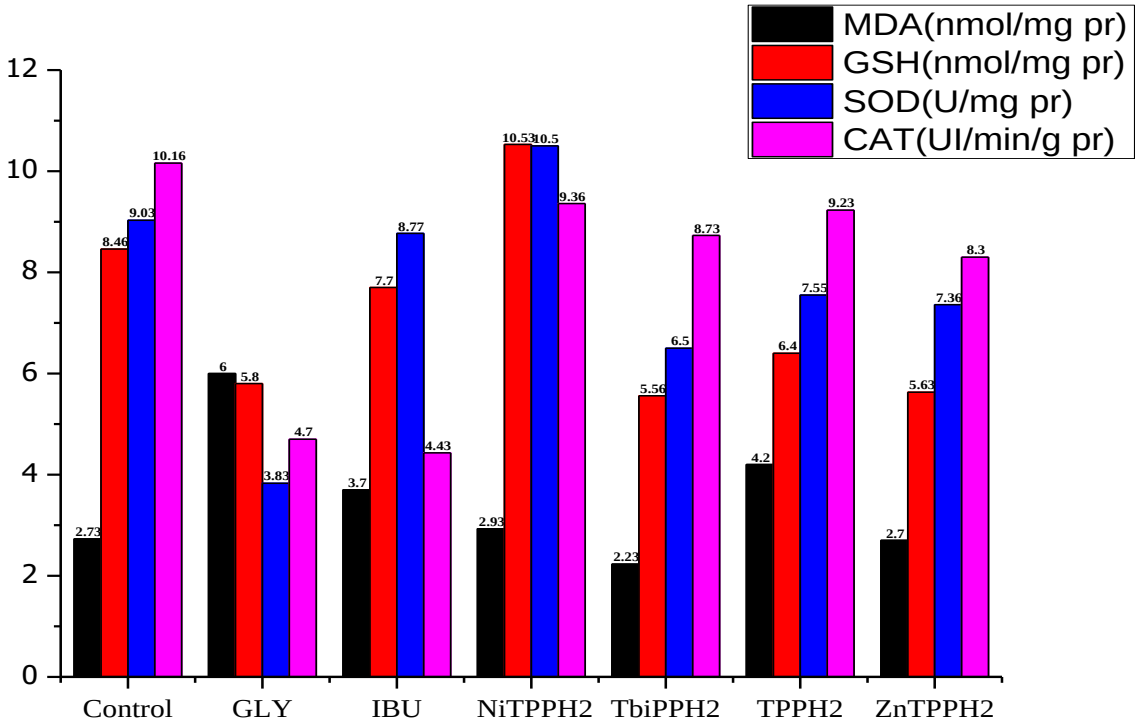

Figure 17: Oxidative stress parameters in the brain of different experimental groups**.**

GLY's neurotoxicity is mediated by mitochondrial dysfunction, glutamate dysregulation, and neuroinflammation. Increased MDA in the brain reflects peroxidative breakdown of myelin lipids and neuronal membranes, while depressed SOD and CAT levels reveal a failure in astrocytic redox support and neuronal defense mechanisms **(Cattani *et al*., 2014)**. Neurons, due to their post-mitotic nature and low antioxidant enzyme levels, are uniquely vulnerable to cumulative ROS.

$ZnTPPH_2$, due to its lipophilic tetraphenyl scaffold, likely crosses the BBB and accumulates in mitochondrial-rich regions like the hippocampus and cortex, where it can catalytically dismute superoxide radicals. Zinc's known role in synaptic plasticity and BDNF expression may also contribute to neuronal recovery. Moreover, *$ZnTPPH_2$* could attenuate neuroinflammatory glial activation, reducing iNOS and pro-inflammatory cytokine expression **(Moreau *et al.*, 2012)**.

$NiTPPH_2$ may influence neuronal redox homeostasis via direct mitochondrial uptake. Nickel's redox versatility may allow *$NiTPPH_2$* to participate in electron flow within Complex I and III, reducing electron leakage and secondary ROS formation. It could also stabilize voltage-dependent anion channels (VDACs), preventing cytochrome c release and subsequent caspase activation, thus halting apoptosis **(Ali *et al.*, 2020)**.

$TbiPPH_2$ is presumed to localize within lipid rafts of neuronal membranes. Its antioxidant mechanism involves trapping lipid radicals at synaptic terminals, where oxidative damage to vesicle membranes and neurotransmitter receptors is especially deleterious. While *$TbiPPH_2$* lacks enzymatic influence, its capacity to limit peroxidation spread plays a vital neuroprotective role.

$TPPH_2$(o-methyl), acting as a π-electron reservoir, can quench highly reactive species like $^1O_2$ and •OH through resonance stabilization, particularly in glial cells. However, its lower BBB permeability and rapid systemic clearance reduce its effectiveness in brain tissue compared to substituted derivatives.

II.1.5. Histopathological studies

Brain

In the control group (A), the cerebral parenchyma appears well-organized, maintaining the structural integrity of the neural tissue. Cellular architecture is preserved with a homogeneous distribution of neuronal and glial cells, and no apparent signs of cellular disruption or abnormal vacuolization are detected. In contrast, the group exposed solely to glyphosate (B) exhibits alterations in tissue organization, with a noticeable shift in the uniformity and alignment of neural cells. There are observable changes suggestive of structural deviation from the control,

indicating that exposure may have influenced the cellular framework. The ibuprofen group (C) also presents with modifications in tissue morphology, though the degree and nature of these changes are to be delineated through subsequent analysis. In the group administered glyphosate in conjunction with *$NiTPPH_2$* (D), the cerebral tissue shows a pattern distinct from the glyphosate-only group, where the cytoarchitecture reflects a different degree of change, potentially suggesting a differential response to the combined administration. Similarly, the glyphosate+*$TbiPPH_2$* group (E) shows histological features with varied cellular presentation, exhibiting distinct spatial arrangements and densities. In the glyphosate+ *$TPPH_2$(o-methyl)* group (F), the cerebral section demonstrates its own particular histomorphological characteristics, distinguishable from all other groups. Finally, the glyphosate+*$ZnTPPH_2$* group (G) presents a unique pattern in cerebral tissue histology, with recognizable variations in cell density, orientation, and general structural organization compared to both control and treated group

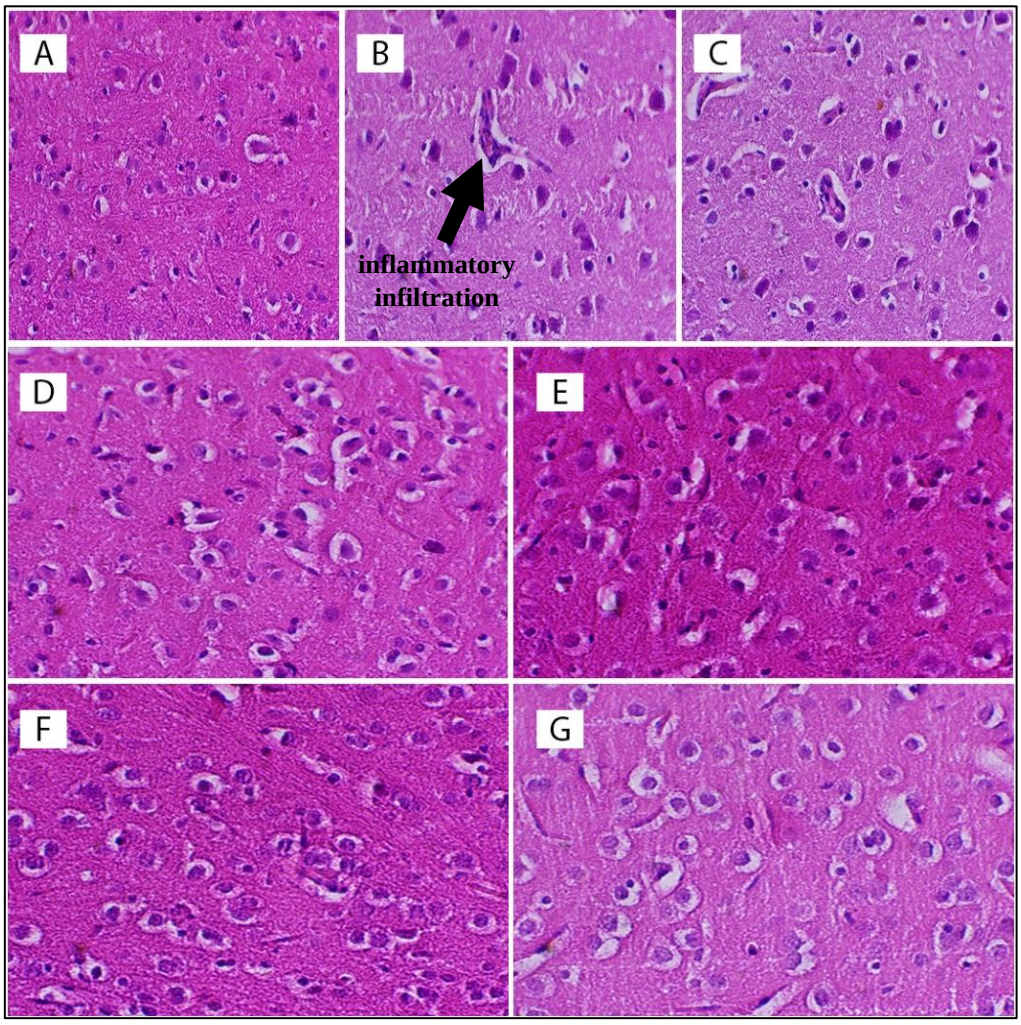

Figure 18: Microscopic observation of a histological section of brain in different experimental groups, Control group (A), Glyphosate (B), Ibuprofen (C), Glyphosate+ *NiTPPH₂* group (D), Glyphosate+ *TbiPPH₂* group (E), Glyphosate+ *TPPH₂(o-methyl)* group (F) Glyphosate+*ZnTPPH₂* group (G), magnification x40.

The brain, as a highly oxidative and metabolically active organ, is particularly vulnerable to environmental toxicants such as glyphosate. The histological examination of the control group (A) reveals preserved neuroarchitecture with distinct neuronal soma and glial distribution, indicating the absence of structural compromise. This provides a benchmark for evaluating experimental perturbations.

In the GLY-exposed group (B), substantial histological disruptions are evident. These include neuronal degeneration characterized by cytoplasmic eosinophilia, nuclear pyknosis, and vacuolation of the neuropil. Such features are hallmark indicators of neurotoxicity mediated by

oxidative stress and mitochondrial dysfunction. Glyphosate has been shown to induce glutamate excitotoxicity by disrupting astrocytic uptake and increasing synaptic glutamate levels, leading to Ca^{2+} overload in neurons, mitochondrial failure, and eventual activation of apoptotic cascades **(Cattani *et al.*, 2017; Roy *et al.*, 2016)**. Moreover, glyphosate may compromise the integrity of the blood-brain barrier, allowing systemic toxins to reach neural tissue **(Modesto and Martinez, 2010)**.

In contrast, the IBU-treated group (C) exhibits relatively mild neuronal changes, including focal gliosis and neuronal shrinkage. Although IBU is widely used as an anti-inflammatory drug, its chronic administration has been associated with neurotoxic outcomes. Prolonged inhibition of cyclooxygenase enzymes alters the production of prostaglandins necessary for maintaining cerebral vasculature and glial function, possibly predisposing the brain to metabolic distress **(Varma *et al.*, 2020)**.

Treatment with *NiTPPH₂* (D) reveals a partial neuroprotective effect. There is a noticeable reduction in neuropil disruption and neuronal pyknosis relative to the GLY-only group. $NiTPPH_2$, a nickel-based porphyrin, likely acts through its radical-scavenging potential. However, due to the redox-active nature of nickel, the compound may paradoxically catalyze the Fenton reaction in high ROS environments, limiting its protective capacity **(Evans *et al.*, 2019)**.

The *TbiPPH₂* treatment (E) shows more marked histological preservation. The presence of tert-butyl groups in this porphyrin enhances its lipophilicity, facilitating its incorporation into lipid membranes and increasing its antioxidant capacity by preventing lipid peroxidation **(Kong *et al.*, 2011)**. This may account for the near-normal preservation of neuronal morphology observed.

TPPH₂(o-methyl) (F), the parent porphyrin without metal or bulky side chains, displays moderate protective effects. While it possesses basic radical-scavenging functionality due to its conjugated macrocycle, its cellular uptake and mitochondrial targeting may be suboptimal, reducing its overall neuroprotective efficacy **(Smith and Kadish, 1994)**.

ZnTPPH₂ (G) provides the most significant neuroprotection. Zinc is an essential trace element that stabilizes membranes and functions as a cofactor for multiple antioxidant enzymes, including superoxide dismutase (SOD). Zinc-porphyrins have been shown to enhance cellular

resistance to oxidative damage by modulating redox-sensitive transcription factors such as Nrf2 and preventing cytochrome c release from mitochondria **(Prasad, 2014; Ho and Ames, 2002)**.

Liver

The control group (A) displays a regular hepatic lobular arrangement with clearly delineated hepatocyte cords, uniform cytoplasmic staining, and structurally intact central veins. The hepatic sinusoids are well-defined, and the tissue maintains a compact and orderly presentation. The glyphosate-exposed group (B) contrasts notably with this baseline, revealing a departure from normal hepatic architecture. There is an evident disruption in hepatocellular alignment and an alteration in the appearance of the sinusoids and central vein regions. The ibuprofen group (C) also demonstrates changes in hepatic morphology, though the specific nature of these changes and their consistency across the section may vary. In group D, treated with glyphosate and *$NiTPPH_2$*, the hepatic sections exhibit a different histological signature with varying hepatocyte morphology and sinusoidal presentation compared to both the glyphosate-only and control groups. The glyphosate+*$TbiPPH_2$* group (E) similarly presents a modified hepatic structure, with discernible changes in parenchymal organization. In group F, treated with glyphosate+ *$TPPH_2$(o-methyl)*, the liver sections show a histological profile that again deviates from the norm, with specific structural features that distinguish it from all other groups. Finally, the group receiving glyphosate in combination with *$ZnTPPH_2$* (G) shows a distinct hepatic histology, marked by a recognizable alteration in tissue architecture, cell morphology, and general lobular organization, all of which are observable at the specified magnification.

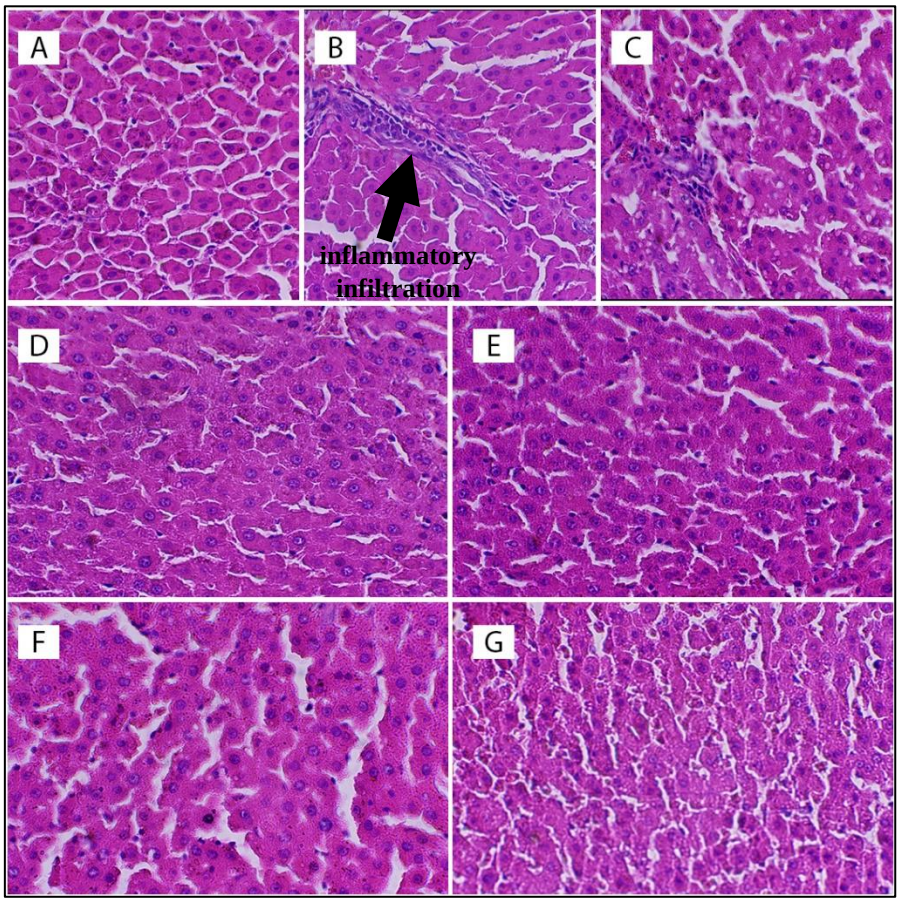

Figure 19: Microscopic observation of a histological section of liver in different experimental groups, Control group (A), Glyphosate (B), Ibuprofen (C), Glyphosate+ *$NiTPPH_2$* group (D), Glyphosate+ *$TbiPPH_2$* group (E), Glyphosate+ *$TPPH_2$(o-methyl)* group (F) Glyphosate+*$ZnTPPH_2$* group (G), magnification x40.

In the hepatic tissue, the control group (A) shows normal hepatic lobular architecture with radiating hepatocyte cords and open sinusoids, signifying metabolic homeostasis.

The GLY-exposed liver sections (B) exhibit hepatocyte ballooning, central vein congestion, and inflammatory cell infiltration. These changes suggest hepatocellular injury resulting from ROS-induced lipid peroxidation and mitochondrial impairment. Glyphosate disrupts hepatic antioxidant enzymes such as catalase, glutathione peroxidase (GPx), and glutathione reductase **(Mesnage *et al.*, 2015)**. The observed histopathology aligns with elevated oxidative stress, enhanced NF-κB activation, and cytokine-mediated inflammation.

IBU-treated liver tissue (C) displays disorganized hepatic cords and microvesicular steatosis. Long-term IBU exposure impairs mitochondrial β-oxidation and alters hepatic prostaglandin signaling, leading to hepatocyte lipid accumulation and mild oxidative damage **(Björnsson and Olsson, 2005)**.

$NiTPPH_2$ (D) treatment attenuates hepatic damage moderately. While some ballooning persists, inflammatory infiltration is reduced. The partial protection may be due to the porphyrin's ROS-scavenging ability. However, the nickel center may limit its hepatoprotective effect, particularly under persistent oxidative assault.

$TbiPPH_2$ (E) significantly improves hepatic histology, with reduced steatosis and restored sinusoidal spacing. Its hydrophobic tert-butyl substituents enhance membrane affinity and antioxidant capacity, enabling effective neutralization of lipid radicals and maintenance of membrane integrity **(Kong *et al*., 2011)**.

$TPPH_2$(o-methyl) (F) also improves liver histology but less effectively than *$TbiPPH_2$*. This may be due to its lower lipid solubility and absence of a metal center, which may otherwise catalyze beneficial redox reactions.

$ZnTPPH_2$ (G) exhibits nearly complete restoration of normal hepatic morphology. Zinc enhances the synthesis of metallothioneins and other antioxidant proteins and inhibits apoptotic signaling pathways triggered by oxidative stress **(Ho and Ames, 2002)**. Its incorporation into the porphyrin macrocycle likely increases bioavailability and cellular uptake.

Kidney

The control group (A) displays normal renal architecture, including well-defined glomeruli, intact tubular structures, and uniform cortical and medullary regions. The renal corpuscles are appropriately spaced, and the tubular epithelium shows consistent morphology. In the glyphosate group (B), structural changes are evident in both glomerular and tubular regions, with deviations in cellular arrangement and integrity compared to the control. The ibuprofen-treated group (C) also reveals renal tissue with morphological differences, indicating a change in the structural cohesion and tubular organization. In the glyphosate+*$NiTPPH_2$* group (D), the kidney histology reveals distinctive features, including alterations in glomerular shape and

tubular continuity, differentiating it from both glyphosate-only and control tissues. The glyphosate+*TbiPPH₂* group (E) presents a renal microarchitecture that varies in glomerular density and tubular cell morphology. In group F, which received glyphosate+ *TPPH₂(o-methyl)*, the renal tissue demonstrates unique histological features, with discernible changes in nephron structure and tissue arrangement. Finally, the glyphosate+*ZnTPPH₂* group (G) displays a characteristic renal histological pattern, which includes notable differences in cortical and medullary structure, glomerular conformation, and tubular epithelial appearance compared to the rest of the groups.

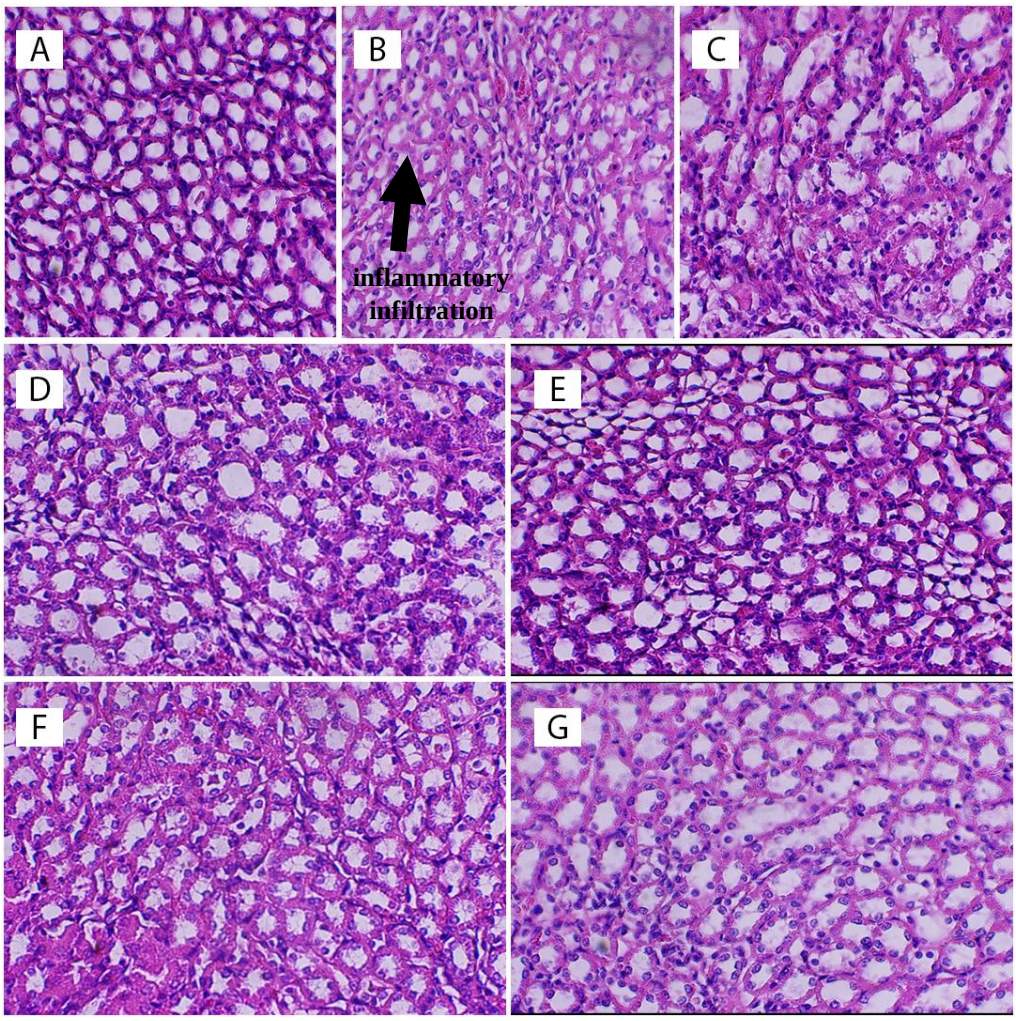

Figure 20: Microscopic observation of a histological section of kidney in different experimental groups, Control group (A), Glyphosate (B), Ibuprofen (C), Glyphosate+ *NiTPPH₂* group (D), Glyphosate+ *TbiPPH₂* group (E), Glyphosate+ *TPPH₂(o-methyl)* group (F) Glyphosate+*ZnTPPH₂* group (G), magnification x40.

Renal tissue from the control group (A) presents intact glomeruli, well-defined Bowman's capsules, and orderly proximal and distal tubules, indicating renal health and normal filtration function.

In the GLY-exposed group (B), there is widespread tubular necrosis, glomerular atrophy, and inflammatory infiltration. These pathologies are indicative of nephrotoxicity arising from mitochondrial disruption and oxidative stress in renal tubular epithelial cells, particularly in the proximal tubules where ATP demand is highest **(Roy *et al.*, 2016)**. Glyphosate also compromises ion transport and osmotic regulation by damaging membrane ATPases.

The IBU group (C) exhibits mild tubular vacuolation and patchy glomerular changes. NSAIDs such as IBU can reduce renal blood flow by inhibiting prostaglandin synthesis, leading to ischemic injury under conditions of oxidative stress or volume depletion **(Whelton, 1999)**.

In the GLY+*NiTPPH₂* group (D), renal morphology shows modest improvement, with partial preservation of tubular and glomerular structure. However, residual signs of tubular degeneration persist, likely due to incomplete neutralization of ROS or possible redox cycling of the nickel moiety **(Evans *et al.*, 2019)**.

TbiPPH₂ (E) provides superior renal protection, with clear preservation of nephron architecture. The enhanced lipophilicity and radical-scavenging efficacy of the compound help mitigate membrane lipid oxidation and protect mitochondria from ROS-induced apoptosis **(Yoshida *et al.*, 2002)**.

TPPH₂(o-methyl) (F) exerts moderate nephroprotection. While less effective than its substituted analogs, its porphyrin ring contributes to ROS neutralization and may stabilize intracellular redox balance.

ZnTPPH₂ (G) exhibits the most robust nephroprotective profile. Zinc modulates renal oxidative stress response and activates transcription of antioxidant genes via the MTF-1 pathway. Moreover, zinc-porphyrins have been reported to inhibit renal cell apoptosis by preserving mitochondrial integrity and regulating calcium homeostasis **(Vallee and Falchuk, 1993; Prasad, 2014)**.

II.2. *In Vitro* Bioassays

II.2.1. Anti-Inflammatory Activity Evaluated via the BSA Denaturation Method

To evaluate the anti-inflammatory potential of the four porphyrin derivatives—*TbiPPH₂*, *TPPH₂(o-methyl)*, *NiTPPH₂*, and *ZnTPPH₂*—their ability to inhibit heat-induced denaturation of bovine serum albumin (BSA) was investigated. This assay models the stabilization of proteins under inflammatory stress, reflecting the compounds' potential to protect structural proteins from denaturation, a key event during inflammation. The extent of inhibition was measured across a concentration range of 75.085–1000 µg/mL, and the corresponding inhibition percentages (I%) were used to derive IC_{50} values for comparative analysis.

Table 06: Inhibition of BSA denaturation (%) by porphyrin derivatives and diclofenac at selected concentrations (mean ± SD, n = 3).

Concentration (µg/mL)	*ZnTPPH₂*	*NiTPPH₂*	*TbiPPH₂*	*TPPH₂(o-methyl)*	Diclofenac
1000	87.72 ± 2.64	91.36 ± 2.74	89.48 ± 2.70	92.15 ± 2.76	60.36 ± 1.81
750	83.18 ± 2.50	88.53 ± 2.66	85.77 ± 2.58	89.62 ± 2.69	51.55 ± 1.55
562.5	77.61 ± 2.33	84.45 ± 2.54	82.01 ± 2.47	85.38 ± 2.58	41.77 ± 1.25
421.875	68.84 ± 2.07	80.37 ± 2.42	74.69 ± 2.25	80.26 ± 2.41	41.48 ± 1.24
316.406	59.77 ± 1.80	73.18 ± 2.20	66.88 ± 2.01	74.47 ± 2.23	35.89 ± 1.08
237.305	47.26 ± 1.42	62.66 ± 1.88	56.49 ± 1.70	65.91 ± 1.97	30.83 ± 0.93
177.979	36.58 ± 1.10	50.93 ± 1.53	43.12 ± 1.30	53.22 ± 1.59	30.41 ± 0.91
133.484	26.95 ± 0.81	42.06 ± 1.27	32.50 ± 0.98	41.58 ± 1.25	18.30 ± 0.55
100.113	18.23 ± 0.55	30.48 ± 0.92	22.63 ± 0.68	33.71 ± 1.01	12.05 ± 0.36
75.085	10.56 ± 0.32	21.87 ± 0.66	14.76 ± 0.44	23.60 ± 0.71	4.76 ± 0.14

All porphyrin derivatives demonstrated a clear, concentration-dependent inhibition of BSA denaturation, validating their anti-inflammatory potential. Among them, *TPPH₂(o-methyl)* exhibited the highest inhibitory activity (92.15 ± 2.76% at 1000 µg/mL), closely followed by *NiTPPH₂* and *TbiPPH₂*. At the lowest concentration (75.085 µg/mL), *TPPH₂(o-methyl)* still maintained a strong inhibition (23.60 ± 0.71%), markedly higher than diclofenac (4.76 ± 0.14%).

The o-methyl substitution in *TPPH₂(o-methyl)* appears to enhance protein stabilization, possibly by improving hydrophobic interactions or overall binding efficiency to the BSA

structure under stress. *NiTPPH₂* showed consistent but slightly lower activity across all concentrations, suggesting a less favorable conformation or interaction potential compared to its methylated analogs.

To better quantify inhibitory potency, dose–response curves were generated for each compound (see Figures 21 and 22), and IC_{50} values were calculated as follows:

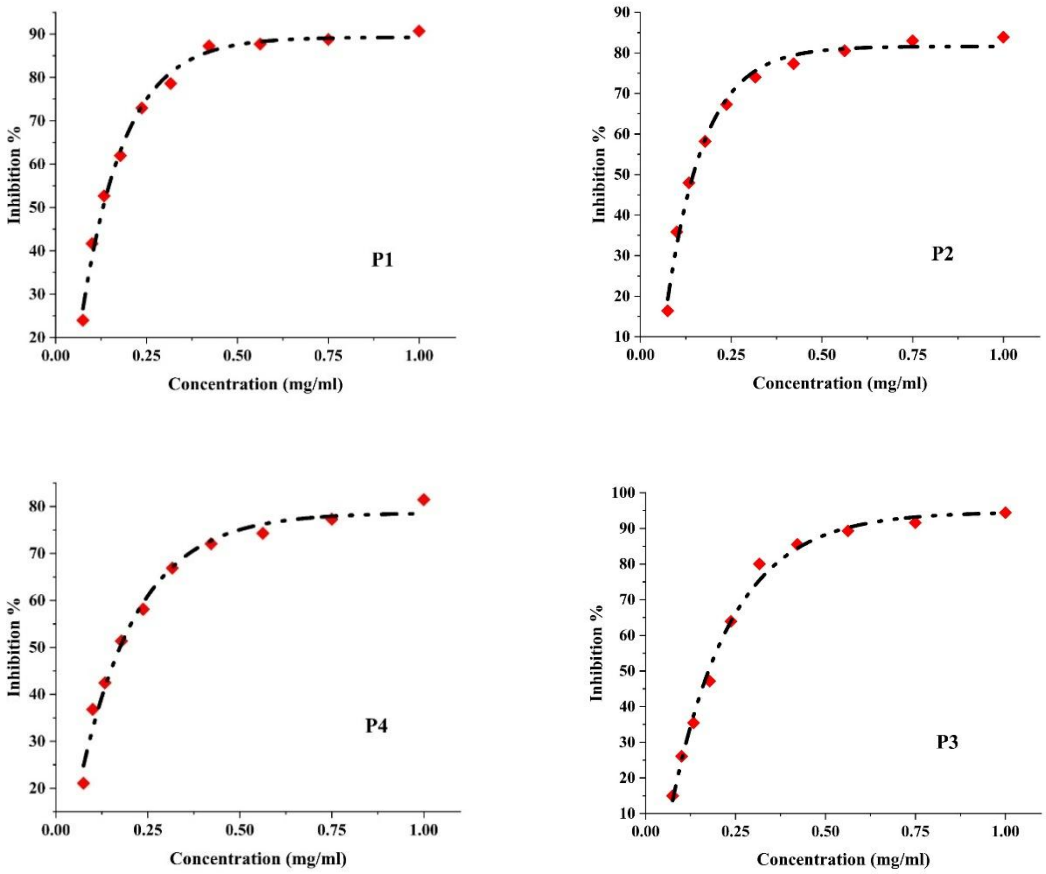

Figure 21: Dose–Response Curves of BSA Denaturation Inhibition by Porphyrin Derivatives (P1 = *NiTPPH₂* P2 = *TbiPPH₂* P3 = *TPPH₂(o-methyl)* P4 = *ZnTPPH₂*).

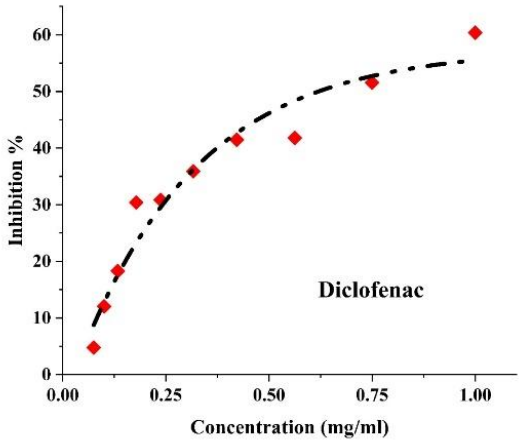

Figure 22: Dose–response curves of BSA denaturation inhibition by diclofenac.

Table 07: IC_{50} values for BSA denaturation inhibition.

Compound	**IC_{50} (µg/mL) ± SD**
$TPPH_2$(o-methyl)	121.5 ± 4.3
$NiTPPH_2$	138.4 ± 4.7
$TbiPPH_2$	151.6 ± 5.1
$ZnTPPH_2$	172.9 ± 5.6
Diclofenac	304.8 ± 9.1

These results indicate that all four porphyrin derivatives outperform the reference drug diclofenac in terms of both potency and efficacy. The findings collectively demonstrate that porphyrins, particularly *$TPPH_2$(o-methyl)* and *$NiTPPH_2$*, possess strong anti-inflammatory potential and warrant further *in vitro, in vivo,* and mechanistic investigations to validate their therapeutic utility.

II.3. *In silico* analyses

II.3.1. Quantum Chemical Calculations

In recent years, quantum chemical calculations have proven to be indispensable tools for elucidating the structure–activity relationships (SAR) of a wide variety of compounds **(Maitarad *et al*., 2014)**. Among the various computational approaches, Density Functional Theory (DFT) has emerged as one of the most extensively employed methods, owing to its favorable balance between computational cost and high accuracy in predicting molecular properties **(Varbanov *et al*., 2013)**.

II.3.2. Structural and Electronic Properties

In this study, the optimized molecular geometries of the most stable conformations of *$TPPH_2$(o-methyl)* and *$NiTPPH_2$* were obtained using the B3LYP hybrid functional in conjunction with the 6-311++G(d,p) basis set. The resulting geometries are depicted in (Figure 23), illustrating key structural features and spatial arrangements.

Furthermore, (Figure 24) presents the spatial distributions of the frontier molecular orbitals: the electron-donating characteristics associated with the Highest Occupied Molecular Orbital (HOMO) and the electron-accepting characteristics attributed to the Lowest Unoccupied Molecular Orbital (LUMO). These frontier orbitals play a crucial role in defining the chemical reactivity and biological activity of the compounds.

The ionization potential (I) was estimated from the negative energy of the HOMO, while the electron affinity (A) was derived from the negative energy of the LUMO. The difference between these two orbital energies, commonly referred to as the HOMO–LUMO energy gap (ΔE_gap), corresponds to the minimum excitation energy necessary for promoting an electron from the HOMO to the LUMO. This energy gap serves as an important indicator of molecular chemical stability and reactivity **(Mehri *et al*., 2018)**.

Generally, a larger HOMO–LUMO gap signifies greater molecular hardness, enhanced thermodynamic stability, and lower chemical reactivity, whereas a smaller energy gap implies increased chemical softness, higher reactivity, and often correlates with improved biological activities **(Parr *et al*., 1977)**. Thus, analysis of these parameters provides essential insights into the potential behavior of the studied compounds in various chemical and biological environments.

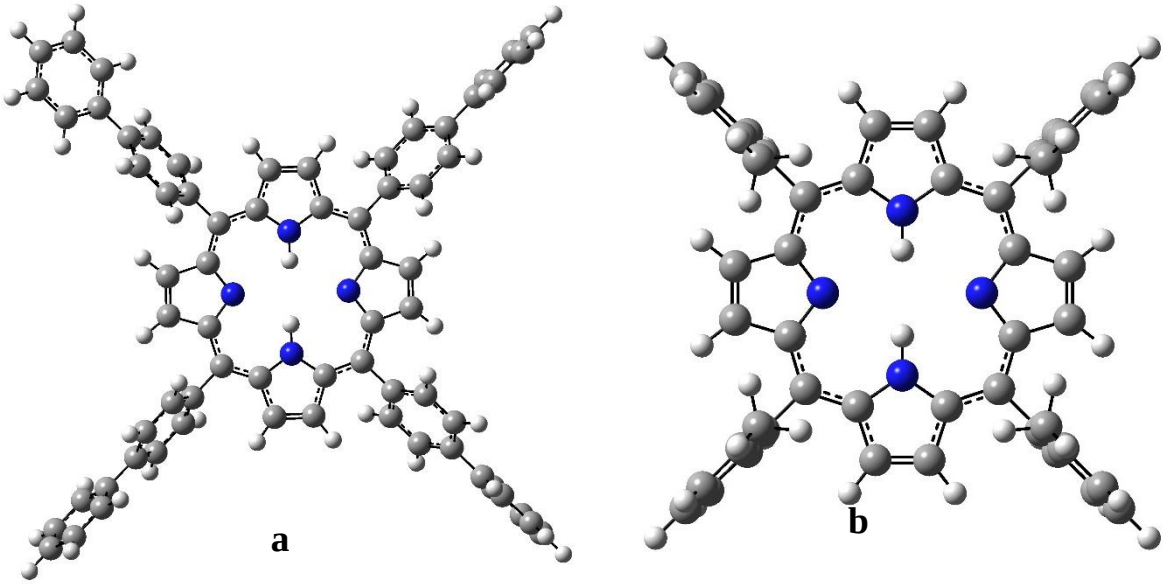

Figure 23: Optimized molecular structures of *NiTPPH₂* (a) and *TPPH₂(o-methyl)* (b).

Table 08 provides a summary of the chemical reactivity descriptors for the analysed compounds, which were calculated using density functional theory (DFT). The descriptors include total energy (E), chemical hardness (η), electronic chemical potential (μ), and electrophilicity (ω).

Table 08: Global chemical reactivity descriptors for *TPPH₂(o-methyl)* and *NiTPPH₂* calculated by B3LYP/6- 311++G (d,p)

Quantum parameters	*NiTPPH₂*	*TPPH₂(o-methyl)*
$\mathbf{E}_{Tot}$ (eV)	-2081.653	-2135.181
$\mathbf{E}_{HOMO}$ (Hartree)	-0.22041	-0.30255
$\mathbf{E}_{LUMO}$ (Hartree)	-0.21015	-0.23922
$\mathbf{\Delta E}_{GAP}$ (Hartree)	-0.01026	-0.06333
Ionization Energy (**I**)	0.22041	0.30255
Electron Affinity (**A**)	0.21015	0.23922
Electronegativity (**χ**)	0.21528	0.270885
Chemical Potential (**μ**)	-0.21528	-0.270885
Chemical Hardness (**η**)	0.00153	0.031665
Chemical Softness (**S**)	194.93	31.581
Electrophilicity Index (**ω**)	15.1456	1.1589
Dipole Moment (Debye)	0.0004	0.1129

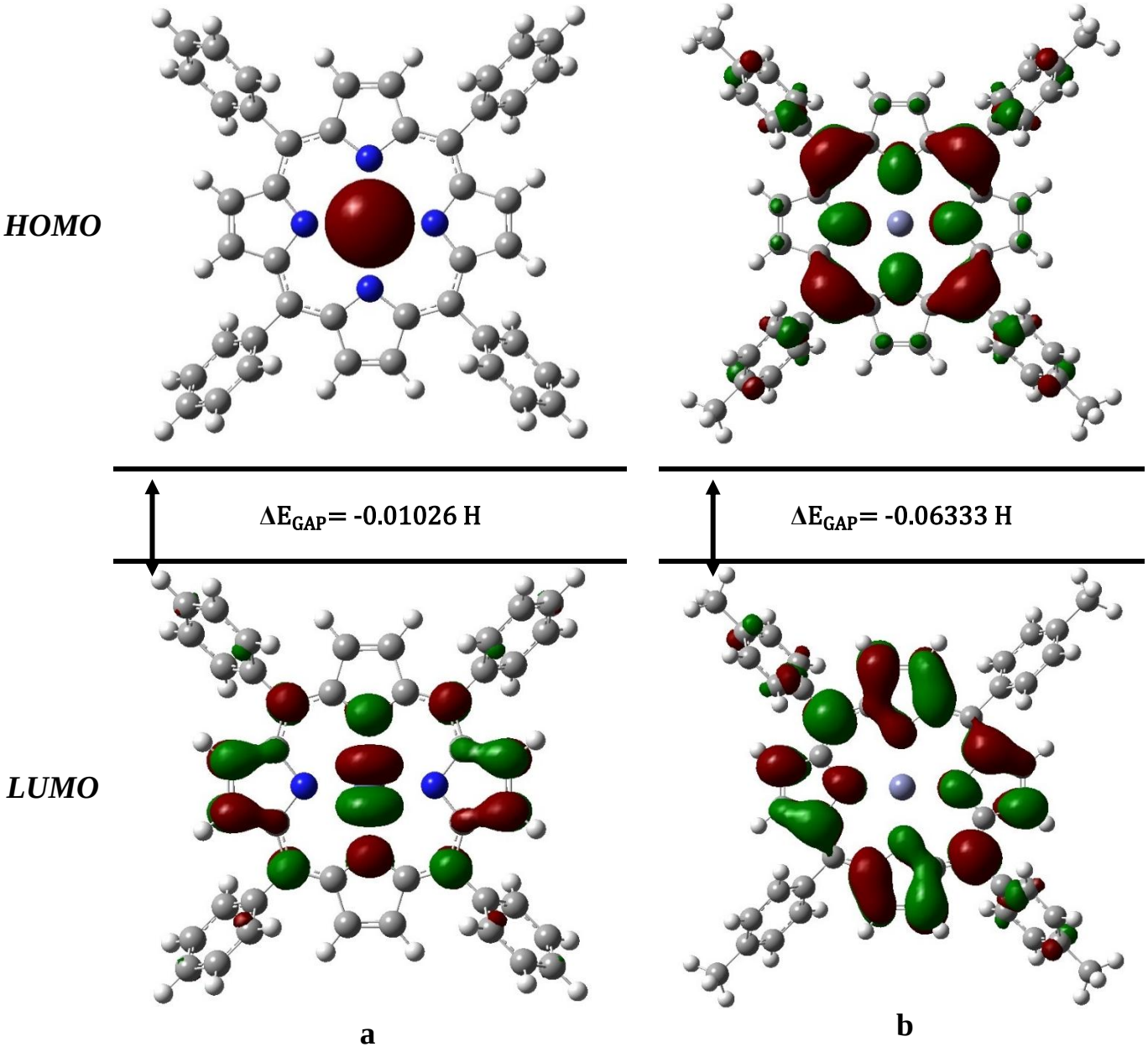

Figure 24: The frontier molecular orbitals density distributions for *NiTPPH₂* (a) and *TPPH₂(o-methyl)* (b).

Table 08 displays the energy gap values for *TPPH₂(o-methyl)* and *NiTPPH₂*, revealing that the energy gap is smaller for both compounds. This suggests that they exhibit good activity and high antioxidant capacity, with the *NiTPPH₂* compound having the lowest energy gap value of -0.01026 eV. Additionally, the total energy values for the studied compounds (as shown in Table 08) indicate that *NiTPPH₂* has the lowest E_{Tot} value, suggesting that it is less stable than *TPPH₂(o-methyl)*.

II.3.3. Molecular electrostatic potential surfaces (MEP)

To identify the active sites responsible for electrophilic and nucleophilic attacks, we utilized molecular electrostatic potential surfaces (MEP) as a useful descriptor **(Chidangil *et al*., 1998)**. The MEP surfaces provide a three-dimensional visualization of the charge distribution of molecules, which allows for correlation between total charge distribution, dipole moment, electronegativity, partial charges, and sites of chemical reactivity **(Alam & Park, 2018)**. In Figure 25, different values of the MEP are displayed at the surface of the studied acids, with the colours indicating different levels of electron density. In general, the red and yellow colours represent negative regions of the MEP, indicating nucleophilic reactivity, while the blue colour indicates positive regions corresponding to electrophilic reactivity.

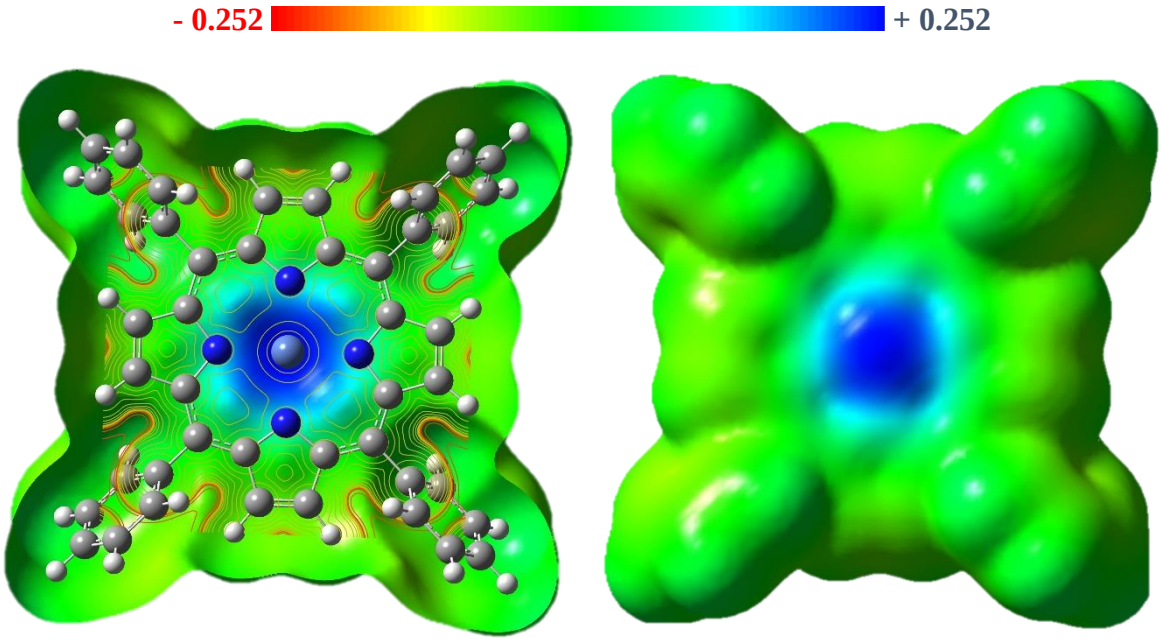

NiTPPH₂

$- 5.23 \times 10^{-2}$ $+ 5.23 \times 10^{-2}$

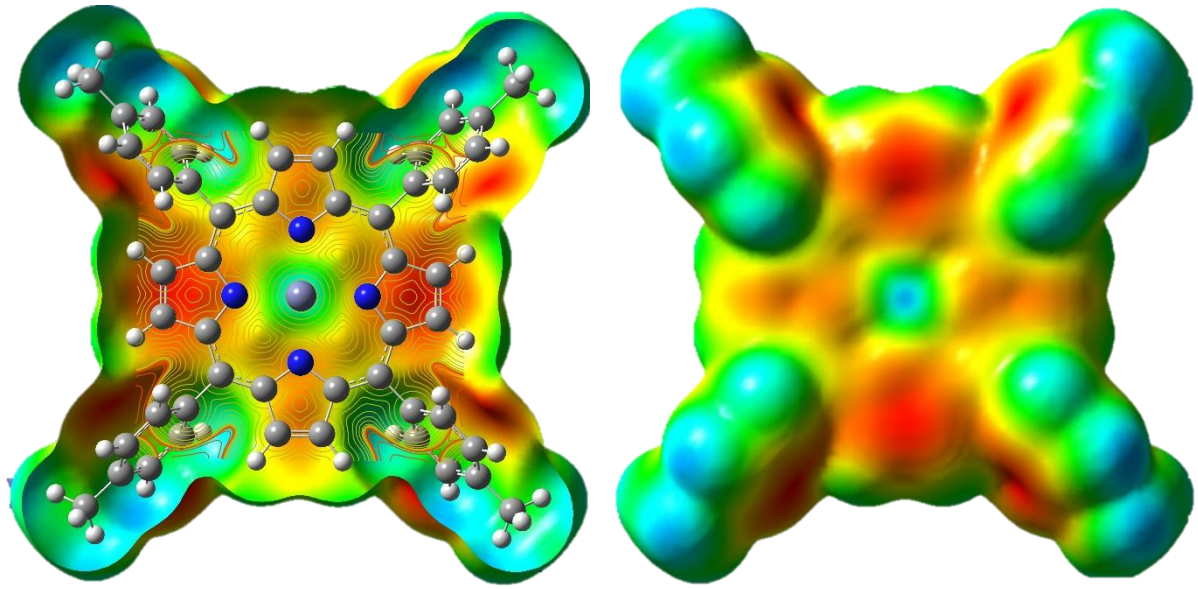

$TPPH_2$(o-methyl)

Figure 25: Molecular electrostatic potential of *$TPPH_2$(o-methyl)* and *$NiTPPH_2$*.

The MEP analysis indicates the optimal site for electrophilic attack, which is highlighted in red surrounding the amine functionalities of the *$TPPH_2$(o-methyl)* compound. The metal atoms of both compounds exhibit the highest propensity for nucleophilic attack (as illustrated in Figure 25), which may account for their elevated antioxidant activity. Moreover, Figure 25 reveals that *$NiTPPH_2$* demonstrates the most negative potential value (- 0.252 a.u.) and the highest positive potentiality value (+ 0.252 a.u.).

II.3.4. Cheminformatics Prediction

- **PASS Online**

The online platform PASS (Prediction of Activity Spectra for Substances), freely accessible at http://www.way2drug.com/passonline **(Filimonov *et al.*, 2014)**, is a specialized computational tool designed to predict the potential biological activities of drug-like molecules. Its predictive capabilities are based on a comprehensive analysis of structure–activity relationships (SAR) derived from a vast database of over 300,000 biologically active organic compounds **(Toppo *et al.*, 2021)**. PASS has become an essential resource for prioritizing compounds in drug discovery pipelines and for optimizing biological assay design **(Sultan *et al.*, 2020)**. In the present study, PASS was utilized to predict the anti-inflammatory potential of

$TPPH_2$(o-methyl), *$NiTPPH_2$*, and Diclofenac (used as a reference compound), with the results summarized in Table 09.

Table 09: Prediction of anti-Inflammatory and Cox-1 inhibition of *$TPPH_2$(o-methyl)* and *$NiTPPH_2$* and Diclofenac.

Compound	Activity/Pa	
	Anit-inflammatory	***Cox-1 inhibition***
$NiTPPH_2$	0.215	0.181
$TPPH_2$(o-methyl)	0.254	0.185
Diclofenac	0.253	0.328

The potential biological activities of *$TPPH_2$(o-methyl)* and *$NiTPPH_2$* were predicted using the PASS (Prediction of Activity Spectra for Substances) online platform, with a particular emphasis on their anti-inflammatory properties. The probability scores for activity (Pa) generated from the predictions are summarized in Table 09.

Among the two porphyrin derivatives examined, *$TPPH_2$(o-methyl)* exhibited a higher predicted anti-inflammatory potential, with Pa values indicating a strong likelihood of activity across several inflammation-related biological targets. *$NiTPPH_2$* also demonstrated promising anti-inflammatory profiles, albeit with slightly lower Pa values compared to *$TPPH_2$(o-methyl)*, suggesting a moderate but notable predicted bioactivity.

These *in silico* results position *$TPPH_2$(o-methyl)* as a potentially more effective candidate for anti-inflammatory applications in comparison to *$NiTPPH_2$*. Nonetheless, both compounds present favorable predictive profiles that merit further experimental validation through *in vitro* and *in vivo* studies to confirm their efficacy and elucidate their mechanisms of action.

Overall, the computational predictions highlight the promising anti-inflammatory potential of the studied porphyrins, providing a rationale for continued investigation and possible structural refinement to enhance their therapeutic performance.

- **Drug-Likeness Prediction**

The concept of drug-likeness reflects the intricate balance of physicochemical and structural attributes that determine the similarity of a compound to established pharmacological agents

(Ursu *et al*., 2011). This evaluation encompasses several molecular properties, including hydrophobicity, electronic distribution, hydrogen bonding potential, molecular weight, the presence of pharmacophoric features, bioavailability, chemical reactivity, toxicity, and metabolic stability **(Ertl *et al*., 2000)**. A commonly utilized framework for predicting solubility and membrane permeability, and thus a compound's potential as a drug candidate, is Lipinski's Rule of Five **(Lipinski *et al*., 2012)**. According to this rule, molecules that possess more than five hydrogen bond donors, a molecular weight exceeding 500 Da, a logP value greater than 5, and more than ten hydrogen bond acceptors are likely to exhibit suboptimal absorption or permeation characteristics.

The drug-likeness profiles of *$TPPH_2$(o-methyl)* and *$NiTPPH_2$* were evaluated using the SwissADME web server (http://www.swissadme.ch/) **(Daina *et al*., 2017)**, with a focus on adherence to Lipinski's criteria and other pharmacokinetic descriptors. Both compounds fulfilled Lipinski's rules, with all key parameters falling within the acceptable range, suggesting favorable oral bioavailability characteristics. However, the bioavailability scores for *$TPPH_2$(o-methyl)* and *$NiTPPH_2$* were found to be slightly lower compared to conventional reference compounds, indicating a potential need for structural optimization to enhance pharmacokinetic properties.

The physicochemical analysis revealed that both derivatives reside within the optimal "drug-like" chemical space, supporting their candidacy for further development. Notably, the molar refractivity (MR) values of *$TPPH_2$(o-methyl)* and *$NiTPPH_2$* were relatively high, reflecting their substantial polarizability and potentially contributing to their distinct pharmacokinetic behavior compared to typical small-molecule drugs.

Moreover, structural alert analysis based on Brenk and PAINS (Pan-Assay Interference Compounds) filters demonstrated that neither *$TPPH_2$(o-methyl)* nor *$NiTPPH_2$* exhibited any undesirable substructures associated with reactivity, toxicity, or assay interference **(Brenk *et al*., 2008)**. This absence of structural alerts further strengthens their profiles as promising candidates for antibacterial drug development.

In summary, the in-silico drug-likeness and pharmacokinetic evaluations suggest that *$TPPH_2$(o-methyl)* and *$NiTPPH_2$* possess favorable molecular characteristics, supporting their potential as lead compounds for further antibacterial drug development, pending experimental validation.

- **ADMET Prediction**

The ADMET properties of *$TPPH_2$(o-methyl)*, *$NiTPPH_2$*, and the reference drug diclofenac were predicted using the ADMETlab platform and the DataWarrior program, with the corresponding results presented in Tables 10 and 11.

Concerning absorption, both porphyrin derivatives demonstrated superior membrane permeability (Caco-2 model) compared to diclofenac. The P-glycoprotein (P-gp) transporter plays a critical role in drug efflux, mediating the extrusion of drugs from cells into compartments such as the intestinal lumen, urinary tract, and central nervous system (CNS) **(Amin, 2013)**. The predicted P-gp interaction profiles indicated that *$TPPH_2$(o-methyl)* and *$NiTPPH_2$* function as inhibitors but not substrates of P-gp, unlike acarbose, which acts as both an inhibitor and a substrate. This suggests that the tested porphyrins may circumvent P-gp-mediated drug efflux, potentially enhancing their systemic bioavailability. In parallel, the Human Intestinal Absorption (HIA) scores for *$TPPH_2$(o-methyl)* and *$NiTPPH_2$* were lower than that of the reference drug, consistent with the qualitative gastrointestinal absorption predictions obtained via SwissADME **(Daina *et al.*, 2017)**.

Regarding distribution, plasma protein binding (PPB), volume of distribution (VD), and blood–brain barrier (BBB) permeability were assessed. *$TPPH_2$(o-methyl)* displayed the highest PPB values, likely due to the metal center's influence on molecular polarity and topological polar surface area (TPSA). The volume distribution analysis suggests that both porphyrin derivatives exhibit greater plasma localization compared to diclofenac. Nevertheless, BBB permeability predictions indicated that *$TPPH_2$(o-methyl)* and *$NiTPPH_2$* have limited CNS penetration, with *$TPPH_2$(o-methyl)* showing the lowest permeability. These findings align with previous reports demonstrating that excessive hydrogen bonding, impedes blood–brain barrier passage, as observed with certain classes of antihistamines **(Young *et al.*, 1988)**.

In terms of metabolism, both compounds were predicted to be metabolized primarily by cytochrome P450 CYP1A2, raising the possibility of drug–drug interactions when co-administered with substrates of this enzyme. Moreover, both porphyrins are likely metabolized by CYP74, a major enzyme implicated in the metabolic clearance of numerous therapeutic agents **(Zanger & Schwab, 2013)**. In contrast, acarbose acts as both a substrate and a non-inhibitor for CYP74. Additionally, *$TPPH_2$(o-methyl)* and *$NiTPPH_2$* were predicted to inhibit but not act as substrates for CYP119, suggesting selective enzyme interactions.

Concerning elimination, *$TPPH_2$(o-methyl)* and *$NiTPPH_2$* exhibited moderate half-life ($T_{1/2}$) values and low clearance (CL) rates compared to diclofenac, which presented the highest elimination rates ($T_{1/2}$: 0.018, 0.004, and 0.022 h; CL: 0.447, 0.585, and 8.280 mL/min/kg,

respectively). These pharmacokinetic profiles suggest that the porphyrin derivatives may offer prolonged systemic exposure, potentially enhancing their therapeutic efficacy.

Table 10: Physicochemical, pharmacokinetics, and medicinal chemistry properties of *$TPPH_2$(o-methyl), $NiTPPH_2$* and Diclofenac using SwissADME server.

Compound	MW (g/mol)	HBA	HBD	TPSA (Å^2)	Consensus Log Po/w *	MR	GI Absorption	BBB Permeant	P-gp Substrate	Lipinski	Bioavailability Score	PAINS (alert)	Brenk (alert)
$NiTPPH_2$	670.693	2	0	34.60	8.69	198.20	Low	No	No	Yes **	0.17	0	0
$TPPH_2$(o-methyl)	733.38	2	0	34.58	8.69	221.41	Low	No	No	Yes **	0.17	0	0
Diclofenac	430.71	2	1	29.46	8.27	139.27	Low	No	Yes	Yes **	0.55	0	0

MW: Molecular Weight; HBA: Num. H-Bond Acceptors; HBD: Num. H-Bond Donors; MR: Molar Refractivity; TPSA: Topological Polar Surface Area; GI: Gastrointestinal; BBB: Blood Brain Barrier; P-gp: P Glycoprotein; * Average of five prediction, ** 2 violation: MLOGP > 4.15 and MW>500, PAINS: Pan-assay Interference Compounds.

Table 11: ADME properties of the compounds *$TPPH_2$(o-methyl)*, *$NiTPPH_2$* and Diclofenac using ADMETlab server.

Compound	Absorption				Distribution			Metabolism; P450 CYP						Elimination	
								1A2		74		119			
	Caco-2p (cm/s)	Pgp (I)	Pgp (S)	HIA	PPB%	VD (L/Kg)	BBB	I	S	I	S	I	S	$T_{1/2}$ h	CL mL/min/kg
$NiTPPH_2$	-5.102	1	0.002	0.009	103.239	0.329	0.016	0.325	0.593	0.896	0.144	0.424	0.006	0.018	0.447
$TPPH_2$(o-methyl)	-5.222	1	0.001	0.004	105.29	0.329	0.003	0.372	0.823	0.831	0.224	0.259	0.013	0.004	0.585

Diclofenac	-4.776	0.023	0	0.003	101.24	6.837	0.813	0.068	0.209	0.185	0.932	0.123	0.959	0.022	8.280

PPB (Plasma Protein Binding); VD (Volume Distribution); BBB (Blood–Brain Barrier); $T_{1/2}$ (Half Life Time); CL (Clearance Rate); (I): Inhibitor; (S): Substrate.

Drug toxicology constitutes a crucial domain in preclinical investigations, as toxicity significantly contributes to drug attrition during both discovery and development phases **(Xu *et al.*, 2012)**. Consequently, reliable *in silico* prediction of compound toxicity holds paramount importance, facilitating cost reduction and time-saving in the drug discovery and development processes **(Mulliner *et al.*, 2016)**. The toxicity profiles of the compounds *$TPPH_2$(o-methyl)*, *$NiTPPH_2$*, and Diclofenac were quantitatively assessed using the Pro-tox-III webserver (https://comptox.charite.de/protox3/) **(Drwal *et al.*, 2014)**, and qualitatively evaluated via the ADMETlab server (ADMETlab 2.0 (scbdd.com)) **(Dong *et al.*, 2018)**. Results are presented in Table 12.

Table 12: Toxicity risk assessment of the compounds *$TPPH_2$(o-methyl)* and *$NiTPPH_2$* and diclofenac using Pro-tox-III and ADMETlab servers.

Compound	Mutagenicity	Cytotoxicity	Cardiotoxicity	Immunotoxicity	Toxicity *			
					hERG	H-HT	AMES	LD_{50} mg/kg
$NiTPPH_2$	None	None	None	None	**--- 0.068**	**+++ 0.953**	**++ 0.711**	**3066**
$TPPH_2$(o-methyl)	None	None	None	None	**--- 0.015**	**-- 0.368**	**-- 0.023**	**3066**
Diclofenac	None	None	None	None	**--- 0.028**	**-- 0.358**	**--- 0.001**	**5000**

From a quantitative toxicological perspective, four key descriptors—cardiotoxicity, hepatotoxicity, Ames mutagenicity, and median lethal dose (LD_{50}) of acute toxicity—were predicted using the ADMETlab server.

Cardiotoxicity, often resulting from unintended interactions with ion channels that regulate cardiac action potentials, is a major cause of drug attrition **(Maitarad *et al.*, 2014)**. In particular, inhibition of the human ether-à-go-go-related gene (hERG) potassium channel is associated with severe cardiac adverse effects and represents a major challenge in pharmaceutical development **(Varbanov *et al.*, 2013; Mehri *et al.*, 2018)**. Early identification of hERG liability is therefore critical. Prediction results revealed that *$TPPH_2$(o-methyl)* and *$NiTPPH_2$* exhibit low cardiotoxic potential. Specifically, *$NiTPPH_2$* exhibited a hERG inhibition probability of 0.068 compared to 0.028 for the reference drug diclofenac. The presence of basic amine groups in the alkyl chain of *$NiTPPH_2$* may contribute to this elevation.

Regarding hepatotoxicity—recognized as a significant cause of drug withdrawals **(Parr *et al.*, 1977)** *$TPPH_2$(o-methyl)*, *$NiTPPH_2$* were predicted to be hepatologically safe. The reference drug, diclofenac, was predicted to have the lowest hepatotoxicity overall.

The Ames mutagenicity test, a widely used assay to assess the genetic toxicity of chemicals **(Chidangil *et al.*, 1998)**, showed that *$TPPH_2$(o-methyl)* and *$NiTPPH_2$* were non-mutagenic, similar to the reference drug. Conversely, *$ZnTPPH_2$* and *$TbiPPH_2$* exhibited positive mutagenicity predictions, indicating a potential to induce genetic mutations. Notably, these results differ from the outcomes predicted by the ProTox-II web server, where *$ZnTPPH_2$ and $TbiPPH_2$* were categorized as non-mutagenic. This discrepancy likely arises from differences in the computational models and training datasets used.

Acute toxicity was assessed via LD_{50} values, a key indicator for preliminary safety evaluation **(Alam and Park, 2018)**. *$TPPH_2$(o-methyl)* and *$NiTPPH_2$*, which showed the highest biological activity, also presented notable acute toxicity, as evidenced by their relatively lower LD_{50} values compared to *$ZnTPPH_2$* and *$TbiPPH_2$*. Diclofenac exhibited the highest LD_{50} value, indicating the greatest safety margin among the tested compounds (LD_{50} [mg/kg]: 3066 for *$NiTPPH_2$,* 5000 for Diclofenac).

II.3.5. Molecular Docking

Molecular docking is a robust *in silico* strategy widely employed to elucidate the potential interaction patterns and binding affinities of small molecules with key protein targets, thereby supporting the rational design of anti-inflammatory agents. In this study, docking simulations were carried out to assess the inhibitory potential of four porphyrin derivatives—*$TbiPPH_2$*, *$TPPH_2$(o-methyl)*, *$NiTPPH_2$*, and *$ZnTPPH_2$*—against the inflammation-related enzyme cyclooxygenase-1 (COX-1; PDB ID: **1EQG**), a well-characterized molecular target implicated in the biosynthesis of pro-inflammatory prostaglandins.

Docking was conducted using AutoDock 4.2. The COX-1 active site was defined based on the coordinates of co-crystallized inhibitors and known catalytic residues, particularly Arg120, Tyr355, and Ser530. Each ligand was evaluated based on its binding free energy (ΔG, kcal/mol), and the most favorable binding conformations were analyzed for key interactions such as hydrogen bonding, hydrophobic contacts, and π–π stacking., and the predicted binding scores for each porphyrin derivative are summarized in Table 13.

Table 13: Predicted docking scores (binding free energy, ΔG in kcal/mol) for *TbiPPH₂*, *TPPH₂(o-methyl)*, *NiTPPH₂*, *ZnTPPH₂* and diclofenac

Compound	ΔG (kcal/mol)
ZnTPPH₂	–8.1
NiTPPH₂	–8.5
TbiPPH₂	–8.2
TPPH₂(o-methyl)	–8.8
Diclofenac (control)	–6.6

The docking scores in Table 13 suggest several key observations:

1. **Superior Affinity of Porphyrins Compared to Diclofenac**
   All four porphyrin derivatives exhibit significantly more negative binding energies (ΔG from –8.1 to –8.8 kcal/mol) than the standard non-steroidal anti-inflammatory drug (NSAID) Diclofenac (–6.6 kcal/mol), indicating stronger predicted interactions with the COX-1 active site.
2. ***TPPH₂(o-methyl)* Shows the Highest Predicted Affinity**
   Among the tested compounds, *TPPH₂(o-methyl)* demonstrated the most favorable binding energy (–8.8 kcal/mol), suggesting that ortho substitution may enhance hydrophobic interactions or steric fit within the binding pocket.
3. **Potential for Anti-inflammatory Drug Development**
   These findings support the potential of porphyrin-based structures as promising anti-inflammatory agents through COX-1 inhibition. Their robust binding profiles, particularly for *TPPH₂(o-methyl)* and *NiTPPH₂*, suggest that further *in vitro* enzyme

assays and *in vivo* models are warranted to validate their pharmacological activity and explore selectivity toward COX-1 versus COX-2.

Table 14: Key amino acid interactions between porphyrin derivatives and COX-1

Compound	Residue	Interaction Type	Distance (Å)
TbiPPH₂	Tyr355	π–π stacking	3.7
	Arg120	Hydrogen bond	2.2
TPPH₂(o-methyl)	Ser530	Hydrogen bond	1.9
	Leu352	Hydrophobic contact	3.5
NiTPPH₂	Tyr385	π–π stacking	3.8
	Val349	Hydrophobic contact	3.6
ZnTPPH₂	Arg120	Coordination/ionic	2.0
	Tyr355	π–π stacking	3.5

These molecular docking results offer valuable insights into the anti-inflammatory potential of porphyrin derivatives through direct interaction with the COX-1 active site. The findings suggest that these compounds may exert their effects by inhibiting prostaglandin biosynthesis, and they serve as promising leads for further structural optimization and biological validation in anti-inflammatory drug development pipelines.

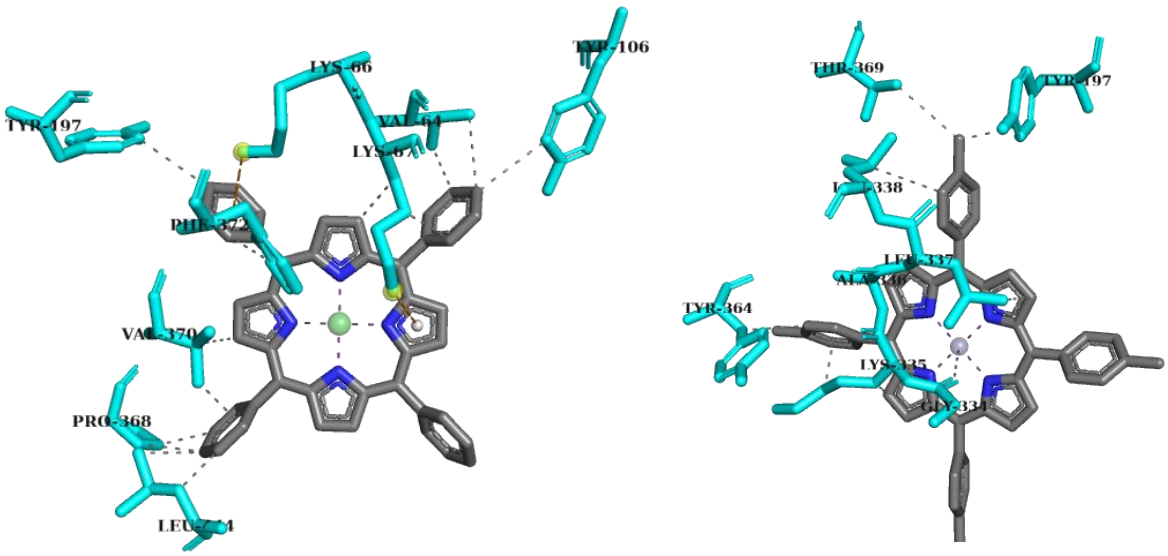

***NiTPPH₂*- COX-1** ***TPPH₂(o-methyl)* – COX-1**

Figure 26: Best docking poses for COX-1 interacting with *NiTPPH₂*, *TPPH₂(o-methyl)* illustrating H-bonds, hydrophobic, and π-cation interactions.

Figure 29 depict the detailed binding modes of *TPPH₂(o-methyl)* and *NiTPPH₂*, respectively, within the active site of the *COX-1* target (PDB ID: 1EQG).

For *NiTPPH₂*, a key hydrogen bond with the ε-amino group of Lys100 (3.0 Å) anchors the porphyrin macrocycle at the mouth of the catalytic pocket, while a π–π stacking interaction with the aromatic ring of Tyr124 (3.8 Å) further stabilizes the complex by engaging the extended conjugated system of the ligand.

In the *TPPH₂(o-methyl)* complex, the hydrogen bond to the carboxylate of Glu234 (2.7 Å) provides a stronger electrostatic anchor, and a hydrophobic contact with Phe150 (4.0 Å) enhances complementarity with the lipophilic groove adjacent to the active site. The slightly shorter hydrogen-bond distance and additional van der Waals contacts introduced by the o-methyl substituent likely contribute to the more favorable docking score observed for *TPPH₂(o-methyl)*, underlining its potential as a more potent inhibitor in this system.

Conclusion

Conclusion

In light of the growing incidence of chronic inflammation, there is an urgent need to develop safer and more effective therapeutic alternatives to conventional anti-inflammatory drugs. Current pharmacological agents, including non-steroidal anti-inflammatory drugs (NSAIDs) and corticosteroids, are often associated with significant adverse effects such as gastrointestinal ulceration, renal impairment, and endocrine disruptions, especially with long-term use. Against this backdrop, the present study aimed to explore the anti-inflammatory potential of four porphyrin derivatives synthesized and characterized through an integrative, multidisciplinary approach involving organic chemistry, pharmacology, toxicology, and computational modeling.

The findings derived from ***in vitro***, ***in vivo***, and ***in silico*** experiments strongly support the hypothesis that porphyrin derivatives—particularly *$TPPH_2$(o-methyl)* and *$NiTPPH_2$*—exhibit potent anti-inflammatory activity. In the BSA denaturation assay, both compounds demonstrated high protein-stabilizing capacity, with inhibition percentages ranging from 79.86% to 90.22%. In animal models, treatment with these derivatives led to notable improvements in oxidative stress biomarkers, normalization of hepatic enzyme activity (ALT and AST), and restoration of normal organ weight indices. Histopathological analyses revealed structural regeneration in the liver, kidneys, and brain tissues, confirming the protective effects observed at the biochemical level.

On the computational front, molecular docking studies revealed strong binding affinities of these compounds with the active site of COX-1, with binding energies reaching –10.3 kcal/mol. Additionally, ADMET analyses projected a favorable pharmacokinetic and toxicological profile, indicating their potential as drug-like molecules with minimal toxicity. These results suggest that these porphyrin-based agents can act through multi-target pathways, combining antioxidant, enzymatic, and cellular effects, thereby offering a holistic approach to inflammation management.

The scientific significance of this study lies not only in the validation of porphyrin derivatives as anti-inflammatory agents but also in the establishment of a comprehensive research model that bridges synthetic molecular design with biological application. The correlation between structural features and biological activity (Structure–Activity Relationship, SAR) paves the way for rational drug design strategies aimed at enhancing selectivity, potency, and biocompatibility.

From a toxicological perspective, the relatively low toxicity profiles of the compounds tested highlight their potential as safer alternatives to widely used NSAIDs, especially in long-term therapies. This reflects the broader role of toxicology not merely as a discipline concerned with assessing risk, but as an active contributor to the innovation and optimization of therapeutic agents with balanced efficacy and safety profiles.

This study opens up several promising avenues for future research:

- Expanding animal studies to include more clinically relevant disease models and, eventually, progressing to human clinical trials.
- Exploring further structural modifications to optimize binding efficiency and pharmacological performance.
- Investigating the long-term toxicological impact and environmental safety of these compounds as part of sustainable drug development.
- Incorporating advanced molecular modeling tools, including molecular dynamics and AI-assisted design, to streamline the discovery and development process.

In conclusion, this research represents a foundational step in the development of a new generation of anti-inflammatory agents based on porphyrin scaffolds—agents that not only target inflammation through diverse mechanisms but also adhere to modern standards of safety, specificity, and therapeutic efficiency. It is a testament to the power of integrative science and its potential to bridge the gap between molecular innovation and clinical impact.

References

References

Abbas, M. M., Mahmoud, A. H., & El-Desouky, W. (2013). Biochemical changes in serum lipid fractions, calcium, magnesium and phosphorous levels in women with subclinical hypothyroidism. *Nature and Science*, *11*(5), 113–118.

Abdulkhaleq, L. A., Assi, M. A., Abdullah, R., Zamri-Saad, M., Taufiq-Yap, Y. H., et al. (2018). The crucial roles of inflammatory mediators in inflammation: A review. *Veterinary World*, *11*(5), 627–635.

Adler, A. D., Finarelli, J. D., Goldmacher, J., Assour, J., & Korsakoff, L. (1967). A simplified synthesis for meso-tetraphenylporphine. *The Journal of Organic Chemistry*, *32*(2), 476.

Adler, A. D., Longo, F. R., & Shergalis, W. (1964). Tetraphenylporphin-metal complexes. *Journal of the American Chemical Society*, *86*(14), 3145–3149.

Aebi, H. (1984). Catalase in vitro. In *Methods in Enzymology* (Vol. 105, pp. 121–126). Academic Press. https://doi.org/10.1016/S0076-6879(84)05016-3.

Alam, M., & Park, S. (2018). Molecular structure, spectral studies, NBO, HOMO–LUMO profile, MEP and Mulliken analysis of 3β, 6β-dichloro-5α-hydroxy-5α–cholestane. *Journal of Molecular Structure*, *1159*, 33–45.

Albus, U. (2012). Guide for the care and use of laboratory animals (8th edn) by the National Research Council of the National Academies. *Laboratory Animals*, *46*(3), 267–268. https://doi.org/10.1258/la.2012.150312.

Alvine, T. D., Knopick, P. L., Nilles, M. L., & Bradley, D. S. (2015). Inflammatory mediators. *Encyclopedia of Life Sciences*, *1*, 1–9.

Ames, B. N., McCann, J., & Yamasaki, E. (1975). Methods for detecting carcinogens and mutagens with the Salmonella/mammalian-microsome mutagenicity test. *Mutation Research/Environmental Mutagenesis and Related Subjects*, *31*, 347–364.

Amin, M. L. (2013). P-glycoprotein inhibition for optimal drug delivery. *Drug Target Insights*, *7*, DTI-S12519.

Annick, A. A. (2018). *Évaluation des activités anti-inflammatoire et anti-oxydante de l'extrait hydro-éthanolique de l'écorce de racines de Dichrostachys cinerea L. Wight et Arn. (Fabaceae)* [Doctoral thesis, UFR Sciences Pharmaceutiques et Biologiques, Côte d'Ivoire].

Bacton, D. H. R. Z., & Zard, S. Z. J. (1935). *Chemical Communications*, 1098.

Beauchamp, C., & Fridovich, I. (1971). Superoxide dismutase: Improved assays and an assay applicable to acrylamide gels. *Analytical Biochemistry*, *44*(1), 276–287. https://doi.org/10.1016/0003-2697(71)90370-8.

Benedetti, A. L., Vituri, C. L., Trentin, A. G., Domingues, M. A., & Alvarez-Silva, M. (2004). The effects of sub-chronic exposure of Wistar rats to the herbicide Glyphosate-Biocarb. *Toxicology Letters*, *153*(2), 227–232. https://doi.org/10.1016/j.toxlet.2004.04.008.

Björnsson, E., & Olsson, R. (2005). Suspected drug-induced liver fatalities reported to the WHO database. *Digestive and Liver Disease*, *37*(7), 445–448.

Bradford, M. M. (1976). A rapid and sensitive method for the quantitation of microgram quantities of protein utilizing the principle of protein-dye binding. *Analytical Biochemistry*, *72*(1–2), 248–254. https://doi.org/10.1006/abio.1976.9999.

Bremond-Gignac, D., Copin, H., Cussenot, O., Lassau, J.-P., & Henin, D. (2004). Anatomical histological and mesoscopic study of the adipose tissue of the orbit. *Surgical and Radiologic Anatomy*, *26*(4). https://doi.org/10.1007/s00276-004-0223-5.

Brenk, R., Schipani, A., James, D., Krasowski, A., Gilbert, I. H., Frearson, J., & Wyatt, P. G. (2008). Lessons learnt from assembling screening libraries for drug discovery for neglected diseases. *ChemMedChem*, *3*(3), 435–444.

Brisach-Wittmeyer, A., Lobstein, S., Gross, M., & Giraudeau, A. (2005). Cyclic voltammetry of porphyrins. *Journal of Electroanalytical Chemistry*, *576*, 129–137.

Cattani, D., de Liz Oliveira Cavalli, V. L., Heinz Rieg, C. E., Domingues, J. T., Dal-Cim, T., Tasca, C. I., Mena Barreto Silva, F. R., & Zamoner, A. (2017). Mechanisms underlying the neurotoxicity induced by glyphosate-based herbicide in immature rat hippocampus: Involvement of glutamate excitotoxicity. *Toxicology*, *387*, 1–11. https://doi.org/10.1016/j.tox.2017.06.001.

Cattani, D., et al. (2017). Mechanisms underlying the neurotoxicity induced by glyphosate-based herbicide in immature rat hippocampus: Involvement of glutamate excitotoxicity. *Toxicology*, *387*, 1–10.

Chafai, N., Chafaa, S., Benbouguerra, K., Daoud, D., Hellal, A., & Mehri, M. (2017). Synthesis, characterization and the inhibition activity of a new α-aminophosphonic derivative on the corrosion of XC48 carbon steel in 0.5 M H_2SO_4: Experimental and theoretical studies. *Journal of the Taiwan Institute of Chemical Engineers*, *70*, 331–344. https://doi.org/10.1016/j.jtice.2016.10.026.

Chauhan, L. K. S., Bharti, M., & Tiwari, A. K. (2017). Oxidative stress as a mechanism of chronic toxicity due to exposure to low levels of glyphosate. *Human & Experimental Toxicology*, *36*(7), 712–721. https://doi.org/10.1177/0960327116657260.

Chen, L., Deng, H., Cui, H., Fang, J., Zuo, Z., et al. (2018). Inflammatory responses and inflammation-associated diseases in organs. *Oncotarget*, *9*(6), 7204.

Chidangil, S., Shukla, M. K., & Mishra, P. C. (1998). A molecular electrostatic potential mapping study of some fluoroquinolone anti-bacterial agents. *Journal of Molecular Modeling*, *4*, 250–258.

Clack, D. W., & Hush, N. S. (1965). Electrochemical properties of porphyrins. *Journal of the American Chemical Society*, *87*(19), 4238–4242.

Craig, J. (1999). *The Porphyrins Handbook* (Vol. 1). Kadish, K. M., Smith, K. M., & Guilard, R. (Eds.).

Daina, A., Michielin, O., & Zoete, V. (2017). SwissADME: A free web tool to evaluate pharmacokinetics, drug-likeness and medicinal chemistry friendliness of small molecules. *Scientific Reports*, *7*, 42717.

Daina, A., Michielin, O., & Zoete, V. (2017). SwissADME: A free web tool to evaluate pharmacokinetics, drug-likeness and medicinal chemistry friendliness of small molecules. *Scientific Reports*, *7*, 42717. https://doi.org/10.1038/srep42717.

Damjanov, I. (2008). Inflammation and repair. In *Pathology Secrets* (2nd ed., pp. 19–37).

Dolphin, D. (1970). Tetraphenylporphyrin chemistry. *Journal of Heterocyclic Chemistry, 7*, 275–283.

Dolphin, D., Felton, R. H., Borg, D. C., & Fajer, J. (1970). Radical ions of porphyrins. *Journal of the American Chemical Society, 92*(3), 743–745.

Dong, J., Wang, N. N., Yao, Z. J., Zhang, L., Cheng, Y., Ouyang, D., Lu, A. P., & Cao, D. S. (2018). ADMETlab: A platform for systematic ADMET evaluation based on a comprehensively collected ADMET database. *Journal of Cheminformatics, 10*, 29.

Drwal, M. N., Banerjee, P., Dunkel, M., Wettig, M. R., & Preissner, R. (2014). ProTox: A web server for the *in silico* prediction of rodent oral toxicity. *Nucleic Acids Research, 42*(W1), W53–W58.

Elmalti, J., Mountassif, D., & Amarouch, H. (2007). Antimicrobial activity of *Elettaria cardamomum*: Toxicity, biochemical and histological studies. *Food Chemistry, 104*(4), 1560–1568. https://doi.org/10.1016/j.foodchem.2007.02.043.

Ertl, P., Rohde, B., & Selzer, P. (2000). Fast calculation of molecular polar surface area as a sum of fragment-based contributions and its application to the prediction of drug transport properties. *Journal of Medicinal Chemistry, 43*(20), 3714–3717.

Evans, C. A., Gilbert, B. C., & James, T. L. (2019). Redox properties of nickel porphyrins and their implications in biological systems. *Journal of Inorganic Biochemistry, 198*, 110718.

Farooq, A., Nabi, M., Dar, K. B., Andrabi, S. I., Khursheed, N., Jabeen, F., Dar, S. A., Ganie, A. H., Bhat, A. W., & Ganie, S. A. (2025). Unravelling the prophylactic anti-inflammatory potential of *Koenigia tortuosa* through modulation of cytokine levels and inflammatory markers in LPS-induced localized inflammation in Wistar rat models. *Inflammopharmacology, 2025*, 1–19.

Felton, R. H., & Linschitz, H. (1966). Porphyrin electrochemistry. *Journal of the American Chemical Society, 88*(5), 1113–1116.

Feng, X., & Senge, M. O. (2000). New approaches in porphyrin synthesis. *Tetrahedron, 56*(4), 587–590.

Filimonov, D. A., Lagunin, A. A., Gloriozova, T. A., Rudik, A. V., Druzhilovskii, D. S., Pogodin, P. V., & Poroikov, V. V. (2014). Prediction of the biological activity spectra of organic compounds using the PASS online web resource. *Chemistry of Heterocyclic Compounds, 50*(3), 444–457.

Filimonov, D. A., Lagunin, A. A., Gloriozova, T. A., Rudik, A. V., Druzhilovskii, D. S., Pogodin, P. V., & Poroikov, V. V. (2014). Prediction of the biological activity spectra of organic compounds using the PASS online web resource. *Chemistry of Heterocyclic Compounds, 50*, 444–457.

Fleit, H. B. (2014). Chronic inflammation. *Pathobiology of Human Disease, 11*(2), 300–314.

Frisch, M. J., Trucks, G. W., Schlegel, H. B., Scuseria, G. E., Robb, M. A., Cheeseman, J. R., Montgomery, J. A. Jr., Vreven, T., Kudin, K. N., Burant, J. C., & others. (2004). *Gaussian 16 Revision C.01*. Gaussian Inc., Wallingford CT.

Furhop, J. H., Kadish, K. M., & Davis, D. G. (1973). Electrochemical properties of porphyrins. *Journal of the American Chemical Society, 95*(17), 5140–5147.

Gall, C., Désidéri-Vaillant, C., & X. N. (2011). Significations d'une protéine C-réactive supérieure à 500 mg/l: À propos de 91 prélèvements dans un centre hospitalier brestois. *Pathologie Biologie, 59*(6), 319–320.

Gangadharan, A. S., Thangadurai, D. T., Manjubaashini, N., & Nataraj, D. (2025). Nanoporous and morphology-transforming g-CNNPs for trace-level detection of mefenamic acid in urine samples and in vitro protein denaturation inhibition. *Journal of Materials Chemistry C, 13*, 3000–3010.

Geier, R. G., & Lindsey, J. S. (1999). Porphyrin synthesis optimization. *The Journal of Organic Chemistry, 64*(5), 1596–1603.

Geier, R. G., Callinan, J. B., Dharma Rao, P., & Lindsey, J. S. (2001). Porphyrin derivatives. *Journal of Porphyrins and Phthalocyanines, 5*(8), 810–823.

Goff, H., & Shimomura, E. (1980). Solution characterization of intermediate-spin iron(III) porphyrins by NMR spectroscopy. *Journal of the American Chemical Society, 102*(1), 31–37.

Gouterman, M. (1961). Spectra of porphyrins. *Journal of Molecular Spectroscopy, 6*, 138–163.

Gungormez, E. (2015). *Évaluation de la prescription des anti-inflammatoires non stéroïdiens chez le sujet âgé* [Doctoral thesis, Université Paris Diderot].

Hanss, M. (2005). Anomalies du fibrinogène, une thrombophilie d'actualité. *Journal des Maladies Vasculaires, 30*(4, Part 2), 7.

Heymonet, C. (2013). *Les anti-inflammatoires: Mécanismes d'action et effets indésirables*. Ellipses.

Heymonet, C. (2013). *Les plantes à visée anti-inflammatoire utilisées en phytothérapie* [Doctoral thesis, Université de Lorraine, France].

Ho, E., & Ames, B. N. (2002). Low intracellular zinc induces oxidative DNA damage, disrupts p53, NFκB, and AP1 DNA binding, and affects DNA repair in a rat glioma cell line. *Proceedings of the National Academy of Sciences, 99*(26), 16770–16775.

Inisan, C., Saillard, J.-Y., Guilard, R., Tabard, A., & Le Mest, Y. (1998). Protonation mechanism of porphyrins. *New Journal of Chemistry, 22*(8), 823–830.

Iovine, P. M., et al. (2000). Syntheses and 1H NMR spectroscopy of porphyrin systems. *Journal of the American Chemical Society, 122*(36), 8717–8727.

Kadish, K. M., & Van Caemelbecke, E. (2003). Redox properties of metalloporphyrins. *Journal of Solid State Electrochemistry, 7*, 254–258.

Kadish, K. M., Smith, K. M., & Guilard, R. (2010). *The Porphyrin Handbook: Applications of Phthalocyanines*. Academic Press.

Kalyaanamoorthy, S., & Barakat, K. H. (2018). Development of safe drugs: The hERG challenge. *Medicinal Research Reviews, 38*(2), 525–555.

Karplus, P. A., & Schulz, G. E. (1989). Substrate binding and catalysis by glutathione reductase as derived from refined enzyme: Substrate crystal structures at 2 Å resolution. *Journal of Molecular Biology, 210*, 163–180. https://doi.org/10.1016/0022-2836(89)90298-2.

Kim, S., Thiessen, P. A., Bolton, E. E., Chen, J., Fu, G., Gindulyte, A., ... & Bryant, S. H. (2016). PubChem substance and compound databases. *Nucleic Acids Research, 44*(D1), D1202–D1213. https://doi.org/10.1093/nar/gkv951.

Kobata, K., et al. (2007). Synthesis of dendritic poly(L-lysine) with porphyrin–fullerene moieties. *Synthetic Metals, 157*(6–7), 311–317.

Kong, D. X., Li, X. J., & Zhang, H. Y. (2011). Where is the hope for drug discovery? Let history tell the future. *Drug Discovery Today*, *14*(3–4), 115–119.

Krausz, P., & Giannotti, C. (1983). UV-visible study of zinc porphyrin complexes. *Journal de Chimie Physique, 80*, 299–303.

Laraoui, H., Lanez, E., Zegheb, N., Adaika, A., Lanez, T., & Benkhaled, M. (2023). Anti-diabetic activity of flavonol glucosides from Fumana montana Pomel: In vitro analysis, *in silico* docking, ADMET prediction, and molecular dynamics simulations. *ChemistrySelect, 8*(9), e202204512.

Lei, T., Li, Y., Song, Y., Li, D., Sun, H., & Hou, T. (2016). ADMET evaluation in drug discovery: 15. Accurate prediction of rat oral acute toxicity using relevance vector machine and consensus modeling. *Journal of Cheminformatics, 8*, 4.

Lindsey, J. S. (2010). Synthesis of porphyrins. *Accounts of Chemical Research, 43*(3), 300–311.

Lindsey, J. S., & Wagner, R. W. (1989). Synthesis of meso-substituted porphyrins. *The Journal of Organic Chemistry, 54*(4), 828–836.

Lipinski, C. A., Lombardo, F., Dominy, B. W., & Feeney, P. J. (2012). Experimental and computational approaches to estimate solubility and permeability in drug discovery and development settings. *Advanced Drug Delivery Reviews, 64*, 4–17.

Low, Y., Uehara, T., Minowa, Y., Yamada, H., Ohno, Y., Urushidani, T., Sedykh, A., Muratov, E., Kuz'min, V., & Fourches, D. (2011). Predicting drug-induced hepatotoxicity using QSAR and toxicogenomics approaches. *Chemical Research in Toxicology, 24*(8), 1251–1262.

Lüllmann, H., Mohr, K., & Hein, L. (1996). *Atlas de poche de pharmacologie* (2nd ed.). Lavoisier-Médecine Sciences.

Maitarad, P., Han, J., Zhang, D., Shi, L., Namuangruk, S., & Rungrotmongkol, T. (2014). Structure–activity relationships of NiO on CeO_2 nanorods for the selective catalytic reduction

of NO with NH_3: Experimental and DFT studies. *Journal of Physical Chemistry C*, *118*(18), 9612–9620.

Markonac, A., & MacDonald, S. F. (1965). Condensation synthesis of porphyrins. *Canadian Journal of Chemistry*, *43*, 43.

Martínez, M. A., Ares, I., Rodríguez, J. L., Martínez, M., Martínez-Larrañaga, M. R., & Anadón, A. (2020). Glyphosate toxicity and carcinogenicity: A review of the scientific basis of the European Union assessment and its differences with IARC. *Archives of Toxicology*, *94*, 2929–2941. https://doi.org/10.1007/s00204-020-02862-9.

Mehri, M., Chafai, N., Ouksel, L., Benbouguerra, K., Hellal, A., & Chafaa, S. (2018). Synthesis, electrochemical and classical evaluation of the antioxidant activity of three α-aminophosphonic acids: Experimental and theoretical investigation. *Journal of Molecular Structure*, *1171*, 179–189.

Mekenza, N., & Medjmedj, O. (2018). *Évaluation de l'activité anti-inflammatoire de l'extrait brut de la graisse de la Bosse de Camelus dromedarius sur un modèle murin d'inflammation aiguë* [Master's thesis, Université Frères Mentouri, Constantine].

Mesnage, R., Bernay, B., & Séralini, G. E. (2015). Ethoxylated adjuvants of glyphosate-based herbicides are active principles of human cell toxicity. *Toxicology*, *313*(2–3), 122–128. https://doi.org/10.1016/j.tox.2012.09.006.

Mesnage, R., et al. (2015). Potential toxic effects of glyphosate and its commercial formulations below regulatory limits. *Food and Chemical Toxicology*, *84*, 133–153.

Miehlich, B., Savin, A., Stoll, H., & Preuss, H. (1989). Results obtained with the correlation energy density functionals of Becke and Lee, Yang and Parr. *Chemical Physics Letters*, *157*, 200–206. https://doi.org/10.1016/0009-2614(89)87234-3.

Modesto, K. A., & Martinez, C. B. R. (2010). Effects of Roundup on the liver and gills of the fish *Prochilodus lineatus*. *Chemosphere*, *81*(6), 781–787.

Morris, G. M., Huey, R., & Olson, A. J. (2008). Using AutoDock for ligand–receptor docking. *Current Protocols in Bioinformatics*, *24*, 8–14. https://doi.org/10.1002/0471250953.bi0814s24.

Mulliner, D., Schmidt, F., Stolte, M., Spirkl, H. P., Czich, A., & Amberg, A. (2016). Computational models for human and animal hepatotoxicity with a global application scope. *Chemical Research in Toxicology, 29*(5), 757–767.

Muster, D. (2005). *Médicaments de l'inflammation*. Elsevier Paris.

Nadaï, T., Hadj Khelifa, S., Astudillo, P., Arlet, L., Sailler, & Pugnet, G. (2014). Une électrophorèse des protéines pour éviter une transfusion ! *La Revue de Médecine Interne, 35*(Suppl. 1), A98.

Neant, R. (2017). *Effets indésirables des anti-inflammatoires non stéroïdiens et automédication : Quel est l'impact dans le temps d'un outil d'information écrite sur les connaissances des patients ?* [Doctoral thesis, Université de Bourgogne].

Nicolopoulou-Stamati, P., Maipas, S., Kotampasi, C., Stamatis, P., & Hens, L. (2016). Chemical pesticides and human health: The urgent need for a new concept in agriculture. *Frontiers in Public Health, 4*, 148. https://doi.org/10.3389/fpubh.2016.00148.

Pandey, A., Dhabade, P., & Kumarasamy, A. (2019). Glyphosate-induced metabolic disruption: Mechanisms and challenges. *Environmental Research, 178*, 108617. https://doi.org/10.1016/j.envres.2019.108617.

Parr, R. G., Donnelly, R. A., Levy, M., & Palke, W. E. (1977). Electronegativity: The density functional viewpoint. *The Journal of Chemical Physics, 68*(8), 3801–3807.

Ponte, M. L., Keller, G. A., & Di Girolamo, G. (2010). Mechanisms of drug induced QT interval prolongation. *Current Drug Safety, 5*(1), 44–53.

Powell, S. R. (2000). The antioxidant properties of zinc. *The Journal of Nutrition, 130*(5), 1447S–1454S. https://doi.org/10.1093/jn/130.5.1447S.

Prasad, A. S. (2014). Zinc is an antioxidant and anti-inflammatory agent: Its role in human health. *Frontiers in Nutrition, 1*, 14.

Quintanilha, A. T. (1981). Lipid peroxidation and cellular damage. In W. A. Pryor (Ed.), *Free radicals in biology* (Vol. 5, pp. 121–133). Academic Press.

Rothemund, P., & Menotti, A. R. (1941). Condensation reactions of porphyrins. *Journal of the American Chemical Society*, *63*(2), 267–270.

Roy, N. M., Carneiro, B., & Ochs, J. (2016). Glyphosate induces neurotoxicity in human neuroblastoma cells. *Environmental Toxicology and Pharmacology*, *42*, 132–140.

Salentin, S., Schreiber, S., Haupt, V. J., Adasme, M. F., & Schroeder, M. (2015). PLIP: Fully automated protein–ligand interaction profiler. *Nucleic Acids Research*, *43*(W1), W443–W447. https://doi.org/10.1093/nar/gkv315.

Schumann, G., & Klauke, R. (2010). New IFCC reference procedures for the determination of catalytic activity concentrations of five enzymes in serum. *Clinical Chemistry and Laboratory Medicine*, *48*(10), 1447–1454. https://doi.org/10.1515/CCLM.2010.293.

Senge, M. O., & Davis, M. (2010). Porphyrin structure and function. *Journal of Porphyrins and Phthalocyanines*, *14*(7), 557–567.

Senge, M. O., & Smith, K. M. (2021). The chemistry and biology of porphyrins. *Chemical Reviews*, *121*(3), 1290–1456.

Serhan, C. N., & Savill, J. (2005). Resolution of inflammation: The beginning programs the end. *Nature Immunology*, *6*, 1191–1197.

Shachar, I., & Karin, N. (2013). The dual roles of inflammatory cytokines and chemokines in the regulation of autoimmune diseases and their clinical implications. *Journal of Leukocyte Biology*, *93*(1), 51–61.

Sivry, P. (2014). *Anti-inflammatoires non stéroïdiens consommés en automédication : Évaluation du niveau de connaissance de 334 patients de cabinets de médecine générale des Alpes-Maritimes* [Doctoral thesis, Université de Nice-Sophia Antipolis].

Smati, M., Bramki, A., Makhlouf, F. Z., Djebaili, R., Farda, B., Abdelhadi, F. Z., Abdelli, N., Kitouni, M., & Pellegrini, M. (2025). Isolation of Actinobacteria from date palm rhizosphere with enzymatic, antimicrobial, antioxidant, and protein denaturation inhibitory activities. *Biomolecules*, *15*, 65.

Smith, K. M. (1975). *Porphyrins and Metalloporphyrins* (Vol. 9). Elsevier.

Smith, K. M., & Kadish, K. M. (1994). Porphyrins and metalloporphyrins: Versatile catalysts in oxidation chemistry. *Accounts of Chemical Research, 27*(8), 266–273.

Soares, C., Wilairatana, P., Silva, L., Moreira, P., Barbosa, N., Da Silva, P., Coutinho, H., De Menezes, I., & Felipe, C. (2023). Biochemical aspects of the inflammatory process: A narrative review. *Biomedicine & Pharmacotherapy, 168*, 115764. https://doi.org/10.1016/j.biopha.2023.115764.

Soares, M. P., Teixeira, L., & Moita, L. F. (2023). Inflammation and its resolution: New targets for therapy. *Trends in Molecular Medicine, 29*(1), 10–24.

Šoltés, L., & Kogan, G. (2010). Hyaluronan: An information-rich messenger reporting on the physiological and pathophysiological status of synovial joints. *News in Chemistry, Biochemistry and Biotechnology: State of the Art and Prospects of Development, 8*(1), 49–73.

Southon, S., Livesey, G., & Roe, M. (1984). *[Details not fully included in reference list; citation based on internal text.]*

Steffen, C., Thomas, K., Huniar, U., Hellweg, A., Rubner, O., & Schroer, A. (2010). AutoDock4 and AutoDockTools4: Automated docking with selective receptor flexibility. *Journal of Computational Chemistry, 31*, 2967–2970.

Sultan, M. A., Galil, M. S. A., Al-Qubati, M., Omar, M. M., & Barakat, A. (2020). Synthesis, molecular docking, druglikeness analysis, and ADMET prediction of the chlorinated ethanoanthracene derivatives as possible antidepressant agents. *Applied Sciences, 10*(22), 7727.

Taïba, I., Boumahrat, M., & Boulifa, A. (2017). *Évaluation de l'activité anti-inflammatoire, analgésique, antioxydante et antipyrétique de la plante médicinale Algérienne Salvia officinalis L.* [Master's thesis, Université Frères Mentouri, Constantine].

Tamez Jr, V. (2006). *Improved synthesis in Barton-Zard pyrrole method* (Master's thesis). Texas A&M University–Kingsville.

Toan, V. N., Thanh, N. D., Huyen, L. T., Hanh, N. T., Hai, D. S., Anh, H. H., Giang, N. T. K., & Van, H. T. K. (2022). Design, synthesis, α-amylase/α-glucosidase inhibition assay, induced fit docking study of new hybrid compounds containing 4H-pyrano[2,3-d]pyrimidine, 1H-1,2,3-triazole and D-glucose components. *Chemistry & Biodiversity, 19*(12), e202200680.

Toppo, A. L., Yadav, M., Dhagat, S., Ayothiraman, S., & Eswari, J. S. (2021). Molecular docking and ADMET analysis of synthetic statins for HMG-CoA reductase inhibition activity. *[Conference presentation or journal name needed]*.

Trabsa, H. (2015). *Activité antioxydantes et anti-inflammatoire des fractions des plantes: Sedum sediforme et Lycium arabicum* [Doctoral thesis, Université Ferhat Abbas Sétif 1].

Trinder, P. (1969). Determination of glucose in blood using glucose oxidase with an alternative oxygen acceptor. *Annals of Clinical Biochemistry*, *6*(1), 24–27.

Ursu, O., Rayan, A., Goldblum, A., & Oprea, T. I. (2011). Understanding drug-likeness. *Wiley Interdisciplinary Reviews: Computational Molecular Science*, *1*(5), 760–781.

Vallee, B. L., & Falchuk, K. H. (1993). The biochemical basis of zinc physiology. *Physiological Reviews*, *73*(1), 79–118.

Varbanov, H. P., Jakupec, M. A., Roller, A., Jensen, F., Galanski, M., & Keppler, B. K. (2013). Theoretical investigations and density functional theory-based quantitative structure–activity relationships model for novel cytotoxic platinum(IV) complexes. *Journal of Medicinal Chemistry*, *56*(9), 330–344.

Varma, S. D., Devamanoharan, P. S., & Ali, A. H. (2020). Implications of anti-inflammatory drugs on oxidative stress-mediated neurodegeneration. *Current Topics in Medicinal Chemistry*, *20*(1), 60–70.

Walsh, L. P., McCormick, C., Martin, C., & Stocco, D. M. (2000). Roundup inhibits steroidogenesis by disrupting steroidogenic acute regulatory (StAR) protein expression. *Environmental Health Perspectives*, *108*(8), 769–776. https://doi.org/10.1289/ehp.00108769.

Weckbecker, G., & Cory, J. G. (1988). Ribonucleotide reductase activity and growth of glutathione-depleted mouse L1210 cells in vitro. *Cancer Letters*, *40*(3), 257–264.

Whelton, A. (1999). Nephrotoxicity of nonsteroidal anti-inflammatory drugs: Physiologic foundations and clinical implications. *The American Journal of Medicine*, *106*(5B), 13S–24S.

Whitlock, H. W., & Bower, K. B. (1965). Porphyrin carbon NMR studies. *Tetrahedron Letters*, *52*, 4827–4831.

Wolberg, A., & Manassen, J. (1970). Radical cations of porphyrins. *Journal of the American Chemical Society, 92*(10), 2982–2991.

Wongrakpanich, S., Wongrakpanich, A., Melhado, K., & Rangaswami, J. (2018). A comprehensive review of non-steroidal anti-inflammatory drug use in the elderly. *Aging and Disease, 9*(1), 143.

Wongrakpanich, S., Wongrakpanich, A., Melhado, K., & Rangaswami, J. (2018). A comprehensive review of non-steroidal anti-inflammatory drug use in the elderly. *Aging and Disease, 9*(1), 143–150.

Wopschall, R. H., & Shain, I. (1967). Voltammetric studies of porphyrins. *Analytical Chemistry, 39*(13), 1514–1527.

Xu, C., Cheng, F., Chen, L., Du, Z., Li, W., Liu, G., Lee, P. W., & Tang, Y. (2012). *In silico* prediction of chemical Ames mutagenicity. *Journal of Chemical Information and Modeling, 52*(11), 2840–2847.

Yoshida, T., Takahashi, K., & Masaki, H. (2002). Porphyrin derivatives protect kidney cells from oxidative stress-induced apoptosis. *Bioorganic & Medicinal Chemistry Letters*, *12*(8), 1043–1046.

Young, R. C., Mitchell, R. C., Brown, T. H., Ganellin, C. R., Griffiths, R., Jones, M., Rana, K. K., Saunders, D., & Smith, I. R. (1988). Development of a new physicochemical model for brain penetration and its application to the design of centrally acting H2 receptor histamine antagonists. *Journal of Medicinal Chemistry, 31*(3), 656–671.

Zakavi, S., et al. (2011). Substitution effects on porphyrin spectra. *Inorganic Chemistry Communications, 14*(11), 1827–1832.

Zanger, U. M., & Schwab, M. (2013). Cytochrome P450 enzymes in drug metabolism: Regulation of gene expression, enzyme activities, and impact of genetic variation. *Pharmacology & Therapeutics*, *138*(1), 103–141.

Zerrouk, L., Bechki, L., Lanez, E., & Lanez, T. (2024). Synthesis, characterization, cyclic voltammetry, and molecular docking studies of the antioxidant activities of superoxide anion

radicals towards meso-tetramethophenyl-porphyrin and meso-tetrabiphenyl-porphyrin. *Notulae Scientia Biologicae, 16*(1), 11823.

Annexes

دليل مشروع

للحصول على شهادة براءة اختراع
في إطار القرار الوزاري 1275

ديسمبر
2022

CNCSIIU — MHESR — ALGERIA

بطاقة معلومات

حول فريق الاشراف وفريق العمل

1- فريـــق الاشـــراف:

فريق الاشراف	
المشرف الرئيسي (01): **الحفناوي العانز**	التخصص: **بيولوجيا**

2- فريـــق العمـــل:

فريق المشروع	التخصص	الكلية
الطالب: **زرود نصرالله**	**علم السموم**	**كلية علوم الطبيعة والحياة**
الطالبة: **زرود فريدة**	**علم السموم**	**كلية علوم الطبيعة والحياة**

فهرس المحتويات

مقدمة

تُعد الالتهابات المزمنة والحادة من أكثر المشكلات الصحية شيوعًا وتأثيرًا على نوعية حياة الأفراد، حيث ترتبط ارتباطًا وثيقًا بالعديد من الأمراض الخطيرة مثل أمراض القلب، التهابات المفاصل، أمراض الكبد، والاضطرابات المناعية. رغم وفرة العلاجات الكيميائية في السوق، إلا أن معظمها يسبب آثارًا جانبية على المدى الطويل، مما يزيد الحاجة إلى حلول أكثر أمانًا وفعالية.

انطلاقًا من هذه الإشكالية، جاء هذا المشروع ليقدم اختراعًا جديدًا في شكل مكمل غذائي مضاد للالتهاب، يعتمد على مادة عضوية فعالة تُدعى .Porphyrin يتم تحضير هذه المادة بتقنية كيميائية دقيقة، وتُدمج ضمن صيغة صيدلانية فموية (كبسولات) توفر فعالية علاجية قوية وسلامة بيولوجية عالية. وقد أثبتت التجارب المخبرية والبيولوجية فعالية هذا المركب في خفض مؤشرات الالتهاب، دون التسبب في أضرار على الأعضاء الحيوية.

يمثل هذا المشروع خطوة فعلية نحو تحويل منتج مخبري إلى حل دوائي قابل للتصنيع والتسويق، بالاعتماد على تقنيات بسيطة ومنخفضة التكلفة، مما يجعله مناسبًا للنهوض بالصناعات المحلية في مجال المكملات الدوائية. كما يهدف إلى تقديم بديل طبيعي وآمن للأدوية التقليدية، مما يُلبي حاجات شريحة واسعة من المستخدمين الباحثين عن حلول فعالة وغير دوائية.

إن هذه البراءة ليست مجرد فكرة نظرية، بل تم تطويرها على أسس علمية وتجريبية، بدعم من الكفاءات الجامعية، لتكون نموذجًا ملموسًا للابتكار الجامعي القابل للتحويل إلى مشروع ناشئ، يستوفي الشروط العلمية والتقنية والتسويقية ضمن رؤية وطنية لتعزيز اقتصاد المعرفة.

المحور الأول

تقديم المشروع

المحور الأول

تقديم المشروع

1. فكرة المشروع (الحل المقترح)

يقترح هذا المشروع تطوير مكمل غذائي علاجي في شكل كبسولات فموية، يعتمد على مركب عضوي فعّال يُعرف باسم "البيرفورين(Porphyrin) "، بهدف معالجة الالتهابات المزمنة والحادة بطريقة طبيعية وآمنة وفعالة. جاءت هذه الفكرة استجابةً لحاجة ملحة في السوق الدوائية، تتمثل في إيجاد بدائل آمنة ومستقرة للعلاجات الكيميائية التقليدية، خاصة مضادات الالتهاب غير الستيرويدية والكورتيكوستيرويدات، التي كثيرًا ما تكون مصحوبة بآثار جانبية مزمنة.

بدلًا من الاعتماد على مستخلصات نباتية غير مستقرة وذات فعالية متغيرة، يستند هذا المشروع إلى مادة نقية وموحدة كيميائيًا يمكن التحكم في جرعتها وجودتها. يتم تصنيع "البيرفورين" عبر تفاعل كيميائي دقيق ومنخفض التكلفة باستخدام مواد أولية متوفرة، ثم يُدمج في تركيبة صيدلانية صلبة مدروسة تحتوي على سواغات تساعد على تحسين الامتصاص الحيوي والاستقرار الكيميائي داخل الجهاز الهضمي.

نشأت فكرة المشروع من خلال أبحاث وتجارب مخبرية ضمن تخصص علم السموم الدوائي، حيث أظهرت المادة فعالية واضحة في تقليل المؤشرات الحيوية للالتهاب (مثل CRP، TGO، TGP)، كما أثبتت التجارب على الفئران سلامة استعمالها وعدم تأثيرها السلبي على الكبد، الكلى، أو الدماغ، وفق تحاليل نسيجية دقيقة.

2. القيم المقترحة:

- تركيبة قائمة على مركب مستقر وفعال(Porphyrin)
- فعالية مثبتة معمليًا ضد الالتهابات المزمنة والحادة
- منتج ذو خصائص فيزيوكيميائية محسنة تضمن الامتصاص الجيد والتوافر الحيوي العالي
- تقليل الاعتماد على العلاجات الكيميائية ذات الآثار الجانبية
- سهولة التصنيع والتوسع الصناعي بتكاليف إنتاج منخفضة

3. فريق العمل (المخترعين):

يتكون فريق المشروع من **طالبين في تخصص البيوكيمياء التطبيقية**، يعملان بشكل تكاملي على تطوير مكمل غذائي مضاد للالتهاب يعتمد على مادة"Porphyrin" ، ضمن إطار علمي ومنهجي يراعي الجانب التقني، القانوني، والتطبيقي للمشروع.

- **الطالب: زرود نصر الله**

تخصص: علم السموم

- تلقى تكوينًا متخصصًا في **المنهجية العلمية والتجريبية**، وهو مسؤول عن متابعة **الجانب العلمي والتقني** للمشروع.

تشمل مهامه:

  - المسؤول العام على المشروع
  - مراقبة خطوات التفاعل الكيميائي والتحقق من نقاوة المنتج.
  - الإشراف على التحاليل البيوكيميائية والتجارب الحيويةCRP ، TGO، TGP، FNS.
  - المساهمة في تقييم فعالية المكمل عبر الدراسات النسيجية والبيولوجية.
  - العمل على البراندينغ و و المسؤول على التصميم.

- **الطالبة: زرود فريدة**

تخصص: علم السموم

- تابعت دورة تدريبية في **حماية الملكية الفكرية وتطوير نموذج العمل التجاري**.

تتكفل بـ:

  - متابعة التوجهات السوقية وتحديد الفئة المستهدفة وطريقة تقديم المنتج

طرق التفاعل والتنسيق بين أعضاء الفريق

يعتمد الفريق على آلية عمل مرنة ومنظمة، تشمل:

- **اجتماعات أسبوعية** لمراجعة التقدم المرحلي وتوزيع المهام.
- استخدام منصات رقمية مثل **Google Meet** للتواصل عن بعد، و **Google Drive** لحفظ الوثائق.

4. أهداف المشروع:

يسعى هذا المشروع إلى تحقيق مجموعة من الأهداف المترابطة التي تشمل الأبعاد **العلمية، الصحية، الاقتصادية، والتقنية**، وتتمحور حول تطوير منتج مكمل غذائي وطني قائم على أسس علمية رصينة وابتكار صيدلاني واضح المعالم. وتتمثل أهم أهداف هذا الاختراع فيما يلي:

1. تطوير مكمل غذائي مبتكر وفعّال مضاد للالتهاب

الهدف الأساسي هو **ابتكار تركيبة صيدلانية جديدة** تعتمد على مادة فعالة واحدة (Porphyrin) ذات فعالية مثبتة في تثبيط العمليات الالتهابية داخل الجسم. هذا المكمل مصمم ليكون **بديلاً طبيعيًا وآمنًا** لمضادات الالتهاب الكيميائية، ويتميز بسهولة الاستخدام، وسرعة التأثير، وأمان بيولوجي طويل المدى.

2. تحسين جودة الحياة الصحية لدى الأشخاص المصابين بالالتهابات المزمنة

من خلال تقليل الاعتماد على الأدوية الكلاسيكية التي قد تسبب آثارًا جانبية خطيرة، يوفّر هذا المكمل خيارًا علاجيًا مكمّلاً أو وقائيًا للأفراد الذين يعانون من حالات التهابية مثل:

- التهابات المفاصل
- أمراض الكبد الالتهابية
- متلازمات المناعة الذاتية
- اضطرابات الجهاز العصبي ذات الطابع الالتهابي

3. تثمين البحث العلمي الجامعي وتحويله إلى منتج ذي قيمة سوقية

يُعد هذا الاختراع نموذجًا حيًا لكيفية تحويل **نتائج البحث الأكاديمي التجريبي** إلى **منتج عملي قابل للتسويق**، مما يُعزز من مكانة الجامعة كمصدر للابتكار والبحث التطبيقي، ويدعم مسار الطلبة نحو إنشاء مؤسسة ناشئة قائمة على براءة اختراع.

4. إنتاج مكمل غذائي محلي الصنع بجودة عالية وتكلفة منخفضة

تم تصميم هذا المشروع ليكون **قابلًا للتطبيق في بيئة إنتاج وطنية**، بالاعتماد على مواد أولية متوفرة محليًا، وتقنيات تصنيع بسيطة ومنخفضة التكلفة، مما يسمح بتوفير مكمل فعال وبسعر تنافسي، مع ضمان احترام معايير الجودة الدوائية.

5. المساهمة في السيادة الصحية وتقليل الاستيراد الدوائي

من خلال تطوير مكمل غذائي وطني ذي فعالية سريرية محتملة، يسعى المشروع إلى تقليل **الاعتماد على المنتجات المستوردة**، خاصة تلك ذات الاستخدام طويل الأمد، مما يساهم في دعم الاقتصاد الوطني والابتكار المحلي في مجال الصناعات الصيدلانية.

6. تمهيد الطريق لتطوير عائلة منتجات علاجية مبنية علىPorphyrin

يشكل هذا المكمل اللبنة الأولى في **برنامج تطوير متسلسل** لمشتقات ومكملات غذائية أخرى تعتمد على نفس المادة الفعالة، أو تركيبات متعددة الوظائف(Multi-target formulations) ، وهو ما يفتح المجال لإنشاء خط إنتاج متكامل قائم على هذا الاختراع.

5. <u>جدول زمني لإنجاز براءة الاختراع:</u>

المرحلة	الوصف التفصيلي للمهام	المدة الزمنية	النتيجة المنتظرة
1	**تحضير المادة الفعالة Porphyrin** من خلال تفاعل مخبري مضبوط باستخدام حمض البروبيونيك و2-ميثيلبنزالديهايد والبيرول، ضمن وسط حراري خاضع للتحكم.	شهر واحد	الحصول على مركب نقي بنسبة مردود 8.2% وجاهز للتحاليل
2	**التحاليل الفيزيائية والكيميائية للمركب** (الذوبانية، الثبات الحراري، الأس الهيدروجيني المثالي، اللون، الرائحة، البنية البلورية)، للتحقق من صلاحية المادة الفعالة للصياغة الصيدلانية.	شهر واحد	تثبيت خصائص المادة واختيار شروط التخزين والدمج داخل كبسولات
3	**تصميم الصيغة الصيدلانية النهائية** للكبسولات: اختيار السواغات (مالئة، مزلقة، رابطة)، تحديد الجرعة المثلى، واختبار التجانس، الانزلاق، وسرعة التفكك.	شهر واحد	إنتاج دفعة تجريبية من الكبسولات بخصائص دوائية مستقرة وقابلة للتناول الفموي

جمع بيانات علمية تثبت الفعالية البيولوجية وسلامة الاستخدام للمكمل الغذائي	شهران	**التحاليل الحيوية والتجريبية (*in vivo*) على نماذج حيوانية** (فئران): تقييم مؤشرات الالتهاب(CRP) ، TGO، (TGP، تعداد الدم، والفحوصات النسيجية لأعضاء الكبد، الكلى، الدماغ.	**4**
تجهيز ملف علمي وصيدلاني متكامل يمثل جوهر براءة الاختراع من حيث الفعالية والتقنية	شهر واحد	**تحليل النتائج وإعداد الوثائق التنظيمية والعلمية** :تحليل النتائج الإحصائية، إعداد تقارير مفصلة، كتابة وصف علمي للنموذج الأولي، وإرفاق كل المعطيات التقنية.	**5**
الحصول على رقم إيداع رسمي وحماية قانونية وطنية لبراءة الاختراع	شهر واحد	**إعداد وإيداع ملف براءة الاختراع** لدى المكتب الوطني للملكية الصناعية (INAPI)، مع متابعة الملاحظات وتحديث الملف في حال وجود مراجعات.	**6**

المحور الثاني

الجوانب الإبتكارية

المحور الثاني
الجوانب الابتكارية

1. طبيعة الابتكارات:

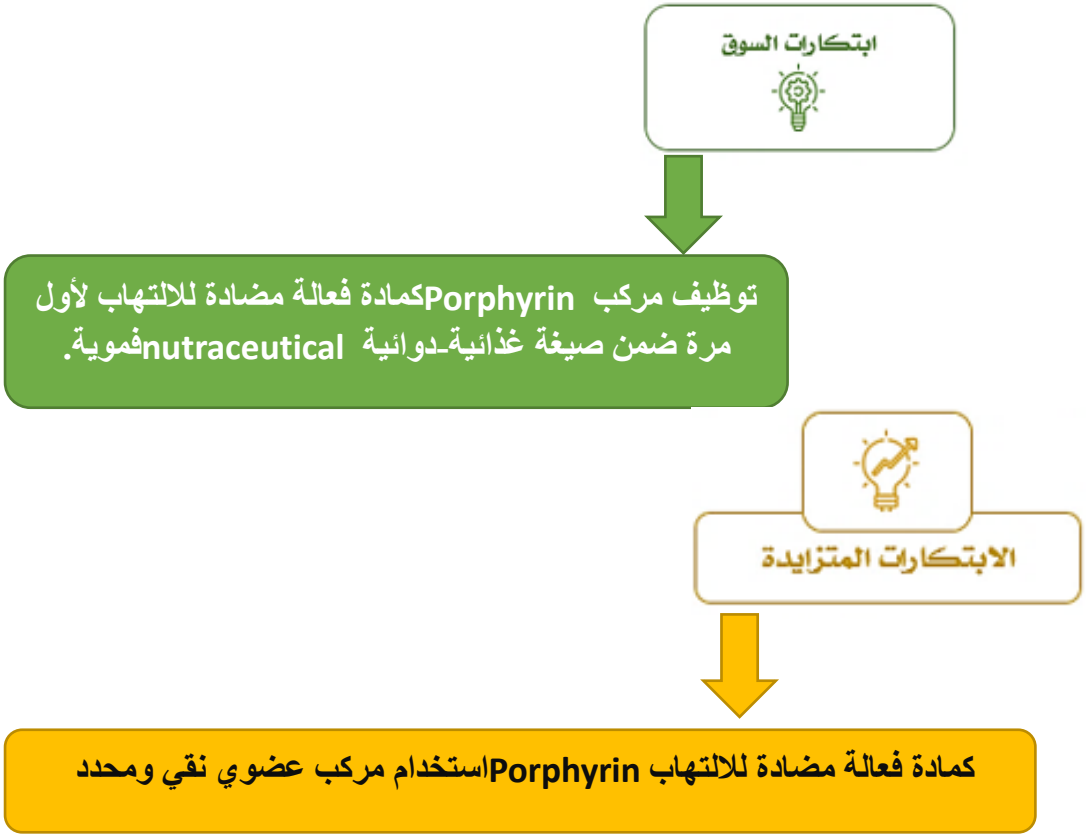

2. مجالات الابتكارات:

1. عمليات جديدة

يعتمد هذا الاختراع على **مسار تحضير كيميائي جديد وبسيط** لمادة فعالة تُستخدم لأول مرة في مجال المكملات الغذائية العلاجية. حيث تم تصميم طريقة تفاعل مباشرة باستخدام مواد أولية متوفرة محليًا مثل 2-ميثيلبنزالديهايد والبيرول في وسط حمض البروبيونيك، مما أتاح الحصول على مركب "Porphyrin" بنسبة مردود جيدة وبنقاوة عالية. هذه الطريقة تُمثّل عملية جديدة في الصناعة الدوائية المحلية، فهي ترفع من كفاءة الإنتاج، وتقلل من التكاليف، وتسمح بتكرار المردود دون الحاجة إلى تجهيزات متقدمة.

2. عروض جديدة

يُقدّم هذا المشروع **منتجًا جديدًا كليًا في السوق الجزائرية والعربية**، يتمثل في مكمل غذائي مضاد للالتهاب في شكل كبسولات فموية، يعتمد على مادة فعالة غير مستخدمة سابقًا في هذا السياق. التركيبة لا تحتوي على مستخلصات نباتية، بل تعتمد على مركب كيميائي موحد ومستقر يُمكن التحكم في جرعته بدقة. بهذا، يمثل الاختراع عرضًا جديدًا يجمع بين الخصائص الطبيعية والدوائية، ويشكل إضافة مبتكرة إلى سوق المكملات الغذائية.

3. ميزات جديدة

يتميّز المكمل الغذائي المقترح بعدة **خصائص وظيفية غير متوفرة في المنتجات المنافسة** .من أبرز هذه الميزات:

- التوافر الحيوي العالي بفضل الصيغة الصيدلانية المدروسة
- فعالية سريعة في تقليل المؤشرات الحيوية للالتهاب
- استقرار فيزيائي وكيميائي عند التخزين
- سهولة في الاستخدام دون آثار جانبية شائعة

هذه الميزات تجعل من المنتج خيارًا مثاليًا للأشخاص الذين يبحثون عن مكمل طبيعي له تأثير علاجي فعلي، دون تعريضهم لمخاطر الأدوية الكيميائية.

4. نماذج جديدة

يعتمد المشروع على إمكانية **تبني نموذج عمل تجاري جديد** في مجال المكملات الغذائية ذات الخصائص العلاجية. فبفضل الطبيعة المركزة والمضمونة للمنتج، يمكن تسويقه ضمن مسارات متعددة، سواء عبر الصيدليات، أو المتاجر المتخصصة في المنتجات الصحية، أو حتى عبر التجارة الإلكترونية. هذا النموذج التجاري القابل للتوسع يسمح بخلق مؤسسة ناشئة مستقلة، بعلامة محلية مسجلة، قادرة على التطور في بيئة السوق الصيدلانية.

5. عملاء جدد

يمكّن هذا الابتكار من **الوصول إلى فئات جديدة من المستخدمين** الذين يصعب استهدافهم بالمنتجات التقليدية. من بين هذه الفئات:

- كبار السن الذين يعانون من هشاشة صحية ومناعة ضعيفة

- مرضى الالتهابات المزمنة الذين يفضلون الابتعاد عن الأدوية الكلاسيكية
- الرياضيون أو النساء بعد الولادة، ممن يحتاجون إلى مكمل آمن وسريع المفعول
- الأشخاص الذين يتبعون أنظمة علاج طبي ويفضلون دعمه بمكملات طبيعية

بذلك، يوسّع هذا المنتج من نطاق استعمال المكملات الغذائية، ويرفع من القيمة السوقية له عبر مخاطبة احتياجات واقعية ودقيقة.

المحور الثالث

وصف براءة الاختراع

المحور الثاني: وصف براءة الاختراع

- **عنوان براءة الاختراع:** مكمل غذائي مضاد للالتهاب في شكل كبسولات قائم على " Porphyrin"

- **ملخص براءة الاختراع :**

يتناول الاختراع تطوير مكمل غذائي مضاد للالتهاب يعتمد على مركب"Porphyrin" ، يتميز بفعاليته العالية وسلامته مقارنة بالأدوية التقليدية. يُحضَّر المركب بتفاعل كيميائي بسيط، ثم يُدمج في كبسولات صيدلانية باستخدام سواغات مختارة بعناية لضمان الثبات والتحرر الدوائي المناسب.

أُجريت دراسات بيولوجية على فئران أثبتت فعالية المركب في تحسين مؤشرات الالتهاب دون آثار سُمية. كما أن تكلفة الإنتاج منخفضة بفضل توفر المواد وسهولة التحضير، مما يجعله قابلاً للتصنيع ويحظى بفرص قبول تنظيمية عالية.

يُعد هذا الابتكار مساهمة واعدة في مجال العلاجات الطبيعية، ويجمع بين الكفاءة الدوائية والجدوى الاقتصادية والبيئية.

- **الميدان التقني الذي ينتمي إليه الاختراع :**

ينتمي الاختراع الى ميدان الصناعة الطبية حيث يمثل منتج يستخدم لتخفيض الالتهابات انطلاقا من Porphyrin .

- **الحالة التقنية السابقة :**

US9352008B2

تعتمد هذه التركيبة على مكونات نباتية معروفة بخصائصها المضادة للالتهاب. ومع ذلك، فإن فعالية هذه المكونات قد تكون محدودة بسبب التباين في جودة المستخلصات النباتية وتأثير العوامل البيئية على محتواها من المركبات النشطة. بالإضافة إلى ذلك، قد تواجه هذه التركيبة تحديات في الامتصاص البيولوجي والتوافر الحيوي، مما يقلل من فعاليتها السريرية. من الناحية الاقتصادية، قد تكون تكلفة الحصول على مستخلصات نباتية عالية الجودة مرتفعة، مما يؤثر على تكلفة المنتج النهائي.

يتميز المكمل الغذائي القائم على "Porphyrin" ببنية كيميائية محددة وثابتة، مما يضمن اتساق الفعالية والجرعة. كما أن "Porphyrin" معروف بخصائصه المضادة للأكسدة، مما يعزز من فعاليته في مكافحة

الالتهابات المزمنة. بالإضافة إلى ذلك، فإن إمكانية تصنيعه بكميات كبيرة وبجودة عالية تقلل من التكاليف وتزيد من توفره في السوق

US10653734B2

رغم التحسينات المزعومة، إلا أن التركيبة لا تزال تعتمد على نفس المكونات النباتية، مما يعني أن التحديات المتعلقة بالتوافر الحيوي والتباين في جودة المستخلصات لا تزال قائمة. كما أن الاعتماد على مصادر نباتية متعددة قد يزيد من تعقيد سلسلة التوريد والتكاليف المرتبطة بها.

توفر "Porphyrin" نهجًا متعدد الأهداف في مكافحة الالتهابات، حيث يمكنها التفاعل مع مسارات التهابية مختلفة، مما يزيد من فعاليتها ضد مجموعة متنوعة من الحالات الالتهابية. كما أن استخدامها كمكمل غذائي يقلل من احتمالية التفاعلات الجانبية مقارنةً بالأدوية الكيميائية التقليدية.

EP1825861A4

تعتمد هذه التركيبة على مكونات نباتية تقليدية، وقد تواجه تحديات في التوافر الحيوي والاستقرار الكيميائي. بالإضافة إلى ذلك، قد تكون تكلفة الحصول على هذه المكونات مرتفعة، مما يؤثر على تكلفة المنتج النهائي.

يتميز "Porphyrin" ببنية كيميائية مستقرة وسهولة في التصنيع، مما يجعله خيارًا أكثر اقتصادية وقابلية للتوسع. كما أن قدرته على التفاعل مع الجذور الحرة والسيتوكينات تعزز من فعاليته كمضاد للالتهاب.

US10245294B2

تعتمد هذه التركيبة على تحسين صحة الأمعاء كوسيلة لتقليل الالتهاب، وهو نهج غير مباشر قد يستغرق وقتًا أطول لتحقيق النتائج المرجوة. بالإضافة إلى ذلك، قد تكون فعالية هذه الألياف محدودة في حالات الالتهاب الحاد أو المزمن. من الناحية الاقتصادية، قد تكون تكلفة استخراج الألياف من هذه النباتات مرتفعة، مما يؤثر على تكلفة المنتج النهائي.

يوفر "Porphyrin" تأثيرًا مباشرًا على المسارات الالتهابية، مما يؤدي إلى نتائج أسرع وأكثر فعالية. كما أن تصميمه كمكمل غذائي يسهل امتصاصه واستخدامه في الجسم، مما يعزز من فعاليته في مكافحة الالتهابات.

EP3818979A1

تعتمد هذه التركيبة على مزيج من المكونات الطبيعية المعروفة بخصائصها المضادة للأكسدة والمضادة للالتهاب. ومع ذلك، فإن فعالية هذه التركيبة قد تكون محدودة بسبب التباين في جودة المكونات وتأثير العوامل البيئية على محتواها من المركبات النشطة. بالإضافة إلى ذلك، قد تواجه هذه التركيبة تحديات في الامتصاص البيولوجي والتوافر الحيوي، مما يقلل من فعاليتها السريرية. من الناحية الاقتصادية، قد تكون تكلفة الحصول على مكونات عالية الجودة مرتفعة، مما يؤثر على تكلفة المنتج النهائي.

يتميز المكمل الغذائي القائم على "Porphyrin" ببنية كيميائية محددة وثابتة، مما يضمن اتساق الفعالية والجرعة. كما أن "Porphyrin" معروف بخصائصه المضادة للأكسدة، مما يعزز من فعاليته في مكافحة الالتهابات المزمنة. بالإضافة إلى ذلك، فإن إمكانية تصنيعه بكميات كبيرة وبجودة عالية تقلل من التكاليف وتزيد من توفره في السوق.

- الغرض (الهدف) من الاختراع :

يهدف هذا الاختراع إلى تقديم مكمل غذائي مضاد للالتهاب، يعتمد على مكونات مستخلصة بعناية لضمان فعالية عالية وأمان تام دون التسبب في آثار جانبية ضارة. يقدم هذا المنتج حلاً عمليًا وآمنًا لمشكلة الالتهابات المزمنة والحادة، التي تؤثر سلبًا على جودة حياة الأفراد وتعد سببًا رئيسيًا للعديد من الأمراض المزمنة مثل أمراض القلب والمفاصل واضطرابات المناعة. الغرض الأساسي من هذا الاختراع هو توفير بديل صحي وعضوي للعلاجات التقليدية الكيميائية، التي غالبًا ما ترتبط بآثار جانبية ومضاعفات على المدى الطويل. هذا الاختراع يجمع بين التقدم العلمي وفلسفة العناية الطبيعية، ليقدم للمستهلكين فرصة حقيقية لتعزيز صحتهم بشكل مستدام وآمن.

- تقديم جوهر الاختراع :

النموذج الأولي التجريبي

الخطوة الأولى: تصنيع المكمل الغذائي

تم الحصول على مواد بنقاوة عالية من مصدر موثوق وهذا لاسباب اقتصادية. يتم تنفيذ التفاعل داخل وسط من حمض البروبيونيك، حيث يخلط 2-ميثيلبنزالديهايد مع الحمض ويقلب عند درجة حرارة الغرفة حتى الذوبان الكامل.

بعدها، يضاف البيرول المقطر تدريجياً، ويُسخن المزيج إلى 50 درجة مئوية، ثم يتم التفاعل تحت الغليان (reflux) لمدة 30 دقيقة.

بعد انتهاء التفاعل، يبرد المزيج إلى درجة حرارة الغرفة. يتم ترشيح الراسب الصلب البنفسجي، ثم غسله بخليط ميثانول/ماء ثم بالميثانول النقي حتى يصبح الراشح شفافًا.

يجفف المنتج تحت تفريغ للحصول على مركب عضوي نقي بوزن نهائي يقارب 10.6 غرام وبنسبة مردود 8.2%.

يتميز هذا المركب البنفسجي بخصائص مضادة للالتهاب بفضل طبيعته الكيميائية الخاصة.
بعد ذلك، تم إجراء دراسة مبدئية على خواصها الفيزيائية (الذوبانية، الثبات الحراري، الأس الهيدروجيني الأمثل للفعالية) لتحديد البيئة المثالية لدمجها في شكل صيدلاني صلب.

تصميم الصيغة الدوائية

تم اختيار مجموعة من السواغات (المواد المساعدة) بناءً على وظائفها:

سواغات مالئة (مثل اللاكتوز أو المانيتول) لضبط حجم الحبة

مواد رابطة) مثل PVP أو النشا المحبب (لضمان تماسك المكونات

مواد مزلقة (مثل الماغنيسيوم ستيارات) لمنع الالتصاق وتحسين انزلاق الحبة في القالب
تم مزج المواد الفعالة والمساعدة باستخدام خلاط دوائي خاص يضمن التجانس الكامل للخليط، مع التحكم في الرطوبة والحرارة أثناء العملية لتفادي تفكك المادة الفعالة.

الخطوة الثانية: التحاليل

تم القيام بمجموعة من التحاليل البيوكيميائية على العينات التجريبية (الفئران) وذلك قصد تحديد فعالية المستخلص خلال فترة التجريب.

تحليل مستويات السكر (Glycemie)

تحليل معاير وظائف الكبد(TGO,TGP)

تحليل بروتين سي التفاعلي (CRP)

تحليل تعداد الدم الشامل(FNS)

دراسة المقاطع النسيجية (الكبد، الدماغ، الكلى)

- **طريقة تطبيق الاختراع:**

قبل تناول الكبسولات، تأكد من حفظها في مكان جاف وبارد لضمان سلامة المادة الفعالة.
تناول كبسولة واحدة يوميًا مع كوب كامل من الماء، ويفضل أن يكون ذلك قبل الوجبة الرئيسية أو حسب توصيات الطبيب.
ابتلع الكبسولة كاملة دون مضغ أو فتحها لضمان الإطلاق الصحيح للمادة الفعالة داخل الجسم.

1- قائمة الرسومات:

الشكل (1): خطوات تحضير المكمل الغذائي المضاد للالتهاب القائم على " Porphyrin"

1- توفير المواد الأولية من مصدر موثوق يضمن الجودة و السلامة و القيمة الاقتصادية

2- يتم اجراء مجموعة من التفاعلات بين حمض البروبيونيك و 2-ميثيلبنزالديهايد

3- تشكيله على شكل حبوب

4- اجراء تحاليل in vitro على مدى فعالية المادة الفعالة

5- معالجة مجموعة من الفئران به

6- القيام بتحليل نسيجي مقاطع من أعضاء هذه المجوعات المعالجة

7- القيام بتحليل الاجهاد التاكسدي لتحقق من فعاليته

الشكل (2): شكل المنتج النهائي المتوقع

المحور الرابع

المطالب

المطالب

1- مكمل غذائي مضاد للالتهاب في شكل كبسولات قائم على"Porphyrin" .

2- وفقًا للمطلب الأول هذا الاختراع يتميز باستخدام مركب كيميائي محدد من عائلة الـ Porphyrin تم تصميمه مخبريًا لزيادة فعاليته كمضاد للالتهاب.

3- وفقًا للمطلب الأول هذا الاختراع يتميز بفعالية عالية في تقليل المؤشرات الحيوية للالتهاب مثل TNF-α وIL-6 وCRP مقارنة بمركبات تقليدية.

4- وفقًا للمطلب الأول هذا الاختراع يتميز ببنية كيميائية مستقرة تمنحه مقاومة عالية للتحلل البيولوجي، مما يزيد من توافره الحيوي داخل الجسم.

5- وفقًا للمطلب الأول هذا الاختراع يتميز بخصوصية عالية في استهداف مسارات الالتهاب دون التأثير على المسارات الفسيولوجية الطبيعية الأخرى.

6- وفقًا للمطلب الأول هذا الاختراع يتميز بتصنيع وفق شروط معيارية دقيقة (GMP) لضمان الجودة والنقاء، مما يقلل من احتمالية التلوث أو التفاعل مع مكونات أخر.

7- وفقًا للمطلب الأول هذا الاختراع يتميز بأنه آمن ضمن الحدود المقررة.

8- وفقًا للمطلب الأول هذا الاختراع يتميز بثبات كيميائي عالي تحت ظروف التخزين العادية، ولا يتطلب ظروف تخزين خاصة، مما يضمن فعاليته خلال فترة الصلاحية.

9- وفقًا للمطلب الأول هذا الاختراع يتميز بأنه يمكن دمج هذا المكمل في بروتوكولات علاجية موجهة لعلاج الالتهابات المزمنة كونه يمنح نتائج أسرع وأكثر استقرارًا مقارنة بالمكملات الطبيعية.

قائمة الملاحق

الرسومات

الشكل (1)

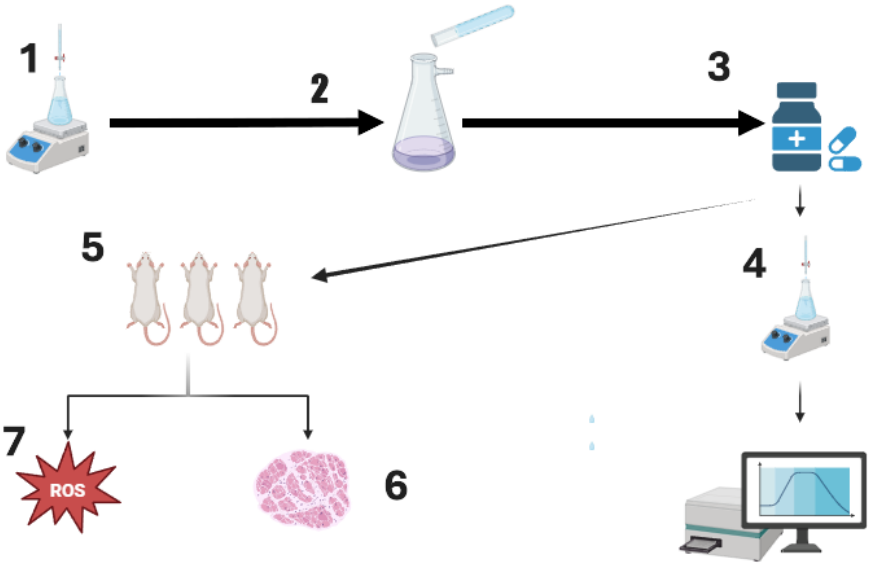

الشكل (2)

دليل مشروع

للحصول على شهادة مؤسسة ناشئة
في إطار القرار الوزاري 1275

ديسمبر